# POLITECNICO DI TORINO

Collegio di Ingegneria Chimica e dei Materiali

**Corso di Laurea Magistrale**
**in Ingegneria Chimica e dei Processi Sostenibili**


Tesi di Laurea Magistrale

# Modeling of a stirred liquid-liquid extraction column in a bio-sourced process



**Relatore**

prof. Daniele Marchisio

**Candidato**

Matia Mazzocco


Dicembre 2017

# Riassunto in Italiano

## Introduzione

La produzione di sostanze chimiche di sintesi prodotte per via petrolchimica rappresenta attualmente una delle vie utilizzate più sfruttate. Si prevede che nei prossimi anni, il mercato dei principali prodotti petrolchimici mostrerà una forte crescita, legato principalmente all'aumento di produzione in diversi settori favorito dalle politiche economiche emanate dai principali governi dell'Asia Pacifica. Inoltre, si prevede che l'impulso positivo sulla domanda sarà legato alla politica dei prezzi bassi attuata dai paesi produttori e allo sviluppo di nuove infrastrutture nelle principali economie emergenti (BRICS) (Grand View Research, 2016). Sebbene questi aspetti comportino una consistente crescita del settore, una delle problematiche dei principali protagonisti del mercato (multinazionali e governi consumatori) è la stretta dipendenza dal petrolio, fonte esauribile e soggetta a fluttuazioni di prezzi in funzione a strategie economico-politiche. Non solo, grazie alla maggior sensibilità ambientale registratasi nel corso degli ultimi anni e allo sviluppo di politiche etiche-sociali, come la riduzione della degradazione ambientale, lo sviluppo economico rurale e di modelli di economia circolare, sono stati attuati degli obiettivi di sviluppo di processi alternativi competitivi nel mercato, che mirino all'indipendenza da fonti fossili. Uno di questi, è la produzione di sostanze chimiche per processi di bioraffineria, ovvero l'insieme dei processi utilizzanti organismi viventi che, attraverso una serie di reazioni biologiche, convertono e modificano un determinato substrato in prodotti chimici e combustibili. Questi processi, definiti processi chimici verdi, rappresentano una valida alternativa rinnovabile alle tecniche di produzione e alle fonti di approvvigionamento classiche, in quanto permettono di utilizzare, per esempio le eccedenze agricole o sostanze vegetali esaurite (oli alimentari). I processi basati sulla sintesi di sostanze chimiche a partire da biomasse, vengono definiti processi di *bio-sourced processes.*

L'oggetto del presente studio è il progetto di un processo di produzione di una sostanza chimica di grande valore industriale, che basa le sue origini su una fonte biologica. In particolare, questo lavoro si focalizza sulla progettazione di un'unità di separazione atta a recuperare i reagenti non convertiti. Nel processo, i reagenti vengono miscelati e inviati in un reattore dove condizioni operative ottimali permetteranno la formazione del composto chiave. La reazione principale è accompagnata da una serie di reazioni indesiderate che consumano una parte dei reagenti. Per questo motivo la conversione viene limitata in maniera tale da evitare la formazione di grandi quantità di sottoprodotti. All'uscita del reattore la miscela composta dal prodotto chiave, dai reagenti non convertiti e dai *by-products* (sottoprodotti della reazione principale e prodotti delle reazioni parassite), viene inviata nella zona dedicata alla separazione. È composta da due unità: la prima, dedicata al recupero del prodotto principale, e la seconda, usata per il recupero dei reagenti non convertiti. La corrente in uscita del reattore è inviata nella prima unità composta da una colonna di distillazione, dove il prodotto principale viene recuperato, separato dai reagenti non convertiti e dai sottoprodotti, e inviato all'unità di purificazione. I sottoprodotti e i reagenti non convertiti sono inviati nella seconda unità di separazione. Il recupero di quest'ultimi, permetterà quindi, previo spurgo, il loro ricircolo nel processo designato (Figura 1). Dato l'elevato numero di componenti all'interno della corrente separata dalla prima unità di separazione, l'applicazione di un'unità di distillazione risulterebbe sconveniente, in quanto per una buona efficienza di separazione si dovrebbe operare con una colonna ad elevato numero di piatti e con un rapporto di riflusso elevato e quindi economicamente poco interessante. Per questo motivo, nella seconda unità di separazione è stata applicata un'estrazione liquido-liquido. Si tratta di un'operazione unitaria

basata sulla differenza di affinità di una sostanza in due fasi generalmente immiscibili, in cui la separazione è legata al trasferimento di uno o più componenti dalla fase di alimentazione alla fase del solvente estrattore.

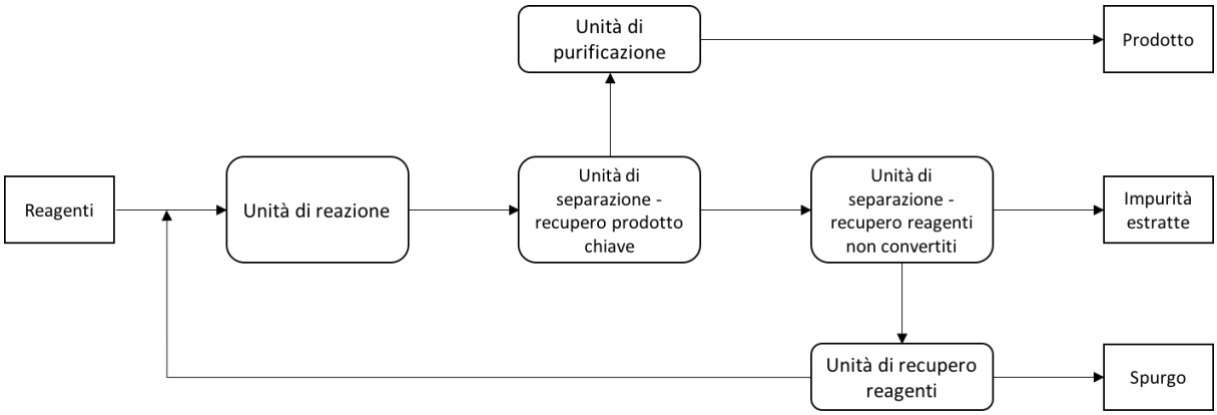


**Figura 1:** Diagramma a blocchi del processo in esame

L'alimentazione, la quale a fine processo risulterà impoverita di alcuni dei suoi componenti è definita raffinato. Il solvente arricchito è definito estratto. Alcuni studi di fattibilità condotti hanno permesso di valutare il tipo di solvente (di natura organica) e l'apparecchiatura estrattiva più adatti per l'applicazione industriale. L'alimentazione, composta dai reagenti non convertiti e dai sottoprodotti, viene inviata in una colonna di estrazione. La colonna, agente in controcorrente, permetterà un buon contatta tra le fasi d'alimentazione e solvente estrattore. Le impurità presenti nella fase alimentata, chimicamente più affini al solvente, si trasferiranno nell'altra fase. Il raffinato verrà inviato nell'unità di riciclo e spurgo, mentre l'estratto verrà inviato nell'unità di recupero del solvente (Figura 2).

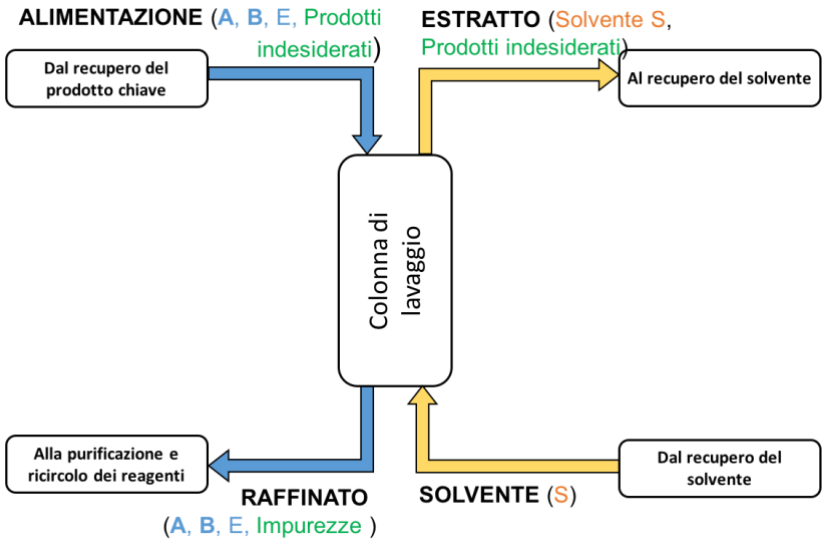


**Figura 2:** Schema dell'unità estrattiva per il recupero dei reagenti

Inoltre, è stato verificato che durante l'intero processo è presente un'ulteriore reazione parassita. Questa reazione d'equilibrio caratterizzata da due step principali, catalizzata in

ambiente acido ($A + B \leftrightarrow F$ e $F + A \leftrightarrow G + E$), consuma una parte dei reagenti da recuperare (A, B) trasformandoli in una specie chimica (G) molto affine al solvente estrattore (S). Questo prodotto, durante la fase di estrazione, si trasferirà totalmente nella fase del solvente, abbassando la quantità di reagente recuperabile, influenzando direttamente il costo totale del funzionamento del processo. Per ovviare a questo problema è stata introdotta una seconda unità estrattiva in grado di recuperare, con un opportuno solvente, il componente G.

L'idea è quella di riuscire, non solo a riconvertire il componente spostando l'equilibrio verso i reagenti, ma anche quello di utilizzare un solvente che sia molto affine ai reagenti A e B, in modo tale da recuperare la maggiore quantità di G. La scelta del solvente da utilizzare ricade quindi sul componente E. L'estratto organico, uscente dalla prima colonna, contenente le impurità estratte e il prodotto da riconvertire, viene inviato in una seconda colonna, dove è messo in contatto con il secondo solvente. La reazione, spostata a sinistra, permetterà la formazione dei componenti iniziali nella fase S, i quali, si troveranno in una fase molto affine. L'estratto della seconda colonna in questo caso verrà miscelato con l'alimentazione del processo estrattivo e inviato nella prima colonna (Figura 3). La prima unità è definita colonna di lavaggio mentre la seconda, che permette di contro-estrarre i reagenti viene denominata di contro-lavaggio. Quest'ultima applicazione permetterà di evitare la perdita di una quantità di reagenti.

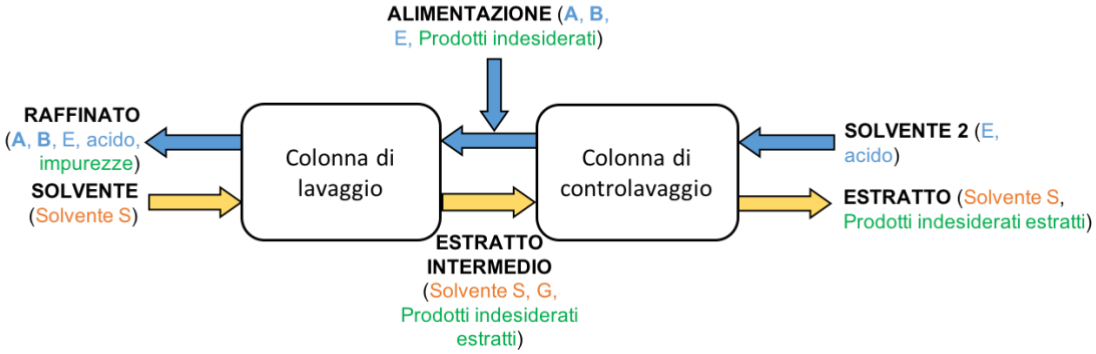


**Figura 3:** Schema delle colonne in serie dell'unità di recupero dei reagenti non convertite. (Figura 2.4 pagina 4)

Data la complessità del problema, è necessario utilizzare una colonna pilota al fine di studiarne il funzionamento ottimale (Mohanty 2000). L'impianto pilota in esame è rappresentato da una colonna funzionante in controcorrente agitata. Generalmente una colonna d'estrazione viene progettata mediante l'uso metodi grafici con il calcolo degli stadi di equilibrio (*Number of theorerical stages*, NTS) nel caso siano presenti degli elementi divisori (piatti), oppure, nel caso di una contatore differenziale (colonne a bolle, *packed tower,* colonne agitate) con il metodo delle unità di trasferimento di massa (NTU *o Number of mass transfer unit*). Ma, a causa della presenza di variazioni di proprietà lungo la colonna, fenomeni idrodinamici complessi, e casi di alimentazioni multicomponente, questi metodi a volte non permettono di ottenere risultati apprezzabili. Lo sviluppo di un modello matematico più dettagliato in grado di valutare accuratamente la concentrazione di soluto lungo la colonna, l'efficienza d'estrazione, le quantità di solvente utilizzate in funzione delle condizioni operative, geometriche e delle proprietà fisiche, è quindi preferito rispetto ai metodi classici, che a volte mostrano deviazioni non trascurabili (Ziegler e Li 1967).

L'obiettivo principale di questo lavoro è quindi la determinazione di un modello matematico in grado di descrivere l'impianto pilota di estrazione liquido-liquido. Il risultato avrà come fine il calcolo dei costi fissi e dei costi operativi del processo descritto. Il modello verrà sviluppato su una colonna Kuhni ECR32 prodotta dalla Sulzer®. Tale *pilot miniplant*, colonna ad alte prestazioni ma per portate liquide limitate, è adatto alle applicazioni di *scale-up*. Nella prima parte del lavoro sono state formulate delle ipotesi che hanno permesso la derivazione matematica del modello, ottenendo un sistema di equazioni differenziali. Il sistema di equazioni risulta legato a cinque parametri relazionati alle variabili operative e geometriche della colonna e possono essere stimati attraverso delle correlazioni matematiche disponibili in letteratura (Hlawitschka 2013, Lo *et al.* 1983 e Leybros 2004). Per determinare il set di correlazioni che possa meglio descrivere il funzionamento della colonna, sono stati condotti degli esperimenti sull'unità estrattiva utilizzando un sistema ternario standard (Hemmati *et. al.* 2015) composto da acqua, acetato di butile e acetone. I risultati ottenuti sperimentalmente sono stati quindi confrontati con il modello matematico. Nella seconda parte del lavoro, il set di correlazioni e il modello ottenuto per il sistema standard ternario verranno applicati al caso reale, sia nel caso di lavaggio e sia in quello di contro-lavaggio, confrontandone le prestazioni con le diverse prove sperimentali svolte in precedenza.

**Modellazione matematica**

La Kuhni ECR32 (Sulzer ®) è una colonna di 1.8 m e diametro di 32 mm agitata meccanicamente da 64 turbine Rushton a 6 pale, tramite un motore collegato all'asse centrale (Figura 4). Sono presenti degli anelli forati (o di coalescenza), che hanno lo scopo di dividere la colonna in 64 compartimenti, massimizzando l'efficienza di estrazione e diminuendo i miscelamenti assiali. Nella parte superiore e inferiore sono presenti due decanter che permettono di separare le fasi. Un sistema di pompe peristaltiche permette il pompaggio dell'alimentazione e del solvente e la regolazione delle loro portate volumetriche. Gli anelli di coalescenza possono essere cambiati e sostituiti, aumentando o diminuendo l'area dedicata al passaggio dei liquidi disponibile. La colonna, grazie al suo piccolo diametro, limita le grandi portate (10-11 Litri/ora), permettendo un risparmio in termini di sostanze utilizzate.

Le due fasi vengono inviate alla colonna per mezzo di pompe. Dalla parte superiore della colonna entra il liquido a densità maggiore, mentre il liquido a densità minore è alimentato dalla parte inferiore, in modo tale da garantire un movimento delle fasi legato alla differenza di densità. In funzione del metodo di caricamento della colonna, una fase sarà continua mentre l'altra sarà dispersa. La prima, presente in quantità maggiore, è distribuita continuamente lungo la colonna. La seconda, dispersa all'interno della fase continua, è formata da gocce polidisperse. A causa della variazione delle proprietà fisiche lungo la colonna, come la densità, la viscosità e la tensione interfacciale del sistema, è possibile verificare che le dimensioni e il numero delle gocce tendono a variare continuamente. Alcune gocce coalescono tra di loro, altre sulla superficie dell'anello formando un film continuo, mentre causa dell'agitatore delle gocce si rompono. L'alimentazione e il solvente vengono pompati alle estremità opposte della colonna. Le gocce della fase dispersa salendo (o scendendo) nei diversi compartimenti vengono miscelate grazie agli agitatori che garantiscono un buon contatto tra le fasi. Il trasferimento di materia avviene per tutta la lunghezza utile della colonna. Le due fasi si separeranno nei decanter, dove verranno raccolte e inviate all'uscita. L'equilibrio idraulico della colonna, legato quindi all'altezza dell'interfaccia delle fasi nel decanter, è regolato per mezzo di un sifone servocomandato, collegato all'uscita nella parte bassa della colonna. In questi tipo di colonne, le variabili operative risultano essere:

- il grado di agitazione (espresso come velocità di rotazione delle turbine);
- la portata totale di liquido;
- il rapporto delle portate tra le due fasi, definito rapporto estratto su raffinato (E/R).

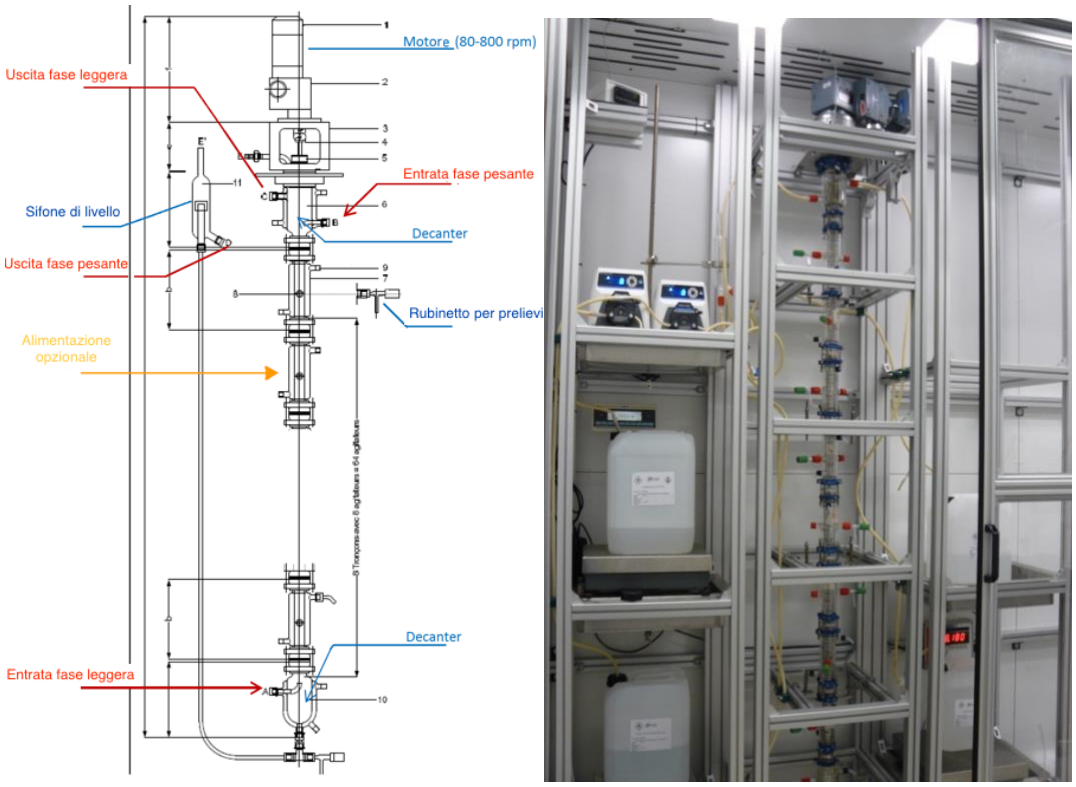


**Figura 4:** Schema della colonna e delle principali ingressi e uscite (a) e foto della colonna nel laboratorio (IFP Lione) (b).

Gli anelli rappresentano un'ulteriore variabile operativa geometrica. Infatti, l'area libera al passaggio dei flussi e quindi, la differente sezione vuota dell'anello influenza l'efficienza di estrazione, per quanto la sua sostituzione richieda lo spegnimento dell'unità.

A portate volumetriche e a rapporti E/R costanti, un aumento di velocità di rotazione porta alla formazione di gocce di grandezza inferiore, le quali avendo una velocità inferiore tendono a concentrarsi maggiormente nella colonna, aumentando dunque la quantità di fase dispersa nel sistema. L'aumento della rotazione fa aumentare la turbolenza del sistema, favorendo il trasporto di materia e la superficie di scambio, dunque, l'efficienza di estrazione. Il volume di fase dispersa sul volume totale viene definito hold-up. A basse rotazioni l'hold-up aumenta linearmente. Quando la fase dispersa si trova nel compartimento con un volume sufficientemente alto, l'aumento diventa esponenziale. Questo punto viene definito *flooding*, o punto di allagamento, dove si registra una brusca perdita di efficacia di estrazione. All'aumentare della portata volumetrica totale, le velocità di rotazione che conducono all'allagamento sono minori. Inoltre, è possibile notare che riducendo l'area libera di passaggio dell'anello forato il rischio di allagamento del compartimento aumenta.

Per la definizione del modello, è necessario analizzare il sistema reale e formulare delle ipotesi che possano semplificare e permettere di descrivere matematicamente le sue complessità. Come già detto, se si osservasse un compartimento della colonna, si vedrebbe uno sciame di gocce che attraversano la fase continua, miscelata dall'agitatore, trasferendo

materia tra le fasi. Il sistema viene definito polidisperso in quanto le gocce presentano diametri diversi. La prima ipotesi del modello è descrivere la fase dispersa come un continuo (Figura 5 (b)). La seconda ipotesi è descrivere ogni compartimento come se fosse un reattore agitato (*continuous stirred tank reactor* CSTR), ovvero un elemento perfettamente miscelato dove le concentrazioni in ogni punto delle due fasi interno all'elemento corrispondono a quelle delle uscite. Inoltre, si può dire che la colonna sia rappresentabile come una cascata di CSTR, essendo formata da compartimenti agitati in serie. Dato l'alto numero di elementi in serie, il sistema può essere pensato come un *plug flow reactor* (PFR), ovvero come un sistema monodimensionale, dove la concentrazione nelle due fasi varia in maniera continua lungo l'asse della colonna. Un'ulteriore ipotesi sta nel descrivere il trasporto di massa con il modello a doppio film. All'interfaccia sarà presente un salto di concentrazione dovuto alla diversa affinità del soluto ai due solventi. Il parametro che quantifica il fenomeno è definito coefficiente di ripartizione. Il modello a pistone descritto però non risulta del tutto soddisfacente. Pratt e Hanson (1982) elencarono una serie di fenomeni che rendono il modello a pistone, in certi casi, inadatto alla descrizione di un sistema d'estrazione (Ziegler e Li 1967). Questi fenomeni sono collegati ad esempio alla presenza di profili radiali di velocità nella fase continua, ad una distribuzione delle dimensioni delle gocce che comporta distribuzioni di velocità della fase dispersa, turbolenze locali, alla retro-miscelazione (*back-mixing)* e alla miscelazione in avanti *forward-mixing*. Questi effetti sono stati raccolti e quantificati in un termine matematico definito flusso dispersivo (Figura 5c ).

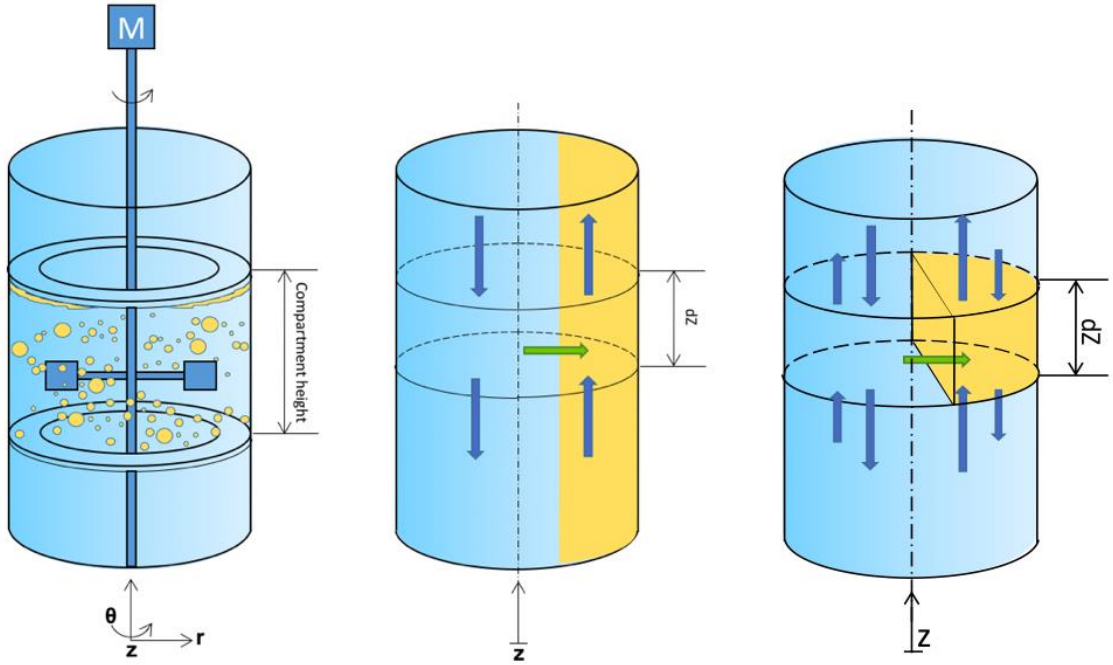


**Figura 5:** Raffigurazione di un compartimento della colonna Kuhni. Dettaglio (a), Modello a pistone (b) e modello dispersivo (c) (Figura 4.1 pagina 9)

Nel modello dispersivo, questi fenomeni vengono descritti da un'equazione simile alla prima legge di Fick (equazione 1), dove il flusso dispersivo di materia è proporzionale al gradiente di concentrazione di un componente i lungo l'asse e a un coefficiente di dispersione.

$$J_{ax,i} = -D_{ax}\frac{dC_i}{dz} \tag{1}$$

I coefficienti di dispersione della fase continua e dispersa sono ricavati sperimentalmente per mezzo di correlazioni. Tramite un bilancio di massa locale (figura 4.6 pagina 15), e dalle opportune ipotesi sviluppate, è stato ricavato un sistema di equazioni differenziali (equazione 2).

$$\begin{cases} (1-\varphi)\dfrac{dC_{c,i}}{dt} = D_{axc,i}\dfrac{d^2C_{c,i}}{dz^2} - v_c\dfrac{dC_{c,i}}{dz} - k_{Oc}a\left(C_{c,i} - C^*_{c,i}\right) \\ \varphi\dfrac{dC_{d,i}}{dt} = D_{axd,i}\dfrac{d^2C_{d,i}}{dz^2} + v_d\dfrac{dC_{d,i}}{dz} + k_{Oc}a\left(C_{c,i} - C^*_{c,i}\right) \end{cases} \quad (2)$$

Nell'equazione 2, sono presenti diversi parametri necessari per risolvere il problema. I principali sono:

- hold-up;
- area specifica, legato al diametro equivalente o di Sauter (equazione 5.11);
- coefficiente di scambio di materia globale;
- coefficienti di dispersione assiale (fase continua e fase dispersa).

I parametri vengono stimati usando correlazioni semi-empiriche o empiriche, legati alle proprietà fisiche del sistema, condizioni operative (velocità di rotazione delle turbine, portate in ingresso) e geometriche. In letteratura sono disponibili, per diverse tipologie di colonne, un numero elevato di correlazioni. Le principali sono state riportate nel capitolo 5 (pagina 17). L'hold up rappresenta la frazione di volume della fase dispersa rispetto il volume totale, e può essere descritto attraverso una correlazione sviluppata da Kumar e Hartland (1995). Questa equazione, basata su più di 7000 dati sperimentali per diversi tipi di colonne e condizioni operative è formata da diversi gruppi adimensionali elevati a potenza da dei coefficienti ricavati dal *fitting* sperimentale. Sulla base della precedente equazione, gli autori hanno sviluppato anche delle correlazioni predittive empiriche per il diametro medio equivalente (Kumar e Hartland 1996) e in accordo con la teoria del doppio film, per i coefficienti di scambio di materia della fase dispersa e continua (Kumar e Hartland 1999). Quest'ultima vede l'estensione dalle correlazioni atte a descrivere i coefficienti di trasferimento di materia per le due fasi alle colonne di estrazione, correlandole a variabili come l'hold-up e la potenza dissipata per l'agitazione. Nel lavoro di Hlawitschka (2013) sono presenti una serie di correlazioni per il calcolo del coefficiente di dispersione assiale delle due fasi. Per il coefficiente di dispersione della fase continua, Kolb (2002) estese la correlazione di Breysse (1983), che inizialmente era stata sviluppata per colonne di grandi diametri, alla colonna Kuhni DN32. Steinmetz (2007) presentò una correlazione per una colonna Kuhni DN32. Le correlazioni per la stima del coefficiente di dispersione della fase dispersa sono state sviluppate sulla base del numero adimensionale di Bodestein. Hlawitschka (2013) elencò diverse correlazioni, come il lavoro di Bauer (1976) e di Steinmetz (2007). Conoscendo i parametri dell'equazione 2, per un sistema tri-componente in condizioni stazionarie e con coefficiente di ripartizione costante, le equazioni differenziali presentano una soluzione analitica, la quale è stata riportata in Appendice 2. Il metodo analitico è stato implementato su un foglio di calcolo e permette di determinare direttamente le concentrazioni di estratto e raffinato, nonché il profilo di concentrazione. La Figura 6 mostra l'andamento della concentrazione delle due fasi per una colonna descritta dal modello a pistone e dal modello a dispersione. Come è possibile vedere, oltre ad un salto di concentrazione (discontinuità) tra le

due entrate, la presenza di un termine dispersivo tende a smorzare la differenza di concentrazione tra le due fasi. Poiché, la differenza di concentrazione rappresenta la forza spingente del processo di separazione, la su riduzione ne pregiudica una perdita delle prestazioni d'estrazione. Se si volesse descrivere le prestazioni come il numero di piatti teorici richiesti (NTS), si vedrebbe che la presenza della dispersione assiale fa aumentare il numero di piatti richiesto, e dunque, per ottenere lo stesso risultato, sarà necessario utilizzare una colonna più alta (Figura 4.3 pagina 9).

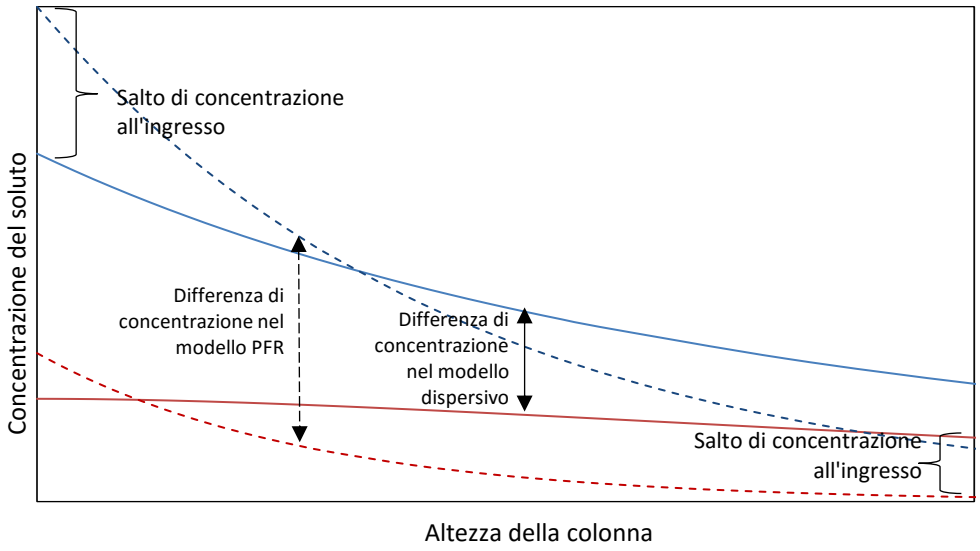


**Figura 6:** Modello a pistone (linea tratteggiata) e modello a dispersione (linea continua) a confronto. Le curve in rosso sono in riferimento alla fase dispersa, le blu alla fase continua. (Figura 4.2 pag. 9)

## Metodi sperimentali:

Per determinare il miglior set di correlazioni da inserire nel modello matematico, sono state condotte una serie di prove sperimentali utilizzando l'unità d'estrazione Kuhni ECR32. Le prove sono state fatte usando un sistema liquido ternario standard (Hemmati *et. al.* 2015). Il sistema standard scelto, presenta una tensione interfacciale media ed è composto da due solventi immiscibili, acetato di butile e acqua, e un soluto, acetone (Tabella 1). Per distinguere meglio le due fasi è stato aggiunto il rosso di Sudan I, un colorante apolare miscelato con l'acetato di butile. Le prove sono state svolte, con trasferimento di materia dalla fase continua (acqua e acetone) alla fase dispersa (acetato di butile e Sudan I), in un range di portate totali da 4 a 10 L/h e da rapporti E/R da 1.5 a 2.5.

**Tabella 1:** Proprietà fisiche del sistema ternario a 20°C (Hemmati et. al. 2015)

| **Componenti / fasi** | **Densità ($kg/m^3$)** | **Viscosità (mPa· s)** | **Tensione superficiale ed interfacciale ($J/m^2$)** | **Diffusività molecolare ($m^2/s$) x $10^9$** |
|---|---|---|---|---|
| Acqua | 998.2 | 1.003 | 0.0727 | - |
| Acetato di butile | 881.5 | 0.73 | 0.0249 | - |
| Acetone | 790.5 | 0.322 | 0.0234 | - |
| Continua | 994.9-995.8 | 1.075-1.088 | 0.0124-0.0132 | 1.01-1.06 |
| Dispersa | 879.6-881,4 | 0.723-0.738 | | 2.15-2.18 |

La prima parte ha come obiettivo la determinazione della mappa del *flooding* per la miscela data e valutarne i punti ottimali di funzionamento. La mappa dell'allagamento permette, fissato il rapporto E/R, di valutare la velocità di rotazione che causa l'allagamento (o critica) in funzione delle diverse portate volumetriche (Figura 6.1 pagina 30). I punti di funzionamento ottimale saranno presi in considerazione nella seconda parte, dove una serie di campionamenti fatti in diversi punti della colonna, unito ad una valutazione fotografica delle dimensioni delle gocce, ha permesso di ottenere una quantità di informazioni che sono state usate per ricavare il migliore set di correlazioni da implementare nel modello a dispersione.

Nella prima parte, per valutare l'hold-up, sono stati presi in considerazione due metodi: il metodo del campionamento veloce (*fast sampling method*) e il metodo dell'arresto della colonna (*shut down method*). Nel *fast sampling method,* l'hold-up è valutato da una serie di campionamenti effettuati attraverso le porte laterali della colonna, dopo un tempo sufficientemente lungo affinché le condizioni di stabilità idrodinamica venissero raggiunte. Valutando il volume di fase dispersa rispetto al volume della fase continua, è stato possibile calcolare l'hold-up per ogni singolo campione prelevato. Il risultato è infine mediato. Nello *shut down method*, l'hold-up viene valutato su tutta la colonna. A condizioni di stabilità idrodinamiche raggiunte, viene arrestata la marcia del motore e vengono chiuse le valvole di immissione del liquido. Aspettando il tempo di separazione delle fasi, viene calcolata la quantità di volume della fase dispersa occupata nella colonna. Conoscendo il volume della colonna, è possibile risalire all'hold-up. Le prove vengono fatte per portate volumetriche costanti a velocità di agitazione crescente. La velocità di rotazione in cui si raggiunge il 30% di hold-up (condizione incipiente allagamento) è detta $N_{critica}$. Diagrammando la velocità di rotazione critica in funzione delle portate totali (a parità di E/R), si ottiene la mappa del *flooding*. Il costruttore della colonna consiglia di lavorare ad una velocità di rotazione pari all'80% di quella critica, dato che generalmente in queste condizioni si hanno efficienze d'estrazione ottimali.

La seconda parte sperimentale prevede un'analisi più approfondita. Le condizioni operative utilizzate sono quelle ottimali determinate dal primo test sperimentale. Per ogni prova in questa parte verrà valutato:

- tempo per il raggiungimento dello stazionario;
- il diametro medio equivalente ($d_{32}$);
- il salto di concentrazione della fase continua in ingesso;
- la concentrazione lungo la colonna attraverso dei prelievi in tre porte laterali;
- concentrazione in uscita di raffinato ed estratto;
- hold-up.

Impostate le condizioni operative, la colonna viene portata a regime idrodinamico e ad intervalli regolari sono effettuati dei campionamenti della fase raffinato ed estratto in uscita. I campioni sono stati analizzati usando una tecnica gascromatografica. Grazie a delle rette di taratura costruite usando uno standard a concentrazione nota, il segnale del rilevatore (FID) è stato correlato alla concentrazione di soluto. Quando la differenza concentrazione di soluto tra due campionamenti a tempi successivi è relativamente bassa, si può affermare che la colonna ha raggiunto lo stato stazionario.

Usando una Nikon D300 è stato possibile ricavare una serie di foto delle gocce all'interno della colonna, che ha permesso in fase di *post-processing* di ricavare il diametro di Sauter (equazione 5.10). È stato aggiunto un colorante organico (rosso del Sudan) che ha permesso di distinguere nettamente le due fasi, originalmente trasparenti. Successivamente un prelievo nei pressi dell'ingresso della fase continua ha permesso di valutare il salto di concentrazione

ed è stato condotto usando una siringa. Utilizzando le porte laterali, sono stati eseguiti tre prelievi in modo da poter valutare la concentrazione lungo la colonna. L'hold-up è stato valutato usando il metodo *shut-down*.

**Risultati e discussioni**

Le prove idrodinamiche hanno permesso di calcolare, come detto, un numero considerevole di valori di hold up e la curva del *flooding*. Analizzando i risultati dati in Figura 7.3 (pagina 34) dove è riportato l'andamento dell'hold-up per i due metodi differenti in funzione dell'agitazione del sistema, è possibile notare come l'hold-up mostri l'andamento già discusso teoricamente. Inoltre, il *flooding* per i due metodi proposti viene raggiunto per gli stessi valori di agitazione. Per contro, per basse velocità di rotazione sono presenti delle differenze di circa 5% tra i due metodi. Il metodo *fast sampling* essendo fatto con prelevamenti su tre porte laterali della colonna, può causare una deviazione rispetto al valore vero, in quanto il liquido prelevato potrebbe modificare l'idrodinamica locale nella colonna influenzandone il prelevamento successivo. Inoltre, dalle misurazioni fatte, l'hold-up tende a variare molto lungo la colonna. Questo può essere legato al fatto che le proprietà fisiche del sistema, come la densità, la viscosità, ma soprattutto la tensione interfacciale, variano lungo la zona d'estrazione. La variazione continua di queste proprietà può causa una variazione assiale dell'hold-up. L'influenza del prelievo unito alle variazioni delle proprietà possono portare ad un risultato leggermente deviato dell'hold up medio, rispetto a quello calcolato con il *shut down method*. Si è preferito optare per quest'ultimo metodo in quanto valuta il parametro medio nella colonna e non è soggetto a possibili deviazioni come per il primo metodo. Nel grafico in Figura 7.2 (pagina 33) è stata tracciata una retta parallela all'asse delle ascisse di valore 30%, utilizzata per calcolare la velocità critica di rotazione. Raccolti tutti i valori del numero critico di agitazione vengono inseriti nella mappa dell'allagamento (Figura 7.4 pagina 34). In questa figura è mostrata la curva dell'allagamento e la curva di funzionamento ottimale in funzione della portata totale nel caso E/R = 1.5.

Le prove del trasferimento di massa sono state utili per ricavare le diverse concentrazioni che verranno confrontate con il modello. I principali risultati sono stati elencati in Tabella 7.2 (pagina 35), dove le performance della colonna sono state espresse in NTS, calcolati usando l'equazione di Kremser (equazione 7.1) (Laddha *et al.* 1978). Le analisi cromatografiche per campioni in intervalli di tempo successivi hanno permesso di capire in quanto tempo il sistema tende alle condizioni stazionarie, generalmente raggiunte in 2 ore per alte portate di liquido (10 Litri/ora) e 4.5 ore per basse portate (4 Litri/ora). Per il calcolo della dimensione delle gocce è stato preso come riferimento una grandezza caratteristica della colonna nota e rapportata al diametro delle gocce. I diametri sono indicati in tabella 7.3 (pagina 36). In accordo con gli studi di Laso (1986) e Kentish (1997), per avere una buona dispersione statistica devono essere considerate almeno 300 gocce. Infine, il campione prelevato in testa (ingresso fase continua) e i tre campioni prelevati dalle porte laterali hanno permesso di avere un'idea di come la concentrazione sia distribuita lungo l'unità estrattiva. Nella Tabella 7.4 (pagina 36) è elencato il salto di concentrazione misurato nelle diverse prove. Si può notare che all'aumentare dell'agitazione e portata, il salto di concentrazione tende ad aumentare.

Per valutare il miglior set di correlazioni trovate in letteratura inizialmente è stato fatto uno studio di sensibilità dei parametri in considerazione. Valutando il rapporto incrementale dell'NTS calcolato in funzione della variazione dei parametri dell'equazione 4.6, è stato possibile definire un ordine di sensibilità dei parametri. (Figura 8.1 pagina 39). Si può notare che il coefficiente di dispersione assiale della fase continua ha una sensibilità molto bassa rispetto agli altri parametri. In base a questo primo risultato, per descrivere la dispersione

assiale della fase continua viene scelta direttamente la correlazione di Steinmetz (2007), un'equazione sviluppata per la colonna Kuhni DN32. Non avendo fatto test specifici per il trasporto di materia, viene fissata la correlazione di Kumar e Hartland (1999) per le due fasi. Infatti le correlazioni sviluppate per il trasferimento di materia di norma hanno un buon grado di accuratezza. L'equazione di Kumar e Hartland (1999) risulta essere applicata su una serie di dati sperimentali raccolti e può essere utilizzata per una vasta gamma di colonne d'estrazione.

Per la valutazione dell'hold-up sono stati analizzati due metodi differenti. Il primo metodo, empirico, prevede l'uso di correlazioni derivanti sperimentalmente per il calcolo diretto dell'hold-up. Il secondo metodo, seguendo un approccio fisico, permette di determinare l'hold-up medio sulla base del diametro di Sauter e della velocità relativa delle gocce nella colonna. Il primo metodo utilizza un'equazione empirica derivante dallo studio di Kumar e Hartland (1995) basata su un numero elevato di esperimenti condotti a diverse condizioni operative. L'equazione è formata da una serie di gruppi adimensionali elevati a potenza da un coefficiente ottenuto dal fitting sperimentale. Basandosi su un numero elevato di dati sperimentali, su tipi di colonne e su diversi sistemi liquidi, ha permesso di diventare una delle correlazioni predittive più interessanti, in quanto assicura, nel range studiato dagli autori, basse deviazioni rispetto ai dati sperimentali. In Figura 8.2 (pagina 38) è mostrato il *parity plot* che mette a confronto l'hold-up calcolato sperimentalmente con quello predetto dalla correlazione. La deviazione, molto alta, è di circa il 40%. Modificando la correlazione di Kumar e Hartand (1995) indicata in tabella 8.2 (pagina 41), ha permesso di ottenere un buon accordo con i valori sperimentali, malgrado limiti l'applicazione solo al range studiato. La figura 8.3 (pagina 39) compara i dati sperimentali con l'equazione modificata. Nel secondo metodo, o metodo fisico, per risalire all'hold-up si ricorre a delle equazioni che descrivono la velocità con cui le gocce si muovono lungo i compartimenti. Secondo la definizione dettata dalla prima ipotesi del modello sviluppato, è possibile definire una velocità relativa o *relative slip velocity* della particella, definita dall'equazione (1):

$$v_{rs} = \frac{v_d}{\varphi} + \frac{v_c}{(1-\varphi)} \tag{3}$$

Dove $v_d$ e $v_c$ rappresentano le velocità superficiali (espresse in maniera assoluta) della fase dispersa e della fase continua. La velocità relativa per una singola goccia può essere inoltre calcolata a partire dalla velocità terminale, tenendo conto dell'effetto del rallentamento dei compartimenti e dell'interazione con le altre gocce detto effetto di sciame o di *swarm* (si veda sezione 5.3) (equazione 2).

$$v_{rs} = u_t k_v (1-\varphi)^m = u_k (1-\varphi)^m \tag{4}$$

A partire dal diametro equivalente delle gocce della fase dispersa e sapendo le equazioni 1 e 2, è stato sviluppato un sistema iterativo che permette di determinare l'hold-up (Figura 8.6 pagina 42). Questo approccio "fisico" ha una potenzialità elevata perché permette di svincolarsi dalle equazioni empiriche frutto di *fitting* sperimentali e di legare l'hold a correlazioni idrodinamiche più generali. Il metodo fisico offre questo grande vantaggio, ma i risultati si mostrano essere inaccurati e per certi valori non è assicurata la convergenza (figura 8.7 e figura 8.8 pagina 43). Modificando la correlazione del fattore di rallentamento di Fang

(Fang *et al.* 1995) è stato possibile ottenere un accordo soddisfacente tra i dati sperimentali e di predizione del modello (figura 8.9 pagina 43).

Per il diametro di Sauter, in letteratura sono state trovate due correlazioni empiriche: Kumar and Hartland 1996 e Fisher (1973). I modelli presentati nel *parity plo*t in figura 8.4 (pagina 40) mostrano una deviazione inferiore al 20% con uno stesso grado di accuratezza rispetto ai risultati sperimentali. In questo caso viene scelta la correlazione di Kumar e Hartland (1996) in quanto, differentemente dalla correlazione di Fisher, non dipende dall'hold-up.

La determinazione della miglior correlazione del coefficiente di dispersione assiale della fase dispersa è avvenuta valutando la minor deviazione dell'NTS sperimentale rispetto all'NTS ricavato dalle simulazioni. L'NTS viene calcolato inserendo nel simulatore il diametro sperimentale, l'hold-up sperimentale, mentre per il coefficiente di dispersione della fase continua e del coefficiente di trasferimento di materia sono state usate le correlazioni scelte precedentemente. Ogni correlazione della fase dispersa disponibile viene testata ed è calcolata la deviazione percentuale dall'NTS sperimentale. In figura 8.1 (pagina 44) si riporta l'andamento dell'errore dall'NTS sperimentale per le quattro correlazioni della fase dispersa. Il risultato mostra che la correlazione di Bauer (1976) offre il miglior accordo, confermando inoltre il risultato ottenuto da Hlawitschka (2013).

Le correlazioni prese in esame sono state analizzate, dove possibile, singolarmente. In questa ultima fase tutte le correlazioni verranno implementate nel simulatore per valutare la performance in termini di NTS. Inoltre, essendo l'hold-up e il diametro dei parametri importanti, si confronteranno anch'essi con i risultati sperimentali raccolti. Sono stati selezionati due possibili scenari composti da *set* di correlazioni distinte. La differenza principale tra i due è la scelta del metodo di calcolo dell'hold-up in quanto nello scenario 1 viene preso in considerazione il metodo implicito, mentre nello scenario 2 viene scelto la correlazione empirica di Kumar e Hartland (1995). In figura 8.3 (pagina 41) sono riportate in dettaglio le correlazioni scelte per i due scenari. Inoltre, in modo da avere una gamma di simulazioni che possano mostrare il comportamento di ogni singola correlazione sui risultati finali, per ogni scenario le tre correlazioni scelte sono state inserite e non modificate, in modo da avere nove risultati ampiamente confrontabili. Avendo fissato la correlazione del coefficiente del mass transfer di Kumar e Hartland (1999) e quella di Steinmetz (2007), rimangono libere le correlazioni dell'hold-up, del diametro medio e del coefficiente di dispersione assiale della fase dispersa. Queste correlazioni verranno utilizzate sia originali, sia modificate in diversa combinazione tra di loro (figura 8.6 pagina 45). I criteri generali per la miglior scelta di equazione sono:

- Grado di modifica. Il set deve avere un risultato accurato con il minor numero di equazioni modificate;
- Grado di errore. È necessario scegliere il set di correlazioni che dia una deviazione limitata rispetto ai dati sperimentali.

I risultati delle simulazioni sono stati riportati nei diagrammi a barre in figura 8.11 (pagina 46) e in figura 8.12 (pagina 46). Lo scenario preso in considerazione è il secondo, nonostante mostri una deviazione di circa 38% sull'hold-up, la deviazione riferita all'NTS è di poco inferiore al 10%.

Le correlazioni scelte sono quelle non modificate, in quanto la loro modifica fa perdere la validità al di fuori delle condizioni studiate. Stando ai criteri di valutazione definiti, in tabella 2 sono riportati le correlazioni scelte.

**Tabella 2:** Correlazioni scelte per il modello dispersivo (tabella 8.7 pagina 46)

| Hold-up | Diametro equivalente | Dispersione assiale (continua) | Dispersione assiale (dispersa) | Coefficiente di scambio di materia |
|---|---|---|---|---|
| Kumar and Hartland (1995) | Kumar and Hartland (1996) | Steinmetz (2007) (1) | Bauer (1976) | Kumar and Hartland (1999) |

I grafici mostrati in figura 7 e nelle figure 8.15, 8.16 e 8.17 (pagina 48) riportano in ascisse la concentrazione di acetone (soluto) nella fase continua (acquosa) e in ordinate la concentrazione di acetone nella fase dispersa organica. Il grafico mostra l'andamento della coppia di punti (concentrazione) lungo la colonna e mostra la presenza della dispersione assiale sia della fase continua che nella fase dispersa. La curva arancione mostra l'andamento della retta di equilibrio, valore termodinamico che indica l'equilibrio tra le due fasi. La retta nera indica la linea del bilancio di massa. La retta blu, quella del modello della dispersione. I punti sperimentali (3 campioni, punto estratto, raffinato, e salto di concentrazione) si trovano in accordo con il modello analizzato con basse deviazioni. Nella tabella 3 sono indicati i principali risultati per lo scenario scelto.

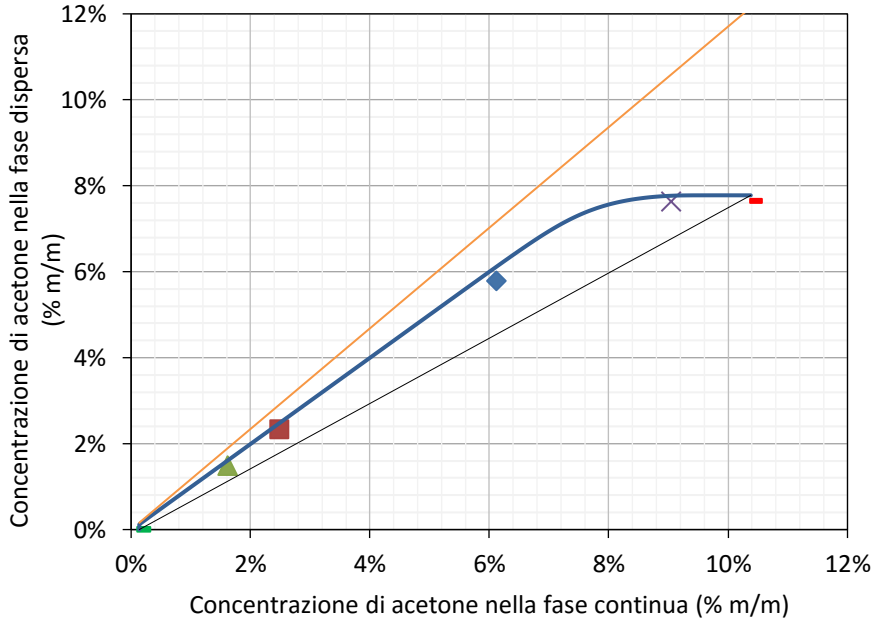


**Figura 7:** Modello dispersivo e punti sperimentali per la prova D185-177 (8.13 pagina 47).
♦Campione 1, □ Campione 3, Δ Campione 4, — estratto, – raffinato, x salto di concentrazione all'ingresso della fase continua

Si può quindi affermare che la descrizione con un modello a dispersione della colonna Kuhni DN32 permette di ottenere un buon risultato in termini di performance. Il modello a pistone puro, in questo caso, non avrebbe assicurato una descrizione efficace. Anche in una colonna di queste dimensioni ridotte, i fenomeni dispersivi non sono trascurabili. Questo risultato mostra come un modello semplice, come quello dispersivo, possa essere in grado di descrivere le performance di estrattore con un certo grado di precisione.

**Tabella 3:** Modello dispersivo e parametri sperimentali in confronto

| N° Test | Hold up % | | Diametro medio (mm) | | Numero di stadi teorici | |
|---|---|---|---|---|---|---|
| | Valore sperimentale | Valore predetto | Valore sperimentale | Valore predetto | Valore sperimentale | Valore predetto |
| D185-177 | 14.9 | 22.6 | 0.97 | 0.69 | 9.5 | 8.9 |
| D185-178 | 14.8 | 22.4 | 0.81 | 0.59 | 10.3 | 9.0 |
| D185-179 | 9.3 | 17.2 | 0.51 | 0.48 | 8.1 | 8.5 |
| D185-180 | 13.1 | 20.0 | 0.50 | 0.46 | 6.6 | 7.1 |

La seconda parte dello stage ha avuto come scopo l'applicazione del modello dispersivo con il set di correlazioni scelto precedentemente. Nel caso reale, il sistema diventa più complesso perché si ha la presenza diversi soluti, ma anche perché il grado di ripartizione di una o più specie chimiche può influenzare la ripartizione nelle fasi degli altri soluti e quindi il trasferimento di materia. Uno studio precedente a questo lavoro basato su analisi cromatografiche condotti ha permesso di sviluppare una correlazione tra il coefficiente di ripartizione e la concentrazione dei solventi nelle due fasi equazione 6 (equazione 9.2). L'equazione differenziale (eq. 5) invece tiene conto dell'effetto della variazione di velocità superficiale locale causato dalla variazione della densità delle fasi.

$$\begin{cases} (1-\varphi)\dfrac{dC_{c,i}}{dt} = D_{axc,i}\dfrac{d^2C_{c,i}}{dz^2} - \dfrac{d(v_c \cdot C_{c,i})}{dz} - k_{Oc}a\left(C_{c,i} - C^*_{c,i}\right) - R_{i,c} \\ \varphi\dfrac{dC_{d,i}}{dt} = D_{axd,i}\dfrac{d^2C_{d,i}}{dz^2} + \dfrac{d(v_d \cdot C_{d,i})}{dz} + k_{Oc}a\left(C_{c,i} - C^*_{c,i}\right) - R_{i,d} \end{cases} \quad (5)$$

dove il coefficiente globale di scambio risulta correlato al coefficiente di ripartizione:

$$\frac{1}{\mathrm{k_{OV,c}}} = \frac{1}{\mathrm{k_c}} + \frac{1}{\mathrm{mk_d}} \quad (6)$$

con m coefficiente di ripartizione definito dal modello sperimentale (7):

$$\mathrm{m}^{\frac{aq}{org}} = m_i^0\left(m_i^{min} + (1 - m_i^{min})\exp(-\frac{T}{\tau})\right) \quad (7)$$

e il parametro T, dipendente dalla quantità locale dei componenti A, B ed E (8):

$$\mathrm{T} = \frac{m_A + m_B}{m_E} \quad (8)$$

Come già detto, nel caso del controlavaggio bisogna tenere conto anche della presenza della reazione chimica. In questo caso la simulazione analitica del modello dispersivo non risulta

applicabile, e per determinare l'efficienza di estrazione è stato utilizzato un risolutore sviluppato su Fortran (IFP 2016-2017) che permette di risolvere una serie di sistemi di equazioni differenziali riportato dall'equazione 5. Il risolutore Fortran prevede l'inserimento dei dati input tramite un foglio di testo di formato .txt, che fa risultare scomoda l'esecuzione delle simulazioni. Per questo motivo, è stata sviluppata un'interfaccia grafica su un foglio Excel che permette di selezionare le diverse portate in input, di lanciare la simulazione e di raccogliere i dati in output direttamente sul foglio di calcolo. Inserendo l'alimentazione e la sua composizione, il foglio calcola direttamente le proprietà fisiche dell'input (grazie ad una banca dati di sostanze pure caricata) e in base alle condizioni operative e geometriche calcola il valore delle correlazioni scelte. Tramite una macro sviluppata in VBA, i parametri e gli altri input verranno implementati sul risolutore. Il foglio permette quindi di lavorare in un ambiente *user friendly* e di sfruttare appieno le potenzialità del risolutore sviluppato in Fortran.

Utilizzando il risolutore, sono stati presi in considerazione due esperimenti condotti nella colonna in modalità "lavaggio" (IFP 2016). Si riportano quindi le efficienze di separazione delle diverse sostanze presenti nell'alimentazione (Figure 9.3 e 9.4 pagina 53). Nel primo caso, per la maggior parte delle specie chimiche si ha una deviazione tra sperimentale e calcolato inferiore al 10%. Una deviazione maggiore è mostrata per il componente J, con un valore di oltre 15%. Nella seconda simulazione, le specie chimiche L, N e J mostrano delle deviazioni anomale.

Le simulazioni per il caso di contro lavaggio sono riportate nelle figure 9.5 e 9.6 (pagina 55). L'obiettivo principale del *back-washing* è di ridurre la perdita di reagenti sotto forma della molecola "G", presente nell'estratto uscente dal washing. Nel primo *parity plot* si riporta in ascisse l'efficienza di separazione della molecola G sperimentale, in ordinate l'efficienza predetta dal modello. Come si può notare, il simulatore risponde bene ai dati sperimentali, con una deviazione media inferiore al 10%. Sono però presenti tre simulazioni che mostrano una discrepanza non banale con i dati sperimentali. Attualmente non è stato verificato il motivo di tale comportamento anomalo.

## Conclusioni

In questo lavoro si è sviluppato un modello matematico che possa descrivere una colonna di estrazione liquido-liquido. Il progetto di sviluppo di un'estrazione chimica di una colonna Kuhni da un caso reale multicomponente, è stato studiato per un sistema standard ternario. È stato confermato matematicamente e sperimentalmente che in una colonna Kuhni DN32 l'effetto della dispersione assiale non può essere trascurato, e dunque l'approccio matematico utilizzando il modello a pistone (PFR) risulta limitante. Invece, il modello dispersivo, che tiene conto degli effetti idrodinamici che deviano dall'idealità del pistone attraverso un flusso di dispersione assiale continua e dispersa, offre, utilizzando un set di correlazioni disponibili in letteratura, un risultato con un buon grado di accuratezza. Il risultato in termini di performance nel caso di uno standard ternario come utilizzato nella parte sperimentale è molto positivo. Il set di correlazioni è costituito da Kumar e Hartland (1995) per l'hold up, Kumar e Hartland (1996) per le gocce, Kumar e Hartland (1999) per i coefficienti di trasferimento di massa, Bauer (1976) per la dispersione assiale nella fase dispersa e Steinmetz (2007) per la dispersione assiale nella fase continua. Per quanto il risultato sulla predizione dei numeri degli stadi teorici (NTS) sia buono, sono state ottenute delle deviazioni nell'ordine del 35% sull'hold-up e del 18% sul diametro medio equivalente. Alcuni possibili errori di misura possono aver influenzato questi risultati, specialmente per il metodo fotografico, in quanto

non è stato preso in considerazione l'effetto ottico della variazione della dimensioni causata dalla curvatura della colonna cilindrica.

È stato possibile confrontare i dati sperimentali sul sistema reale, nel caso dell'applicazione di un'operazione di lavaggio, con il modello dispersivo implementato in un programma di linguaggio Fortran. L'estrazione nella fase di lavaggio, sotto controllo di trasferimento di massa, risulta molto sensibile alle variazioni di tensioni interfacciale e anche al coefficiente di ripartizione. I risultati nella prima prova simulata mostrano una discreta concordanza rispetto ai dati sperimentali. Nel secondo test invece, i risultati sembrano avere delle deviazioni e in certi casi l'errore risulta anomalo. I principali problemi sono legati alla difficoltà di stimare i coefficienti di ripartizione, alle proprietà fisiche variabili lungo la colonna (specialmente la tensione interfacciale che influisce molto sui parametri idrodinamici come l'hold-up e il diametro delle gocce), alle correlazioni scelte ed errori dovuti all'operazione sperimentale. Comunque, trattandosi di un sistema molto complicato, questo semplice modello matematico offre, rispetto ai dati sperimentali, una buona risposta.

L'applicazione al caso del controlavaggio, è stata presa in considerazione l'estrazione del componente G. Il modello risponde bene ai dati sperimentali, fuorché tre prove che mostrano una deviazione anomala. Studi futuri permetteranno di approfondire e capire la natura di tali errori. La cinetica risulta controllante in quanto le portate volumetriche sono molto basse e si hanno quindi alti tempi di residenza. Le costanti cinetiche e i coefficienti di ripartizione ricavati sperimentalmente mostrano un'alta sensibilità al sistema studiato, mentre risultano meno sensibili, l'hold up, diametro equivalente e gli altri parametri del modello dispersivo.

In conclusione, si può dire che, per quanto in certi casi il modello applicato al caso reale mostri alcune deviazioni (errori che sono frutto di una serie di cause che possono non essere ricondotte al modello stesso), il modello offre dei risultati soddisfacenti e ogni simulazione richiede un tempo computazionale molto ridotto (nell'ordine della decina di secondi). Il modello pseudo omogeneo dispersivo, non considera l'effetto della polidispersione delle gocce. Associando un modello di bilancio di popolazione al modello dispersivo, tenendo conto degli effetti di rottura, e di coalescenza delle gocce è possibile ottenere un risultato decisamente più accurato, non solo in termini di rese di estrazioni calcolate, ma anche da un punto di vista idrodinamico. Infatti tenendo conto della "storia" di ogni goccia, descrivendone la nascita e la morte in funzione delle condizioni operative e delle proprietà del sistema locale è possibile stimare l'andamento della distribuzione delle dimensioni delle gocce e quindi dell'hold-up lungo la colonna. I modelli dispersivi associati al bilancio di popolazione richiedono tempi computazionali maggiori, nell'ordine della decina di minuti (Bunchbender 2012). Sono stati ottenuti dei risultati molto precisi abbinando il bilancio di popolazione a programmi di fluidodinamica computazionale CFD-BPM, che sono in grado di descrivere non solo la polidispersione delle gocce, ma anche l'interazione turbolenta dello *swarm* della dispersione che si crea interagendo con la particolare geometria del compartimento della colonna (Hlawitschka 2013). Questi strumenti sono quindi utili non solo per avere una descrizione precisa di ogni singolo aspetto del sistema e di avere una funzione di supporto al processo in sviluppo, ma anche per permettere una riduzione dei costi e dei tempi sperimentali, sebbene la trattazione matematica sia molto più complessa e richieda un tempo computazionale che può arrivare nell'ordine delle settimane.

# Table of contents

Riassunto in Italiano ..... i
Table of contents ..... xix
List of tables ..... xx
List of figures ..... xxi
List of symbols: ..... xxiii
List of greek symbols: ..... xxiv
List of dimensionless symbols: ..... xxiv
List of subscripts ..... xxv
1 Introduction ..... 1
2 Bio-sourced process ..... 3
3 Kuhni Miniplant extractor ..... 5
4 Model description ..... 9
4.1 General statements and hypothesis ..... 9
4.2 Plug flow ..... 12
4.3 Dispersion model ..... 14
5 Set of correlation ..... 17
5.1 Hold Up ..... 17
5.1.1 Empirical equation ..... 17
5.2 Droplet size ..... 19
5.2.1 Empirical correlation of d32 ..... 19
5.3 Implicit method for d32 and hold up ..... 20
5.3.1 Terminal velocity model ..... 21
5.3.2 Slowing factors and swarm coefficient ..... 23
5.4 Mass transfer coefficient ..... 24
5.5 Axial dispersion ..... 26
5.5.1 Axial dispersion of the continuous phase ..... 26
5.5.2 Axial dispersion of the dispersed phase ..... 27
6 Experiments ..... 29
6.1 Hydrodynamic ..... 29
6.2 Mass transfer experimentation ..... 31
7 Experimental results ..... 33
7.1 Hydrodynamic ..... 33
7.2 Mass transfer analysis ..... 35
8 Post processing and model comparison ..... 37
8.1 Hold up and Sauter mean diameter direct method ..... 38
8.1.1 Hold up ..... 38
8.1.2 Sauter mean diameter direct method ..... 39
8.2 Hold up and Sauter mean diameter physical method ..... 41
8.2.1 Hold up and Sauter mean diameter implicit method ..... 41
8.3 Dispersed axial coefficient correlation ..... 44
8.4 Correlation comparison ..... 44

8.5 Final result ..... 46
9 Axial dispersion 1D model applied to real system ..... 51
9.1 Comparison between two models ..... 51
9.1.1 Analytical extraction vs numerical extraction ..... 52
9.1.2 Analytical vs numerical plug flow reactor ..... 52
9.2 Real system extraction ..... 53
9.2.1 Washing zone - Extraction ..... 53
9.2.2 Back washing zone – Extraction with reaction ..... 54
10 Conclusion ..... 57
Bibliography ..... 59
Ringraziamenti ..... 62
Appendix 1: PID Kuhni DN32 ..... i
Appendix 2: 1D Dispersion model analytical solution ..... ii
Appendix 3: Henshke's model for terminal velocity ..... v
Appendix 4: Experiments ..... vi

## List of tables

Table 3.1: Main characteristics of the Kuhni miniplant (Sulzer®) ..... 7
Table 5.1: Values of Constants of $C_{\Pi}$ $C_{\Psi}$ $C_{\Gamma}$, and Indexes n1-n7 for Kuhni Columns and unified columns proposed by Kumar and Hartland (1995) ..... 18
Table 5.2: Constants used for the Fisher's drop size model for different Authors ..... 19
Table 5.3: Values of Parameters in Kumar and Hartland's equation (1996) for Kuhni (mechanically agitated columns) ..... 20
Table 5.4: Values of constant in Kumar and Hartland mass transfer equation ..... 26
Table 5.5: Constants of equation for axial dispersion coefficient derived experimentally ..... 27
Table 6.1: Physical proprieties of the studied systems at 20°C (Misek et al. 1985) ..... 29
Table 7.1: Operating condition for the experimental tests ..... 35
Table 7.2: Main results of the tests at steady state ..... 35
Table 7.3: Sauter mean diameter and NTS obtained by experimentation ..... 36
Table 7.4: Concentration jump at the inlet of the continuous phase ..... 36
Table 8.1: Constant value and operating condition for modified Kumar Hartland's hold up correlation ..... 39
Table 8.2: Constant values and operating condition for modified Kumar Hartland's correlation ..... 41
Table 8.3: Different scenarios for Hold up evaluation ..... 41
Table 8.4: Parameters chosen for Dax,d evaluation ..... 44
Table 8.5: Two different scenarios chosen ..... 45
Table 8.6: Nine simulations for each scenario. Code is the name ..... 45
Table 8.7: Final set of correlation chosen ..... 46
Table 8.8: Hold up droplet size and NTS experimental/ predicted ..... 49

## List of figures

Figure 2.1: Two steps of the process reaction ..... 3
Figure 2.2: Global reaction ..... 3
Figure 2.3: G equilibrium reaction ..... 4
Figure 2.4: Washing and back-washing scheme ..... 4
Figure 3.1: Kuhni Miniplant scheme (a) and photo of the unit (b) ..... 6
Figure 3.2: Principal geometrical characteristics dimension of the column ..... 6
Figure 4.1: Detailed scheme (a) and model scheme (b) of a Kuhni compartment ..... 9
Figure 4.2: Plug flow model and axial dispersion model comparison ..... 10
Figure 4.3: NTS required for a plug flow without dispersion (a) and with dispersion (b) extraction operation ..... 11
Figure 4.4: Axial dispersion coefficients evolution in funt to impeller speed ..... 11
Figure 4.5: Plug flow local matter balance scheme ..... 13
Figure 4.6: Plug flow with axial dispersion matter balance scheme ..... 15
Figure 5.1: Droplet in an unhindered system(a), Slowing effects due the internals and the rotation (b) and Effect of swarm interaction on a particle (c) ..... 21
Figure 5.2: Terminal velocity in function to the particle diameter for rigid sphere (dotted line) and real particles (continuous line). (Garthe 2006) ..... 22
Figure 5.3: Double film layer theory (Hlawitschka 2013) ..... 24
Figure 6.1: Flooding and operational curve in function of the total flow rate ..... 30
Figure 6.2: Kuhni DN32 column with the red Sudan dye in the dispersed phase ..... 31
Figure 7.1: Fast sampling method hold up for several experimental tests ..... 33
Figure 7.2: Shut down method hold up chart and flooding line (30%) for several experimental tests ..... 33
Figure 7.3: Shut down and fast sampling method comparison ..... 34
Figure 7.4: Flooding curve for Kuhni Column E/R=1.5 e=20% Water/Butyl-Acetate/Acetone system (shut down method) ..... 34
Figure 8.1: Sensitivity study of the five parameters of the dispersion model ..... 37
Figure 8.2: Parity plot of hold-up obtained by correlation of Kumar and Hartland (1995) and experimental values, using shut down method for two cases E/R 1.5 and 2.5 ..... 38
Figure 8.3: Parity plot of experimental hold up (shut down method) versus modified Kumar and Hartland's (1995) correlation with a 40% of deviation (dotted line) ..... 39
Figure 8.4: Parity plot of experimental diameter (photographic method) versus three different correlations and the deviation of 25% (dotted line) ..... 40
Figure 8.5: Parity plot of experimental diameter (photographic method) versus Kumar and Hartland's original correlation and Kumar and Hartland's modified correlation ..... 40
Figure 8.6: Iterative scheme for hold-up evaluation with a "physical" approach ..... 42
Figure 8.7: Parity plot of Scenario 1 (Vignes, Steinmetz, Godfrey and Slater) by using implicit method ..... 42

Figure 8.8: Parity plot of Scenario 2 (Vignes, Fang, Godfrey and Slater) by using implicit method ..... 43
Figure 8.9: Parity plot of Scenario 2 (Vignes, Fang modified, Godfrey and Slater) by using implicit method ..... 43
Figure 8.10: NTS Experimental deviation for several Dax,d correlation ..... 44
Figure 8.11: Scenario 1, Implicit method for hold up, Bauer and Kumar and Hartland (1996) for d32 ..... 46
Figure 8.12: Scenario 2, Kumar and Hartland for hold up, Bauer and Kumar and Hartland (1996) for d32 ..... 46
Figure 8.13: D185-177 model and experimental values concentration plot comparison. E/R=1.5, Q=10.7 L/h and N=396 rpm. ..... 47
Figure 8.14: D185-177 raffinate concentration model/experiment zoomed near the raffinate outlet ..... 47
Figure 8.15: D185-178 model and experimental values concentration plot comparison. E/R=1.5, Q=8.3 L/h and N=440 rpm. ..... 48
Figure 8.16: D85-179 model and experimental values concentration plot comparison E/R=1.5, Q=4.2 L/h and N=517 rpm ..... 48
Figure 8.17: D180 model and experimental values concentration plot comparison. E/R=2.5, Q=4.3 L/h and N=513 rpm ..... 49
Figure 9.1: Numerical and analytical solution comparison for a 1D dispersion extraction problem ..... 52
Figure 9.2: Numerical (Num, dotted line) and analytical (an, continuos line) solution comparison for a PFR 2A+B→C reaction problem. Plot of concentration of species in function of the length of the reactor ..... 52
Figure 9.3: D185-26 Experimental test efficiency comparison ..... 53
Figure 9.4: D185-27 Experimental test efficiency comparison ..... 53
Figure 9.5: Parity plot of G's separation efficiency between the experimental values (x-axis) and the model prediction (y-axis) ..... 54
Figure 9.6: G's efficiency of separation for different operating condition ..... 55

## List of symbols

| Symbol | Unit | Definition |
|---|---|---|
| a | [$m^2$/ $m^3$] | Specific area |
| C | [$kg/m^3$] | Mass concentration |
| d | [m] | Droplet diameter |
| $d_{32}$ | [m] | Sauter mean diameter |
| $D_{ax}$ | [$m^2/s$] | Dispersion coefficient |
| D | [m/s] | Diffusion coefficient |
| $D_{Col}$ | [m] | Column diameter |
| $D_R$ | [m] | Rotor diameter |
| $D_S$ | [m] | Stator diameter |
| e | [ad] | Stator free area |
| E | [ad] | Extraction factor |
| E/R | [ad] | Extract raffinate ratio |
| g | [$m/s^2$] | Acceleration gravitational |
| H | [m] | Column height |
| $H_C$ | [m] | Compartment Height |
| k | [m/s] | Mass transfer coefficient |
| $K_v$ | [ad] | Slowing factor |
| L | [m] | Characteristic length |
| m | [ad] | Swarm coefficient |
| $\dot{m}$ | [kg/s] | Mass flow rate |
| n | [#] | Number of particles/droplets |
| $n_c$ | [ad] | Number of compartments |
| N | [1/s] | Impeller speed |
| NTS | [ad] | Number of theoretical stages |
| P | [W] | Power |
| S | [$m^2$] | Surface area |
| u | [m/s] | Velocity or Interstitial velocity |
| $u_{rs}$ $u_{slip}$ | [m/s] | Slip velocity or relative swarm velocity |
| v | [m/s] | Superficial velocity |
| V | [$m^3$] | Volume |
| $\dot{V}$ | [$m^3/s$] | Volumetric flow rate |

| | | |
|---|---|---|
| x | [ad] | Fraction of transferred component in continuous phase |
| y | [ad] | Fraction of transferred component in dispersed phase |

## List of greek symbols

| Symbol | Unit | Definition |
|---|---|---|
| $\delta_c$ | [m] | film layer thickness |
| ρ | [kg/m$^3$] | density |
| φ | [ad] | dispersed phase hold up |
| Ψ/ϵ | [W/kg] | mechanical power dissipation |
| μ | [Pa s] | viscosity |
| μ$^*$ | [ad] | viscosity ratio (dispersed/continuous) |
| σ | [N/m] | interfacial tension |

## List of dimensionless symbols

| Symbol | Definition |
|---|---|
| $\mathrm{Re_R} = \mathrm{d_R^2 \rho_c N/\mu_c}$ | impeller Reynolds number |
| $\mathrm{Re_d} = \mathrm{d_{32} \rho_d u_d/\mu_d}$ | dispersed-phase Reynolds number |
| $\mathrm{Re_p} = \mathrm{d_{32} \rho_c u_{slip}/\mu_c}$ | droplet Reynolds number |
| $\mathrm{Re_c} = \mathrm{d_{32} \rho_c u_c/\mu_c}$ | continuous-phase Reynolds number |
| $\mathrm{Re_T} = \mathrm{d_{32} \rho_c u_t/\mu_c}$ | terminal velocity droplet Reynolds number |
| $\mathrm{We_R} = \mathrm{d_R^3 \rho_c N^2/\sigma}$ | stirrer Weber number |
| $\mathrm{Sh_c} = \mathrm{d_{32} k_c/D_c}$ | continuous Sherwood number |
| $\mathrm{Sh_d} = \mathrm{d_{32} k_d/D_d}$ | dispersed Sherwood number |
| $\mathrm{Sc_c} = \mathrm{\rho_c/\mu_c D_c}$ | continuous Schimdt number |
| $\mathrm{Sc_d} = \mathrm{\rho_d/\mu_d D_d}$ | Schimdt number |
| $\mathrm{Bo} = vH/Dax$ | Bodestein number |
| $\mathrm{Pe_c} = \mathrm{d_{32} u_{slip}/D_c}$ | continuous-phase Peclet number |
| $\mathrm{Np} = \mathrm{P}/D_R^5 \rho_c N^3$ | modified newton number |
| $\mathbf{P} = \mathrm{\rho_c^2 \sigma^4/g \Delta \rho \mu_c^4}$ | hydrodynamic number |
| $\mathrm{Ar} = \mathrm{d_p^3 g \rho_c \Delta \rho/{\mu_c}^2}$ | Archimede number |

$Np = 1.08 + 10.94/Re_R^{0.5} + 257.37/Re_R^{1.5}$ Kumar and Hartland's power number

## List of subscripts

| Symbol | Definition |
|---|---|
| ace | acetone |
| col | column |
| c | continuous |
| d | dispersed |
| 32 | Sauter mean |
| R | rotor |
| S | stator |
| mas | massic units |
| p | particle |
| ac | aqueous |
| org | organic |
| col | column |
| k | characteristic |
| exp | experiment |
| ov | overall |
| vol | volumetric units |
| x | aqueous |
| y | organic |

# 1 Introduction

The design of new bio-sourced processes is a typical task for a chemical engineer. The development of a biological way to produce chemicals and fuels which can compete into a well-established market, represents a challenge but also a possibility to open into a new era of sustainable chemical industry.

A process leads the production of a chemical by reactants bio sourced. This alternative process is very interesting not only for an economical point of view but also for the development of a "green" way. A reaction needs to assure a good conversion of the reactants, which will follow a separation from the key product and a recovery of unconverted species. Due to the presence of several chemical species inside the stream, recovery process can't be performed properly by distillation. Another kind of operation unit has been tested. Liquid-liquid extraction technique has been taken under consideration, in order to recover the unconverted reactants without a large impact to the final plant cost.

Liquid-liquid extraction (LLE) is a classical unit operation in the chemical industry. Liquid extraction performs separation basing on the different solubility of compounds into two immiscible liquids. A solution feed, composed by a diluent and a solute, is brought in contact to a high solute affinity solvent, causing its transport, depleting the feed and enriching the solvent. So, taking advantage from the different affinity of a solute in two immiscible solvents, it's possible to develop a unit operation that can be applied widely in the chemical industry. Liquid-liquid extraction doesn't require directly a large amount of heat/energy, because its driving force is related to the difference of the solute solubility. However, this process is applied when distillation is impracticable and anti-economical to use. Extraction can be found in different industrial fields such as metallurgy, nuclear processing, chemical and petroleum up to environmental and pharmaceutical engineering and biotechnological applications.

A feasibility study has allowed to verify the possible application of LLE to the given process by using a Kuhni Column DN32 miniplant unit (Unit D0185). The DN32 pilot is an agitated countercurrent column with high performances and low throughput. It's often used for scaling column with diameter up to 100 mm. After a first characterization of the pilot, for evaluating the hydrodynamics, flooding curves and performances has been evaluated. The goal of this extraction unit is to separate impurities from reactants (using a solvent) and perform a back-washing extraction to reconvert reactants from an inevitable equilibrium parasite reaction (using another solvent). In order to create washing and back washing zone of extraction, Kuhni column has set up in series with a packed column. The experiment with a real system and a synthetic system has been conducted with Kuhni and Packed tower and for washing and back-washing, optimal operational conditions have been determined.

One of the principal purpose of the project is to find the best operational condition of the units obtaining good separation efficiencies limiting solvent consumption, minimizing the capital investment and the operating cost as result. In order to know performances and solvent consumption for a wide range of operational conditions, it's possible to develop a mathematical model that can predict the efficiency of separation. The aim of this work is to find an easy way to describe an agitated countercurrent extraction column, developing a predictive model for its performances and hydrodynamics condition, related to the operating condition.

The project work has been divided into two parts. Liquid extraction standard systems are often used to test some units, due to the versatility and simplicity to treat them. Model has

been validated firstly for a standard system and hence extended to the real system. So, in the first part, that represents the core of this work, the research of a good mathematical model for describing a standard ternary system in different operating conditions has been done. Then, in the second part the results obtained allow a multicomponent real system description.

Previous studies have described the column by using a series of CSTR and plug flow model, but now, a new system view with one-dimensional dispersion model has been taken under consideration. In order to determine parameters included into the system of differential equation, correlations from literature have been investigated. Parameters are mathematical terms related to the geometry, operating condition and physical proprieties, that can be described by experimental correlations found in literature. Several correlations have been found in literature and to know a "predictive set" that can be used for describing the column. In order to choose the best set of correlation, ternary standard system experimental tests have been conducted.

The knowledge of a predictive set of correlation of the parameters concerned has allowed to extend the model to the real case study, in which the multicomponent system and chemical reaction make more difficult to predict it. Multicomponent system has to be described taking account of the effect of variation of distribution ratio for each component.

IFP's internal previous work have allowed to describe these phenomena and a study of kinetic of chemical reaction and a feasibility study has been done. By implementing this input into an interface based on Fortran, a mathematical subroutine provides the real results, that can be compared to the experimental test.

The first two chapters are dedicated to the "state of art" in order to explain the problems and the application. Model description and a list of several correlation has been done next. Experimental tests and post processing explain the experiment conducted, the operating condition and the treatment of data obtained. Furthermore, the choice of the best set has been described in the same chapters. Finally, the application of this in the case of washing and back washing has been explained.

# 2 Bio-sourced process

The aim of the green chemistry project is to develop a process for the production of a valuable chemical from a reactant, produced in a biotechnological way. The reaction takes part into two principal steps, is shown in Figure 2.1.

$$A \rightarrow B + D$$

$$A + B \rightarrow 2E + C$$

**Figure 2.1:** Two steps of the process reaction

A reaction concurs in the first step, where moles of A react to form B and D. In the second step, B reacts with A to form C, the key product, and E. Global reaction is shown in the Figure 2.2.

$$2A \rightarrow C + D + 2E$$

**Figure 2.2:** Global reaction

Furthermore, the inevitable presence of secondary reactions in each step, involves to lose a significant amount of the reactants, converted in unwanted by-products. A wide range of organic species have been found and identified but unlikely, the exact composition is unknown.

The development of a separation unit that separates final product from unconverted reactants and by-products, is one of most important goal for this process, because an optimized separation can reduce the operating cost of the entire process.

Two separation units has been developed:

- Key product separation unit (C);
- Unconverted reactants (A and B) and by products separation unit.

The first separation from the other substances is firstly obtained by distillation, that separates into two streams, the key product, sent to purification unit, and the unconverted and by-products sent to the next separation unit. It has been verified that distillation technique is not efficient to separate unconverted reactants from impurities, due a wide range of molecules which have disparate boiling temperatures. For this reason, liquid-liquid extraction unit operation has been taken under consideration for recovering unconverted reagents. In order to eliminate an important fraction of hydrophobic impurities, an apolar solvent has been used as solvent. The extraction unit has to treat a stream composed predominantly by B, E, A and very high number of by-products, sometimes in low concentrations.

During the process, the presence of a parasitic reaction consumes a part of unconverted reactants. This acid catalysed reaction is shown in Figure 2.3, where one mole of A reacts with B to form product F that reacts with another mole of Al forming one mole of G and E. F has a good affinity with apolar compounds (as the solvent used) and during the extraction process a large amount of F shifts to the organic phase. Overall, this phenomenon causes a loss of A and B, increasing the operational cost of the process. In order to regenerate them from F another EEL unit has been developed. It's possible to shift the equilibrium to left mixing extract (formed by the apolar solvent, G and impurities extracted) by using the solvent E and an acid. ELL unit will be divided into two parts:

- Washing zone, where the majorities of impurities are threated and separated by using the apolar solvent.
- Back-washing zone, where a reactive reaction recovering A and B.

$$A + B \leftrightarrow F$$

$$F + A \leftrightarrow G + E$$

**Figure 2.3:** G equilibrium reaction

Figure 2.4 shows a scheme of this extraction unit. The feed, mixed with the outlet from the backwashing zone, is sent to the first column (the washing column) where the extraction of the principal impurities occurs. Solvent (apolar S) allows the extraction process; a large quantity of by-products is separated. Hence, organic extract stream moves to the back-washing column where an extraction-reaction takes place. The raffinate, outlet of washing column, will be composed by A, B and residual of impurities, while the extract in outlet of back washing column, will be composed by Apolar solvent and the impurities extracted.

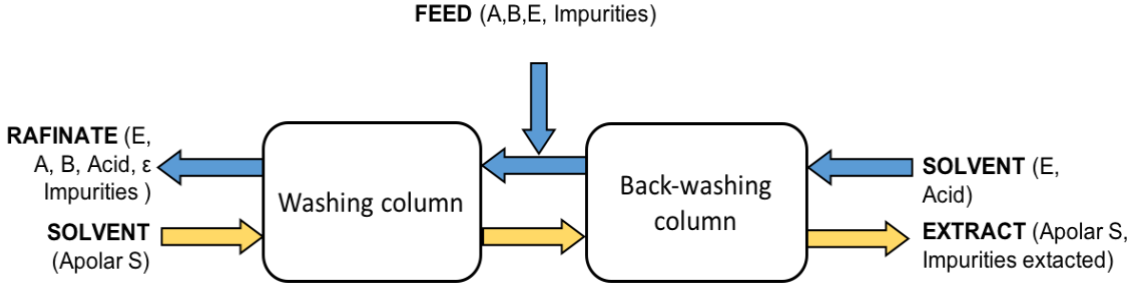


**Figure 2.4:** Washing and back-washing scheme

The objectives required for the liquid-liquid extraction operation unit has been reported as follows:

- extract from the extraction feed the maximum of apolar impurities, in particular the light ones that can accumulate into the process;

- minimize losses of unconverted reactants and recycling back in the reaction unit;

- minimize the Opex / Capex costs of this operation. This consists in particular of minimizing the flow rates of solvents, optimizing the design of the extractors.

These objectives can be performed developing a mathematical model in order to describe the intrinsic characteristics unit operation like mass transfer, hydrodynamic and figure out to the overall performance of extraction. Sometimes the complex behaviour of extraction is not easily to predict, complex geometry, variation of distribution ratio, local velocity and local physical proprieties (such as interfacial tension, density) can affect directly hydrodynamics and performance. Hence, the design of industrial extractor requires in addition to scale up procedure some laboratory and pilot investigations with the system concerned. In the design field, for estimating the height of the column, graphics method and simplified equations are used. For example, for staged column is common to use the number of theoretical stages method (NTS), and, for a differential contactor the HTU/NTU approach. For the first height estimation, these methods can provide a good result, but, these methods have been tested and the solutions weren't satisfactory (IFP 2015).

# 3 Kuhni Miniplant extractor

In the chemical field, countercurrent columns are often used. Overall, this kind of columns allow a good mass transfer, thanks to the high concentration gradient between the phases. Generally, they are gravimetric extractors, so for this reason the light phase is charged at the bottom the column, and the heavy phase to the top, in order to have an ascendant and descendant convective flow due the difference of density between two liquids. As already said, it's important make some experimentation tests in order to evaluate performances for the process desired.

Several types of countercurrent columns are used in chemical industry, such as mechanically stirred agitated columns, packed columns, spray columns. In order to perform a good separation, a high value of number of theoretical stages (NTS) has been needed. Mechanically agitated columns, thanks to an external energy source, provide to improve the formation of new droplets increasing the surface and then, the overall performance and efficiency. Mechanically agitated columns can be divided into two groups, rotary agitated, such as Oldshue-Rushton columns, Sheibel, RDC contactor and Kuhni columns and reciprocating such as Karr column. A Kuhni column (Sulzer®) has been chosen to test experimentally, installed in Elbaite laboratory (IFP-EN Solaize) since September 2015.

Kuhni ECR32 is used to feasibility studies and scale-up for industrial column diameters up to 300 mm, and combining experimental results with the model developed, it is possible to compare and validate it. The miniplant extractor (Sulzer®) is a glass column of 32 mm internal diameter separated in 8 sections of 225mm, where each of it is divided in 8 compartments by stator rings. The column is equipped with 20mm Rushton turbines which rotate around a stainless-steel shaft axially connected by an electrical motor. Eight sampling glass ports are available in each section provided by a PTFE tap.

Figure 3.1 (a) illustrates the mini-plant column, in which is possible to see two decanters situated on the top and on the bottom of the column, needed to separate dispersed phase and continuous phase, and the inlet/outlet of the streams. Overall, it's a total height of 2600 mm with an active height of 1800 mm.

In each section, the stator rings superimposed have a predefined opening area and they can be removed and changed, a useful manner to change the NTS available of the columns. In fact, in order to increase performances, it is common to reduce the stator ring opening area.

There is also the possibility to operate with structured packing type Rombopak, or empty. The unit is equipped with a heating jacket able of operating at a temperature of up to 60 ° C.

The heavy phase inlet is located at the top of column, and an adjustable overflow siphon system placed at the same height of the decanter on the top is used to adjust the level of the interface on the column. The light phase moves in the bottom of the column and is recovered in the decanter at the top. Using a sample port, it is possible to inject another feed in the middle of the column in order to reproduce in "washing-backwashing" operation mode. Figure 3.1 (b) offers an overview of unit D0185. It's possible to see the different tank of feed and solvent, placed on a weight scale. On the left, there is a system of peristaltic pump that moves feed and solvent into the column. Geometrical values to know are important to model the column and these principal parameters are shown in the Figure 3.2. The Table 3.1 shows main characteristics of the Kuhni miniplant unit.

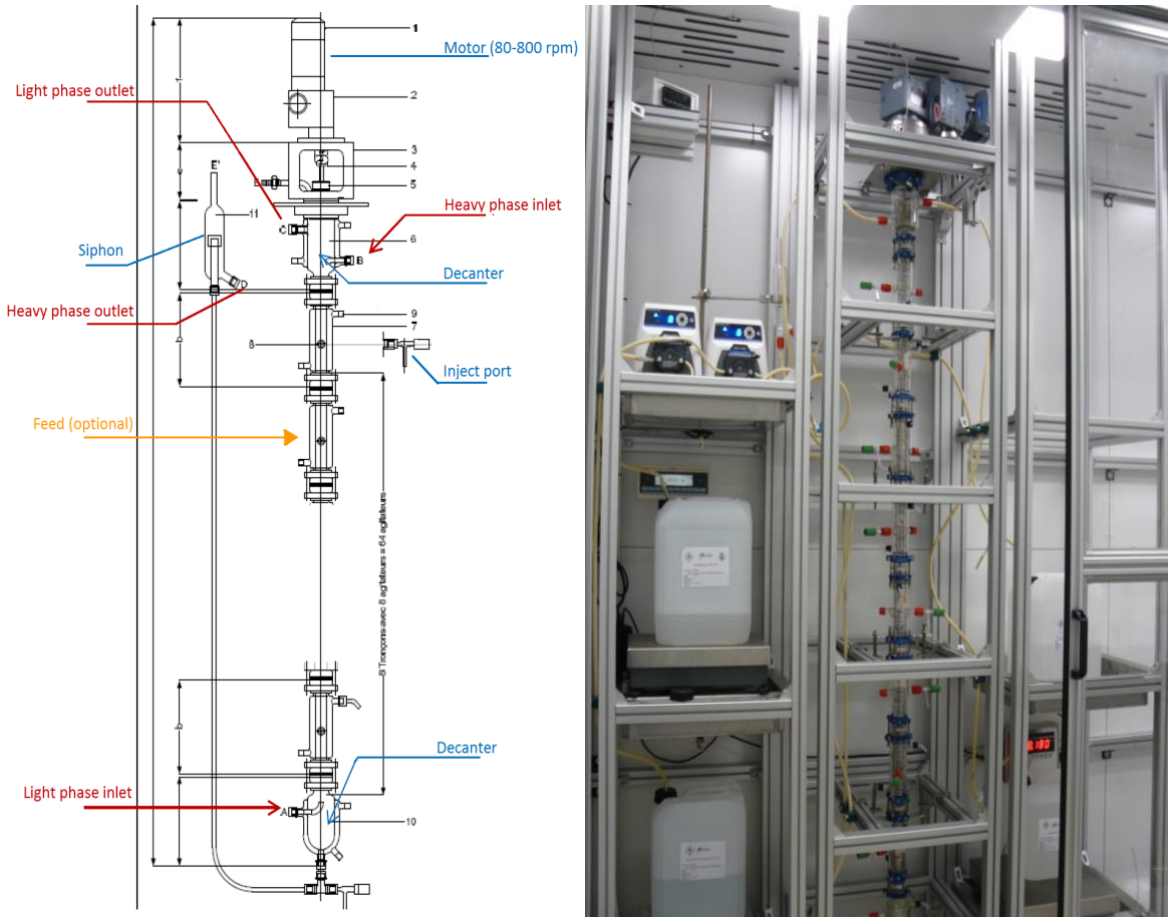


**Figure 3.1: Kuhni Miniplant scheme (a) and photo of the unit (b)**

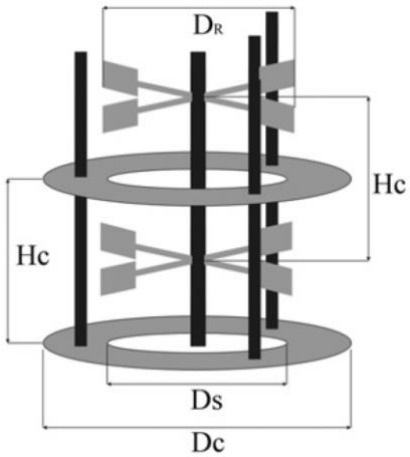


**Figure 3.2:** Principal geometrical characteristics dimension of the column

**Table 3.1:** Main characteristics of the Kuhni miniplant (Sulzer®)

| | | |
|---|---|---|
| Producer | | Sulzer |
| Model | | Kuhni ECR 32/64G |
| Type | | Miniplant LL-Extraction Column |
| Impeller type | | Four blade turbines |
| Stator free area ratio | % | 20 (30,40) |
| Heating jacket | | yes |
| Material column | | Borosilicate glass 3.3 |
| Impeller range of speed | rpm | 80-800 |
| Range of flow rates | L/h | 3-10 |
| Total height | mm | 2600 |
| Effective height | mm | 1800 |
| Section height | mm | 225 |
| Compartment height ($H_c$) | mm | 28 |
| Nominal column diameter ($D_c$) | mm | 32 |
| Impeller diameter ($D_R$) | mm | 20 |

# 4 Model description

## 4.1 General statements and hypothesis

In order to predict the performance of Kuhni column, a mathematical model has been developed. Firstly, it's necessary to formulate a series of hypothesis in function to the nature of the observed system. In Figure 4.1(a) is reported a detailed scheme about the system analysed, where a dispersed phase (yellow) is distributed like a population of droplets into a continuous phase (blue). Geometry plays a fundamental role to the model description. Some work (Hlawitschka 2013) takes account of the geometry of the system and of the population of the droplets, with a high accuracy results but with a very complex treatment. These complex models won't be discussed in this work.

First hypothesis consists in expressing the continuous and dispersed phases like a continuum, mass transfer occurs through the surface between two phases. Model double film has been used (Figure 4.1 (b)). Secondly, it's possible to say that the liquid which moves through the compartment is completely mixed so that its properties can be seen as a uniform and identical to outlet of the element. A number of 64 well mixed compartments can be representing by a CSTR cascade. When the number of stirred elements is high, the system can be described by a plug flow. A number of 64 well mixed compartments can be representing by a CSTR cascade. When the number of stirred elements is high, system can be described by a plug flow.

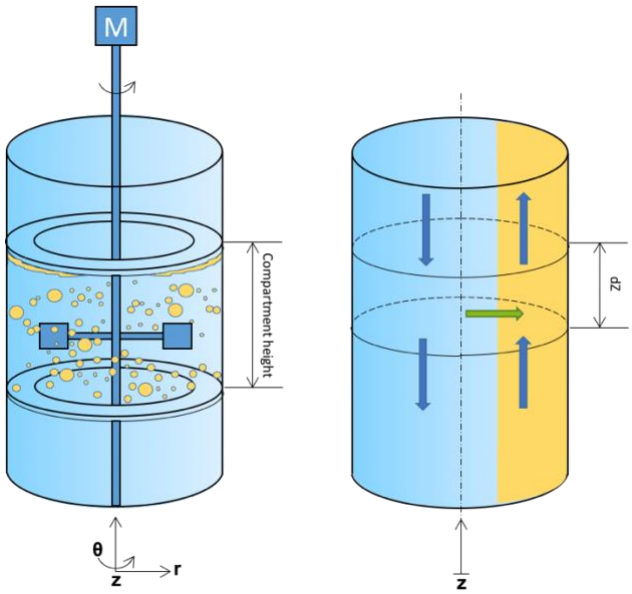


**Figure 4.1:** Detailed scheme (a) and model scheme (b) of a Kuhni compartment

The plug flow model is an easy model that sometimes is predictive for the system observed, but there are many cases in which doesn't correspond to the facts. In fact, the efficiency of an extractor isn't only affected by extraction factor or mass transfer condition, but also by the axial dispersion. The presence of several mixing effects, such as localized high velocities in the continuous phase, entrained droplets with coalescence and breakage effects, non-uniform velocity distribution, back and forward mixing, caused by turbulent eddies in the continuous phase, involves a considerable deviation to the ideal plug flow (Rydberg 2004). These

phenomena are grouped into an effect called axial mixing and overall, they cause a reduction of efficiency of separation (Figure 4.2).

A study Pratt and Hanson (1982) allowed to describe and classify the causes of axial dispersion in liquid-liquid extraction:

- Transport of the continuous phase with the droplets and against the main flow direction.
- Back mixing of the continuous phase in the wake of the droplet swarms.
- Back transport of the continuous phase due to the generation of the double vortex structure in agitated columns.
- A droplet velocity distribution of the different sized droplets caused by breakage and coalescence.
- Channelling of the liquids due to the geometry of the column (e.g. around the stator rings).

These mechanisms whether acting separately or in combination affect the concentration gradient between the phases becoming smaller. Furthermore, a concentration jump at the inlet streams has been found.

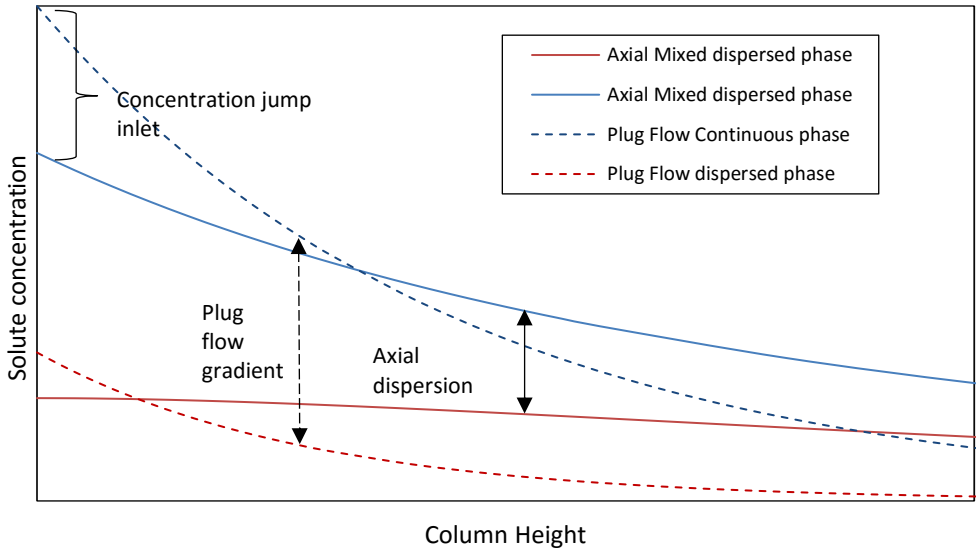


**Figure 4.2:** Plug flow model and axial dispersion model comparison

Extractor performances can be compared to stage columns. If concentration gradient decreases number of theoretical stages required performing the separation increases. But if we consider that theoretical stages available of the column don't change, the extraction result will not be achieved. The given diagram in Figure 4.3 shows the effect of back mixing on the number of theoretical stages. In the X-axis, the concentration of solute in the raffinate is reported, while in the Y-axis the concentration of solute in extract. As it can be seen, the effect of axial mixing provides to decrease the difference of concentration between the phases, reducing the driving force of the mass transfer.

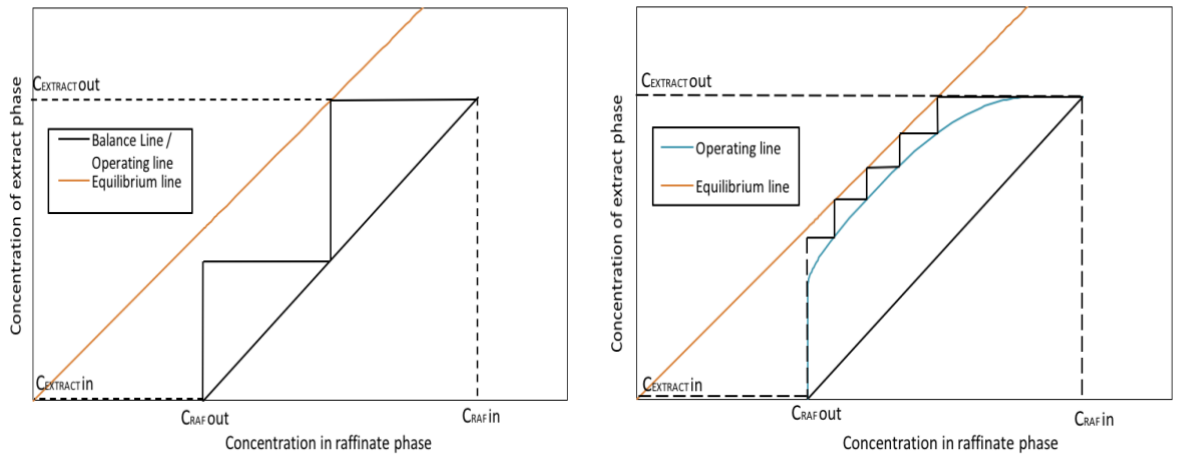


**Figure 4.3:** NTS required for a plug flow without dispersion (a) and with dispersion (b) extraction operation

Ziegler and Li (1967) shown in a ELL application no taking account of the effect of axial dispersion could lead an overestimation of the driving force value from 10% to 30%.

In order to avoid overestimation and hence a performance deviation, plug flow model needs a modification which taking account the effect of axial dispersion. Two models have been found in literature:

- Dispersion model;
- Backmixing model.

The first is an extension of plug flow model. It explains that the effects of axial mixing can be assumed by back diffusional flux in each phase superimposed to plug flow model. Back diffusional flux is based on the Fick's law. The second model describes the axial mixing as a number of no ideal continuous stirred cell connected in series, in which a back flow occurs in each cell. This model is in function of the number of mixing cells in the column. (Lo et al. 1983). In this work, the first model has been chosen, because there are more experimental data, correlations related to it than the second on. In Figure 4.4 is shown a particular behaviour of dispersion.

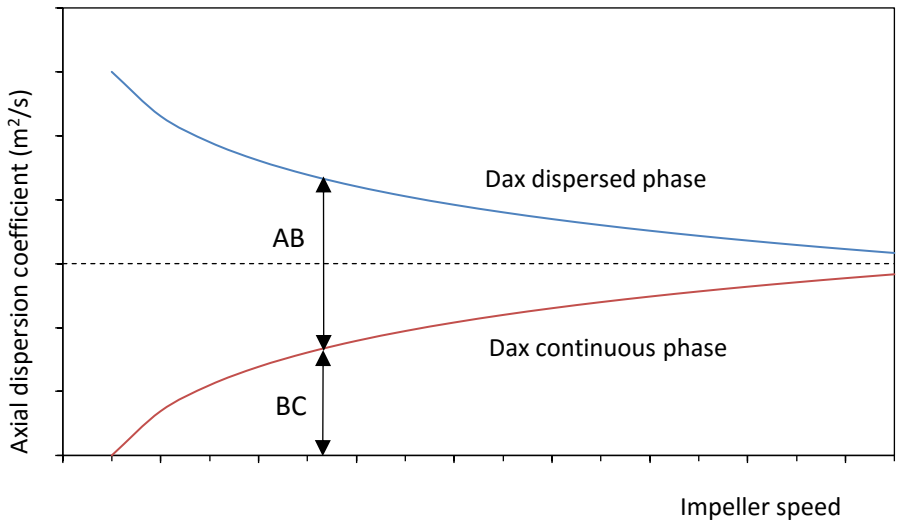


**Figure 4.4:** Axial dispersion coefficients evolution in function to impeller speed

Experimental results (Gourdon 1994) show that if the impeller speed increases, continuous axial dispersion coefficient rises, but dispersed axial coefficient, which has been observed bigger than the continuous, decreases. This paradoxal effect can be explained considering two contributions of dispersed axial dispersion.

- A back mixing effect due the rotational speed of the impeller, related to continuous phase;

- A forward mixing due the distribution of droplets velocity led by the distribution of droplets.

When impeller speed increases dispersed axial dispersion coefficient decreases, and then the distribution of droplets becomes narrower, and the droplets reduce their diameter. For this effect forward mixing become less strong.

This contradiction that can't be explained by dispersion model, show the limitation of this model, also if it offers a good instrument to find reasonable results with a good degree of accuracy. Population balance applied to LLE, with a more complex mathematical approach, leads to explain and count this phenomenon. (Hlawitschka 2013).

## 4.2 Plug flow

In this section, the plug flow model is described. Some hypothesis has been discussed in the section above. By imposing the local matter balance on the given system, the differential equations system has been developed. Plug flow model doesn't take account of the wall effect and velocity profile along the radial direction is constant, and of course, there's no axial dispersion (Lo et. al. 1983).

The hypothesises are:

- Pressure and temperature of the system are constants;
- Low concentration solute (infinite dilution), volumetric flow rate and superficial velocity for each phase along the unit are constants;
- Pseudo-continuous biphasic flow concurrent (pseudo homogenous contactor);
- No wall effect or radial gradient (One dimensional system);
- Double film layer mass transfer theory;
- Volumetric mass transfer coefficients are constants or can be averaged over the column;
- The solvent and raffinate phases are immiscible or have a constant miscibility irrespective of solute concentration;
- The equilibrium relation is linear or can be approximated by a straight line.

Figure 4.5 shows local matter balance for each phase, in which it's possible see the pseudo interface that splits into two continuous parts the phases.

The differential equations system for the solute "i" in each phase (continuous and dispersed) is:

$$\begin{cases} (1-\varphi)\dfrac{dC_{c,i}}{dt} = -v_c\dfrac{dC_{c,i}}{dz} - J_i(z)\cdot a \\ \varphi\dfrac{dC_{d,i}}{dt} = v_d\dfrac{dC_{d,i}}{dz} + J_i(z)\cdot a \end{cases} \tag{4.1}$$

J is the mass transfer flux density for the transferred component, sometimes expressed by the overall mass transfer coefficient and bulk concentrations as driving force:

$$J = k_{OV,c}\left(C_{c,i} - C^{*}_{c,i}\right) \tag{4.2}$$

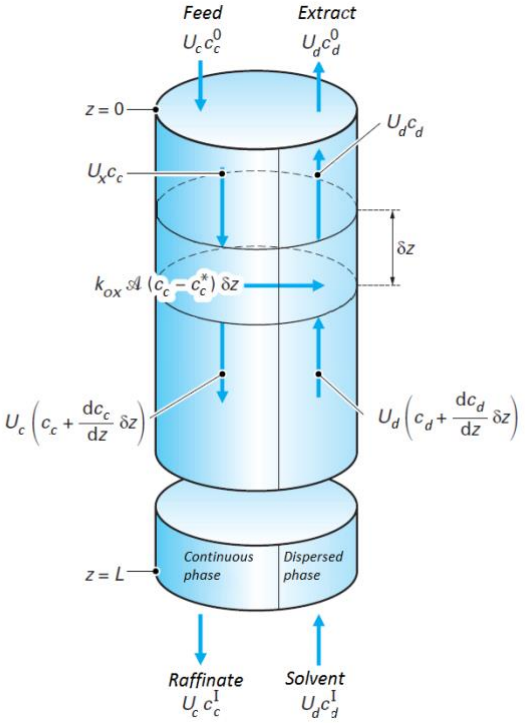


**Figure 4.5:** Plug flow local matter balance scheme Leybros (2004)

In equation 4.2 overall mass transfer coefficient multiplies can be defined by:

$$\frac{1}{k_{OV,c}} = \frac{1}{k_c} + \frac{1}{m \cdot k_d} \tag{4.3}$$

Where:

$$C^{*}_{c,i} = \frac{C_{d,i}}{m_{(vol)}} \tag{4.4}$$

It is important remember that coefficient m, distribution ratio is defined the ratio between the mass concentration (kg/m$^3$) of solute in dispersed phase in equilibrium with continuous phase.

## 4.3 Dispersion model

The turbulent mixing of elements of fluid can be assumed as untidy movement similar to molecular diffusion. Axial mixing is described by a diffusional coefficient, expressed by Fick's law:

$$J_{ax,i} = -D_{ax}\frac{dC_i}{dz} \tag{4.5}$$

Where:

- $J$ matter flux density of axial mixing transport;
- $D_{ax}$ axial dispersion coefficient;
- $\frac{dC_i}{dz}$ concentration of solute gradient.

Then the model involves two transport phenomena:

- an interphase diffusion, related to axial mixing;
- an intra-phase diffusion, related to mass transfer between the phases.

Model is built using these hypothesises (Lo et. al. 1983).:

- Pressure and temperature of the system are constants;
- Low concentration solute (infinite dilution), volumetric flow rate and superficial velocity for each phase along the unit are constants;
- Pseudo-continuous biphasic flow concurrent (pseudo homogenous contactor);
- No wall effect or radial gradient (One dimensional system);
- Double film layer mass transfer theory;
- Volumetric mass transfer coefficients are constants or can be averaged over the column;
- The solvent and raffinate phases are immiscible or have a constant miscibility irrespective of solute concentration;
- The equilibrium relation is linear or can be approximated by a straight line
- Axial mixing is characterized by a turbulent axial diffusion coefficient

A scheme of local mass balance, is shown in Figure 4.6 in which there's the back diffusional flow caused by axial mixing. The differential equations system for the solute "i" in each phase (continuous and dispersed) is:

$$\begin{cases} (1-\varphi)\frac{dC_{c,i}}{dt} = D_{axc,i}\frac{d^2C_{c,i}}{dz^2} - v_c\frac{dC_{c,i}}{dz} - k_{Oc}a\left(C_{c,i} - C^*_{c,i}\right) \\ \varphi\frac{dC_{d,i}}{dt} = D_{axd,i}\frac{d^2C_{d,i}}{dz^2} + v_d\frac{dC_{d,i}}{dz} + k_{Oc}a\left(C_{c,i} - C^*_{c,i}\right) \end{cases} \tag{4.6}$$

As it can be seen, the structure of the equations is pretty similar to the plug flow model, but in 4.6 there's axial dispersion term.

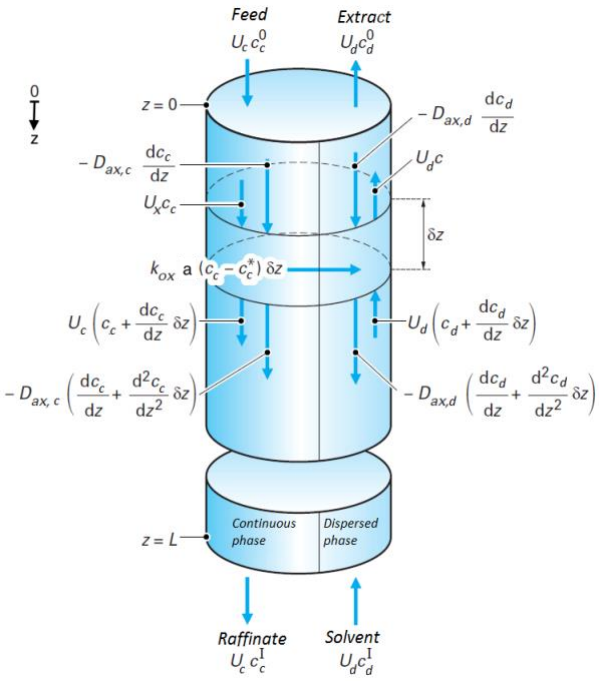


**Figure 4.6:** Plug flow with axial dispersion matter balance scheme Leybros (2004)

In order to solve the problem, four boundary conditions (Lo et al. 1983):

1) In the continuous phase at z=0: Taking the point z=0 where the concentration is $C_{c,0}$ , there are two terms to consider, convective inlet forms the out the boundary to z=0 and convective dispersive outlet from z=0, given by:

$$v_c C_c{}^0 = -D_{ax,c} \left.\frac{dC_c}{dz}\right|_0 + v_c C_{c,0} \tag{4.7}$$

Where $C_c{}^0$ represents the external concentration.

2) At the continuous phase outlet z=L concentrations of internal and external are the same, therefore only one condition is possible:

$$\left.\frac{dC_c}{dz}\right|_L = 0 \tag{4.8}$$

3) In the dispersed phase at z=L, the condition is similar to 1, for pure, $C_d{}^I = 0$

$$0 = -D_{ax,d} \left.\frac{dC_c}{dz}\right|_L - v_d C_{d,L} \tag{4.9}$$

4) At the continuous phase at z=0, the condition is similar to 2:

$$\left.\frac{dC_d}{dz}\right|_0 = 0 \tag{4.10}$$

Equation 4.6 can be solved analytically (See Section A.2 in the appendix).

# 5 Set of correlation

In order to solve the differential equations system, it's required the knowledge of the parameters which can be evaluated empirically by correlation. Several correlations have been found in literature which are related to geometrical, physical and operating variables.

In this section, each parameter is described and related correlations explained.

## 5.1 Hold Up

Hold-up is defined as the volume fraction of the dispersed phase, calculated by:

$$\varphi = \frac{V_d}{V_d + V_c} \tag{5.1}$$

This parameter is related to a specific area of the system. In fact, an increase of hold up leads to increase mass transfer surface i.e. efficiency of extraction.

On the other hand, hold up is useful to calculate the slip velocity. For a Kuhni column, the countercurrent flow of two immiscible phases occurs, so slip velocity is defined by:

$$v_{rs} = \frac{v_d}{\varphi} + \frac{v_c}{(1-\varphi)} \tag{5.2}$$

Where $v_d$ and $v_c$ are respectively the (absolute) dispersed and continuous superficial velocity. Slip velocity is the relative velocity between a drop and the continuous phase, and it is used firstly to determine mass transfer coefficient, because usually the correlation is related to this relative velocity.

### *5.1.1 Empirical equation*

One of most famous correlation is the one developed by Kumar and Hartland (1995), that can predict the hold-up for several types of extraction column and disparate conditions. The empirical equation, based on the knowledge of a wide experimental data (around 7200 measurements), relates hold up as a function of various dimensionless groups:

$$\varphi = \Pi\Phi\Psi\Gamma \tag{5.3}$$

where:

- Π is energy input dissipation dimensionless group;
- Φ is phase flow rates dimensionless group;
- Γ, Ψ are related to geometrical and physical proprieties.

$$\Pi = C_{\Pi} + \left[\frac{\epsilon}{g}\left(\frac{\rho_c}{g\gamma}\right)^{1/4}\right]^{n_1} \tag{5.4}$$

$$\Phi = \left[v_d\left(\frac{\rho_c}{g\gamma}\right)^{1/4}\right]^{n_2} exp\left[n_3 v_d\left(\frac{\rho_c}{g\gamma}\right)^{1/4}\right] \tag{5.5}$$

$$\Gamma = C_{\Gamma} e^{n_6}\left[l\left(\frac{\rho_c}{g\gamma}\right)^{1/2}\right]^{n_7} \tag{5.6}$$

$$\Psi = C_{\psi}\left(\frac{\Delta\rho}{\rho_c}\right)^{n_4}\left(\frac{\mu_d}{\mu_c}\right)^{n_5} \tag{5.7}$$

Where is $\epsilon$ is Energy dissipation $\left[\frac{W}{kg}\right]$ and "e" is stator free open area. Energy dissipation and open stator area are calculated by:

$$\epsilon = \frac{4P}{\pi D_{Col}^2 H_c \rho_c} \tag{5.8}$$

$$e = \left(\frac{D_s}{D_{col}}\right)^2 \tag{5.9}$$

Power is calculated by Newton number or power number (Np) and Kumar and Hartland modified power number.

$$Np = 1.08 + 10.94/{Re_R}^{0.5} + 257.37/{Re_R}^{1.5} \tag{5.10}$$

Two series of dimensionless group's coefficient have been reported in Table 5.1. The first series is the set related to Kuhni columns data only. The second series is the result obtained by using all databank available.

**Table 5.1:** Values of Constants of $C_{\Pi}$ $C_{\Psi}$ $C_{\Gamma}$, and Indexes n1-n7 for Kuhni Columns and unified columns proposed by Kumar and Hartland (1995)

| **Column** | $\mathbf{C_{\Pi}}$ | $\mathbf{C_{\Psi}}$ | | | $\mathbf{C_{\Gamma}}$ | $\mathbf{n_1}$ | $\mathbf{n_2}$ | $\mathbf{n_3}$ | $\mathbf{n_4}$ | $\mathbf{n_5}$ | $\mathbf{n_6}$ | $\mathbf{n_7}$ | **l** |
|---|---|---|---|---|---|---|---|---|---|---|---|---|---|
| | | c→d | d→c | no MT | | | | | | | | | |
| Kuhni | 0.0267 | 1 | 0.56 | 1 | 2.27 | 0.77 | 0.64 | 20.7 | -0.34 | 0 | -0.77 | 0 | $H_C$ |
| Unified | 0.27 | 1 | 1 | 1 | 4.35 | 0.78 | 0.87 | 3.34 | -0.58 | 0.18 | -1 | -0.39 | $H_C$ |

## 5.2 Droplet size

Droplets size is another important parameter to know for designing of a Kuhni column. It affects the hydrodynamic behaviour of the column (i.e. hold up and flooding) and interface of mass transfer. In the previous chapter, different hypothesis has been done to describe 1D axial dispersion model. The dispersed phase is treated as a continuum, where the interphase surface is equal to a monodispersed population of droplets with the same volume of liquid. The diameter that respects this condition is called Sauter mean diameter. It is defined as the diameter of droplets in a mono dispersed swarm with the same value of surface/volume between two phases as the real poly-dispersion:

$$d_{32} = \frac{\sum_{i=1}^{N} n_i d_i^3}{\sum_{i=1}^{N} n_i d_i^2} \tag{5.11}$$

The d32 is used to calculate specific area ($m^2_{interface}/m^3_{extractor}$) related to flux matter density between the phases. It's easy to demonstrate that:

$$a = \frac{\sum S_{dropl}}{V_{col}} = \frac{N_{drop}\pi {d_{32}}^2}{V_{col}} = \frac{\varphi V_{col}}{(1/6)\pi {d_{32}}^3}\frac{\pi {d_{32}}^2}{V_{col}} = \frac{6\varphi}{d_{32}} \tag{5.12}$$

Where the number of (mono dispersed) drop is calculated as the ratio between dispersed volume and volume of single droplet:

$$N_{drop} = \frac{\varphi V_{col}}{(1/6)\pi {d_{32}}^3} \tag{5.13}$$

### *5.2.1 Empirical correlation of d32*

Fisher (1972) proposed a set of equations divided by interfacial tension range, as a function of hold-up:

$$d_{32} = C_1 We_R^{-0.61}(1+2\varphi)\left(1+\frac{11}{{n_c}^{1.22}We_R^{0.5}}\right)d_R \qquad for\ \sigma > 0.012\frac{kg}{m^2} \tag{5.14}$$

$$d_{32} = C_2 We_R^{-0.3} Re_R^{-0.4}(1+2\varphi)\left(1+\frac{11}{{n_c}^{1.22}We_R^{0.5}}\right)d_R \quad for\ \sigma < 0.012\frac{kg}{m^2} \tag{5.15}$$

**Table 5.2:** Constants used for the Fisher's drop size model for different Authors

| $C_1$ (Lo et al. 1983) | $C_1$ (Hufnagl et al. 1991) | $C_2$ (Lo et al. 1983) |
|---|---|---|
| 0.24-0.32 | 0.19 | 2.4-2.8 |

Furthermore, Kumar and Hartland (1996) proposed a set of predictive equations of droplet size for eight different types of extraction columns, based on 2739 experimental data points. For a Kuhni column, it has been used the following equation:

$$d_{32} = \frac{H_c C_\Psi e^n}{\frac{1}{C_\Omega \left(\frac{\gamma}{\Delta\rho g H^2}\right)^{1/2}} + \frac{1}{C_\Pi \left[\left(\frac{\epsilon}{g}\right)\left(\frac{\rho_c}{g\gamma}\right)^{1/4}\right]^{n1} \left[H_c \left(\frac{\rho_{cg}}{\gamma}\right)^{1/2}\right]^{n2}}} \tag{5.16}$$

which "e" term is stator free area ratio, defined by:

$$e = \left(\frac{D_s}{D_{col}}\right)^2 \tag{5.17}$$

**Table 5.3:** Values of Parameters in Kumar and Hartland's equation (1996) for Kuhni (mechanically agitated columns)

| Column | n° data | $C_\Psi$ | | | $C_\Omega$ | $C_\Pi$ | n | $n_1$ | $n_2$ |
|---|---|---|---|---|---|---|---|---|---|
| | | c→d | d→c | no MT | | | | | |
| Kuhni | 702 | 1 | 3.04 | 1 | 1.60 | 0.034 | 0.45 | -0.63 | -038 |

## 5.3 Implicit method for d32 and hold up

Another way to calculate d32 (or hold up) is using an implicit method. As already seen, to determine slip velocity relative absolute velocity difference between the phases is applied (equation 5.2).

But slip velocity can be estimated evaluating the physical path of the droplet. This method, called also "physical method" allows to estimate the value of slip velocity taking account the terminal velocity of a bubble and the other effects which characterize the given system. Hence, in order to estimate slip velocity, it is necessary to evaluate each effect that can affect droplets rise.

Terminal velocity is the highest velocity attainable of a particle that moves through an indefinite fluid. A single drop moves unhindered in a continuum (Figure 5.1 a), so in this case it is possible to write:

$$v_{rs} = u_t \tag{5.18}$$

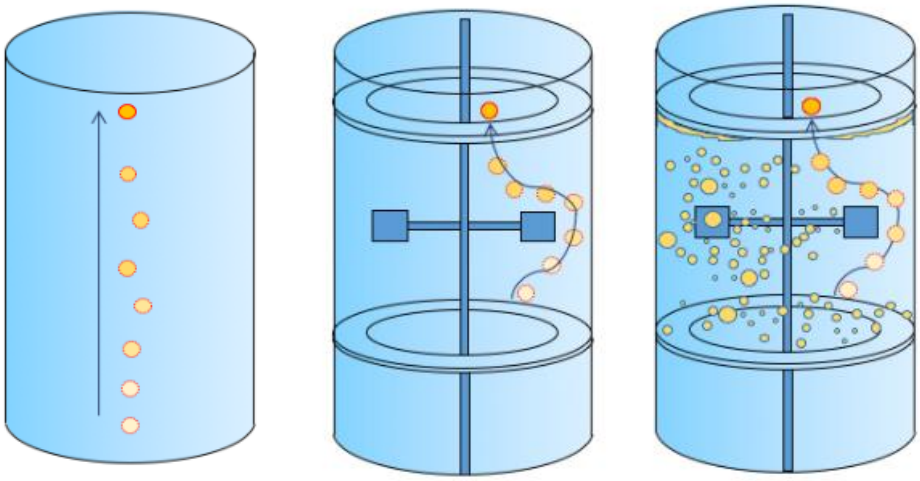

**Figure 5.1:** Droplet in an unhindered system(a), Slowing effects due the internals and the rotation (b) and Effect of swarm interaction on a particle (c)

The presence of internals with a particular geometry or mechanical element in movement (impeller) affects the droplet path. In fact, due this hindered elements, a single drop moves significantly slower through the column (Figure 5.1b). This effect can be expressed by the slowing factor $K_v$ and the slip velocity (also called characteristic velocity) equation becomes:

$$v_{rs} = v_k = u_t K_v \tag{5.19}$$

But in the real system, a huge number of droplets dispersed in the continuous phase with different size moves through the unit. These droplets can coalesce in bigger bubbles or divide into two smaller ones and some of them could coalesce in the stator ring forming a continuous layer of liquid.

In order to describe mathematically these series of effects, it's necessary to consider these droplets interaction between fluid particles, as an effect of "swarm". The swarm effect can be expressed in different mathematical ways.

Godfrey and Slater (1991) proposed an easy form to explain these phenomena. Swarm effect can be expressed as a power law function of hold-up:

$$v_{rs} = u_k(1-\varphi)^m \tag{5.20}$$

Where m is a swarm coefficient, an empirical term in function of Reynolds number of the system.

### *5.3.1 Terminal velocity model*

After an initial short distance, a single drop moves unhindered in a column without internals with constant velocity, and that is called terminal velocity.

Terminal velocity depends on the physical proprieties of the system concerned and the droplet diameter. In fact, if droplet diameter or difference of density between the phases increase, velocity rises.

But velocity doesn't increase infinitively. In fact, (Figure 5.2) Garthe (2006) shows that "below certain value of diameter, the drop moves in the continuum like a rigid drop. An increase of droplet size can take a higher droplet velocity and droplet surface movement, that creates an inner circulation. This effect increases significantly the speed of the droplets. Then, by increasing again the size, circulating drops lead to lose their stability and they become oscillating drops, that will cause a downward tendency of their velocity due to the large surface area exposed to the continuous flow. With an additional increase of volume, the droplets deform from spherical-caps to ellipsoid-plugs which can move slower than rigid spheres due the friction between the phases."

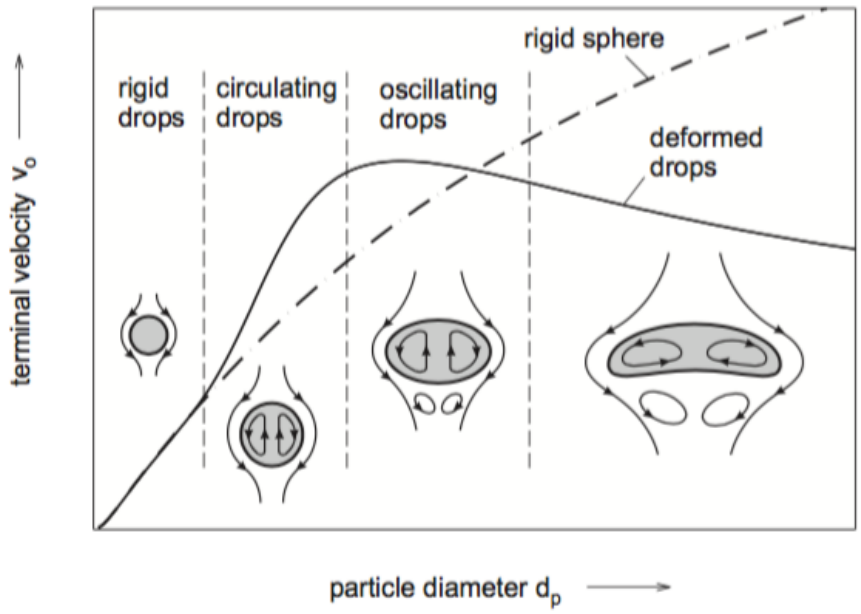


**Figure 5.2:** Terminal velocity in function to the particle diameter for rigid sphere (dotted line) and real particles (continuous line). (Garthe 2006)

Several correlations are available in literature for estimating terminal velocity. According to Leybros (2004), the choice can be done estimating the hydrodynamic number **P**:

$$\boldsymbol{P} = \rho_c^2 \sigma^4 / g \Delta\rho \mu_c^4 \tag{5.21}$$

For low interfacial tension system ($\mathbf{P}<10^5$), Grace et al. (1976) proposed an empirical correlation for rigid and oscillating droplets in contaminated system:

$$u_t = \frac{\mu_c}{d\rho_c} Mo^{-0.149}(J - 0.857) \tag{5.22}$$

$$J = \begin{cases} 0.94H^{0.757} & for: 2 < H < 59.3 \\ 3.42H^{0.441} & for: H > 59.3 \end{cases} \quad (5.23)$$

$$H = \frac{4}{3} EoMo^{-0.149} \left( \frac{\mu_c}{\mu_{water}} \right) \quad (5.24)$$

For high-interfacial tension system (**P**>$10^7$), Vignes (1965) proposed a correlation for circulating droplet:

$$u_t = \frac{d_{32}}{4.2} \left( \frac{g \Delta \rho}{\rho_c} \right)^{2/3} \left( \frac{\rho_c}{\mu_c} \right)^{1/3} \left( 1 - \frac{Eo}{6} \right) \quad (5.25)$$

Grace's correlation doesn't work with drop size smaller than 1 mm and also Baumler et al. (2010) showed that Grace's correlation has a significant deviation from the experimental data for mid and high interfacial standard system.

The correlation given by Hamielec et al. (1963) shows good agreement with the experiments for small drops diameter. In this case the terminal velocity is calculated by the drag coefficient:

$$C_D = \frac{3.05(783(\mu^*)^2 + 2142(\mu^*) + 1080)}{(60 + 29\mu^*)(4 + 3\mu^*) {Re_T}^{0.74}} \quad (5.26)$$

$$C_D = \frac{4 d \Delta \rho g}{3 \rho_c u_T} \quad (5.27)$$

Valid for 4<$Re_T$<100. A good correlation that can describe terminal velocity in each phase is Henscke Model (Henske 2003) and it's reported in the appendix.

### *5.3.2 Slowing factors and swarm coefficient*

Several experimental works (Fang 1996, Garthe 2006, Steinmetz 2007) concerned slowing factor model have been published. Fang (1995) proposed a correlation for 152mm diameter Kuhni column related to geometrical parameter and impeller speed:

$$K_v = 1 - \frac{(1 - e)\gamma}{(1 - \gamma)} \quad (5.28)$$

$$\gamma = 7.18 \cdot 10^{-5} \frac{Re_R}{e} \quad (5.29)$$

Steinmetz (2007) published a correlation for a Kuhni DN32, dependent to geometrical factors, diameter of droplet and impeller speed (Buchbender, 2013).

$$K_v = 0.0028\left(\frac{D_S - D_R}{d}\right) + 0.07227\frac{D}{H_C}exp\left[-0.5\left(\frac{N_P - 1.703}{0.3105}\right)^2\right] \tag{5.30}$$

In order to describe swarm coefficient, Godfrey and Slater (1991) proposed a correlation based on Richardson and Zaki's equation for fluidized system:

$$m = 0.15Re_K^{0.8} \tag{5.31}$$

Swarm coefficient m is in function of Reynolds number, tested on a Kuhni DN150 with an open free area of 20%. This correlation has a hold up range of $0 < \varphi < 0.3$.

## 5.4 Mass transfer coefficient

In literature, different mechanisms are available to describe mass transfer between two phases. According with double film theory, near the interface, in both sides exists a thin stagnant film that represents high resistance of mass transfer (Figure 5.3).

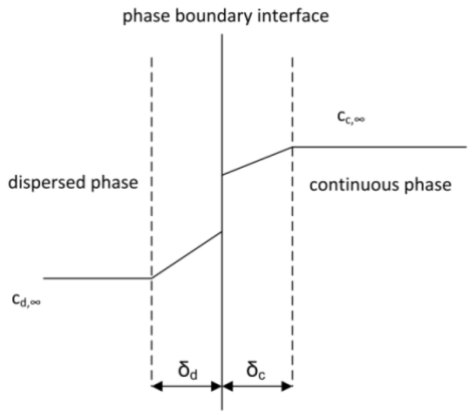


**Figure 5.3:** Double film layer theory (Hlawitschka 2013)

Mass transfer occurs when a difference of concentration between the phases exists. The concentration profile shows a point of discontinuity at the interphase. This jump is related to the difference of affinity of the solute for the phases, a thermodynamic propriety that can be described by the distribution ratio (m).

Into these two stagnant layer the preponderant transport mechanism is the molecular diffusion and in a steady state system where the geometric dimensions of the system are bigger than the film layer, it's possible to express mass flux density as:

$$J = \frac{D}{\delta_c}\left(C_{c,i}{}^{bulk} - C_{c,i}{}^{interface}\right) \tag{5.32}$$

For each stagnant film, matter flux density performs thanks to the difference of concentration between bulk and interface. A useful manner to express this density flux (in steady state condition), is to express the driving force as the difference between the bulk concentration. The final equation has this following form:

$$J = k_{OV,c}\left(C_{c,i}{}^{bulk} - \frac{C_{d,i}{}^{bulk}}{m}\right) \tag{5.33}$$

That can be written:

$$\mathrm{J} = \mathrm{k_{OV,c}}\left(\mathrm{C_{c,i}}{}^{bulk} - \mathrm{C_{c,i}}{}^{*}\right) \tag{5.34}$$

with $\mathrm{k_{Oc}}$ overall continuous phase mass transfer coefficient defined by:

$$\frac{1}{\mathrm{k_{OV,c}}} = \frac{1}{\mathrm{k_c}} + \frac{1}{\mathrm{mk_d}} \tag{5.35}$$

In literature, several models for continuous and dispersed mass transfer coefficient related to Sherwood number have been found. In fact, it is possible to express mass transfer coefficient in function to this dimensionless number:

$$Sh_{phase} = d_{32}k_{phase}/D_{phase} \tag{5.36}$$

Kumar and Harland (1999) proposed an empirical correlation to predict mass transfer coefficients, based on wide experimental data found in literature, for dispersed and continuous phase. For dispersed phase:

$$Sh_d = 17.7 + \frac{3.19 \times 10^3\left(ReSc_d{}^{1/3}\right)^{1.7}}{1 + 1.43 \times 10^2\left(ReSc_d{}^{1/3}\right)^{0.7}}\left(\frac{\rho_d}{\rho_c}\right)^{2/3} \times \frac{1}{1 + \left(\frac{\mu_d}{\mu_c}\right)^{2/3}}\left[1 + C_2\left\{\frac{\Psi}{g}\left(\frac{\rho_c}{g\gamma}\right)^{1/4}\right\}^{n2}\right] \tag{5.37}$$

For continuous phase:

$$\frac{Sh_c(1-\varphi) - Sh_{c\,rigid}}{Sh_{c\infty} - \frac{Sh_c}{(1-\varphi)}} = \tag{5.38}$$

$$5.26Re^{\frac{1}{3}\cdot 6.59\times 10^2 Re^{1/4}} \cdot {Sc_c}^{1/3} \left(\frac{u_{slip}\mu_c}{\gamma}\right)^{4/3} \frac{1}{1+(\frac{\mu_d}{\mu_c})^{1,1}} \left[1 + C_1 \left\{\frac{\Psi}{g}\left(\frac{\rho_c}{g\gamma}\right)^{1/4}\right\}^{n1}\right]$$

With:

$$Sh_{c\,rigid} = 2.43 + 0.775Re_p^{0.5}Sc_c^{1/3} + 0.0103Re_pSc_c^{1/3} \tag{5.39}$$

and Sherwood number in function of continuous Peclet number:

$$Sh_{c\infty} = 50 + \frac{2}{\sqrt{\pi}}{Pe_c}^{0.5} \tag{5.40}$$

Constant are reported in the Table 5.4.

**Table 5.4:** Values of constant in Kumar and Hartland's (1999) mass transfer equation

| Column | $C_1$ $C_2$ |
|---|---|
| Kuhni | 7.5 |

But, for a mass transfer direction from dispersed phase to the continuous phase, Garthe (2006) found the best agreement of his measurements to the model of Kumar & Hartland (1999). Hlawitschka (2013) explains that overall mass transfer coefficient obtained by Kumar's correlations shows a slight deviation from the other correlation compared for high throughput.

## 5.5 Axial dispersion

### *5.5.1 Axial dispersion of the continuous phase*

The description of continuous phase axial dispersion based on the Fick's law, gives a satisfactory result. The most difficult thing is to obtain the correlation from the given column, especially with a large diameter. Back mixing of continuous phase was described through correlations derived from experimental test, found in literature.

By observing these results, there is a direct dependency between Dax,c and impeller speed and the total volumetric flow. In fact, when the rotational speed of the impeller and the flow rate increase, the turbulence inside the compartment rises. On the other hand, by decreasing the stator free area, the dispersion coefficient decreases. A smaller free stator area, which hinders the back mixing of continuous phase, is a limiting factor for the axial dispersion.

Kolb (2002) extended the range of column diameters for the correlation proposed by Breysse et al. (1983), validated from 32 to 600 mm:

$$D_{ax,c} = 0.046Nd_cH_c + 0.14h_cv_c \tag{5.41}$$

Several authors developed for a Kuhni column a correlation based on a particular form:

$$D_{ax,c} = u_c H_c \left( C_1 + C_2 \left( \frac{D_R N}{u_c} \right) C_3 \right) \tag{5.42}$$

The constants values, derived experimentally are shown in Table 5.5.

**Table 5.5:** Constants of equation for axial dispersion coefficient derived experimentally

| Author | Diameter (mm) | $C_1$ | $C_2$ | $C_3$ |
|---|---|---|---|---|
| Kolb (2002) | 32 | 0.203 | 0.031 | $e^{0.5}$ |
| Steinmetz (2007) (1) | 32 | 0.203 | 0.031 | e |
| Steinmetz (2007) (2) | 32 | 0.14 | 0.093 | e |

### *5.5.2 Axial dispersion of the dispersed phase*

Axial dispersion coefficient is often represented by the Bodestein (similar to Peclet number) number introduced as dimensionless number:

$$Bo = \frac{uL}{D_{ax}} \tag{5.43}$$

For a ARD DN150, Bauer (1976) proposed a correlation relating Bodestein number to impeller and dispersed phase characteristic:

$$\frac{1}{Bo} = 0.092 + 1.9 \cdot 10^{-8} Re_R^{1.7} Re_D^{-0.7} \tag{5.44}$$

Hlawitschka (2013) proposed a modification of Bauer's correlation for a Kuhni column DN60:

$$\frac{1}{Bo} = 0.28 + 1.9 \cdot 10^{-8} Re_R^{1.7} Re_D^{-0.7} \tag{5.45}$$

Steinmetz (2004) (1) proposed a correlation for a Kuhni Column DN32, that relates Bodestein number to impeller diameter its rotational speed and interstitial velocity of dispersed phase.

$$\frac{1}{Bo} = 0.056 + 1.19 \cdot 10^{-2} \left( \frac{d_R N}{u_d} \right)^{3.45} \tag{5.46}$$

Steinmetz (2007) (2) proposed a correlation for a Kuhni Column DN80, that relates Bodestein number to impeller diameter its rotational speed and characteristic velocity of dispersed phase (Buchbender et al. 2012):

$$\frac{1}{Bo} = \frac{D_{ax,d}}{v_k H_C} = 0.017 + 1.19 \cdot 10^{-4} {Re_R}^{1.1} {Re_D}^{-0.5} \tag{5.47}$$

# 6 Experiments

In order to evaluate good correlations, we need some additional information. Experiments with a standard system have been conducted on the pilot plant D-185 Elbaite. According to Hemmati et al. (2015), standard systems are divided into three group, in function to interfacial tension. A standard system is composed by three components, two immiscible solvents (organic and aqueous) and a solute. In order to have information that could accord the real system which has a variable interfacial tension, the mid-tension system has been chosen. The feed is composed by water and acetone (solute), and butyl acetate is the organic light solvent. Table 6.1 shows physical proprieties of ternary system used.

**Table 6.1:** Physical proprieties of the studied systems at 20°C (Hemmati *et al.* 2015)

| Components/ phases | Density ($kg/m^3$) | Viscosity (mPa·s) | Superficial and interfacial tension ($J/m^2$) | Molecular diffusivity ($m^2/s$) x $10^9$ |
|---|---|---|---|---|
| Water | 998.2 | 1.003 | 0.0727 | - |
| Butyl Acetate | 881.5 | 0.73 | 0.0249 | - |
| Acetone | 790.5 | 0.322 | 0.0234 | - |
| Continuous | 994.9-995.8 | 1.075-1.088 | 0.0124-0.0132 | 1.01-1.06 |
| Dispersed | 879.6-881,4 | 0.723-0.738 | | 2.15-2.18 |

Experiments have been divided into two groups. Firstly, aim of this part is to find optimal working condition of the column, that can figure out investigating only hydrodynamic behaviour evaluating hold up and flooding, for wide operating values. Secondly, chosen these optimal conditions, experiments for determining droplet size, hold up, axial dispersion have been conducted.

It is important to remember the operative conditions are related to operating variables which are the motor speed rotation, volumetric flow rate and E/R ratio. Stator opening area isn't considered like operating variable because it's a geometrical factor and shut down of the unit is required for modifying it.

Water and acetone (10% m/m), using a peristaltic pump, are sent in the top of the column, filling it. When the column is completely charged, turning on the organic phase pump, butyl acetate is pumped at the bottom of the column and due the difference of density between two phases, it tends to rise along the unit. By using the push button for the impeller motor, agitation will occur allowing mixing inside the compartments.

## 6.1 Hydrodynamic

Aim of this part is determining optimal condition of the column studying its hydrodynamics. A number of 33 operating conditions have been tested, with several flow rates (4-10 L/h) and impeller rotation (300-650 rpm), allowing to determine hold-up in function to propeller speed and flow rate. Concentration of acetone is around 10% w/w in water, opening stator area 20% and mass transfer direction is continuous to dispersed.

Overall, by increasing motor impeller speed, the volume of the disperse phase shows an upward tendency. This can be explained taking account of the effect of the terminal velocity. In fact, the dispersed droplets tend to decrease their size, slowing down their speed along the column. When droplets are slower, their accumulation occur in the compartments, increasing the volume of dispersed phase.

After a continuous slight rise, an increase of agitation leads an exponential increase of the hold up. It means that column reaches flooding point. It means that the column reaches the flooding point. The flooding point is supposed to the minimal agitation of impeller necessary to reach the condition of phases inversion. If the flooding occurs, the column performs no separation.

For different flow rate, evaluating the critical impeller speed that leads flooding, it is possible to draw a flooding curve. The given Figure 6.1 shows a typical diagram of the flooding curve which delimits two zones, the working zone (below the curve) and the not-working zone (above the curve). Optimal working condition are found near flooding curve. Sulzer® suggests to work on a curve called operational curve at 80% of flooding. The operational curve is more or less parallel to the flooding curve optimal working condition should be found around it.

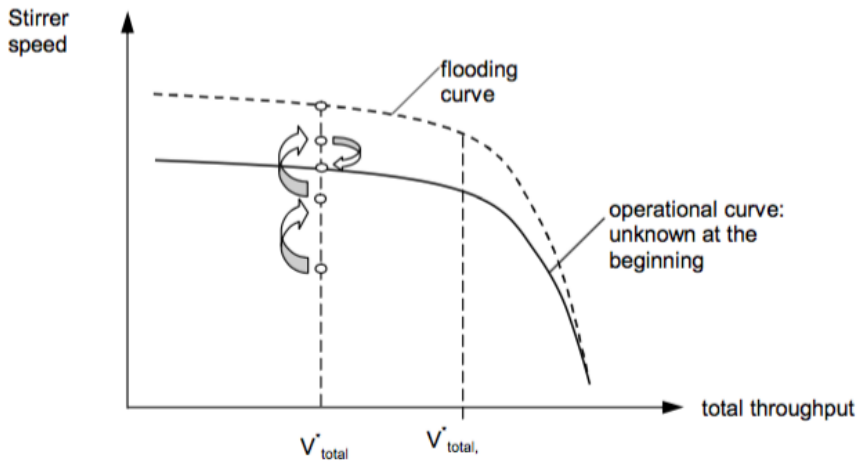


**Figure 6.1:** Flooding and operational curve in function of the total flow rate

To evaluate hold up of dispersed phase, two methods have been proposed:

- Fast sampling measures;
- Shut down measures.

By using the lateral sample ports of the column, it is possible to take a sample of the mixture in different its compartments. After having reached the stable hydrodynamic conditions (around 30-40 minutes in relation to throughput), the samples are extracted and put into separating funnels. The volume of the dispersed and the continuous phases are evaluated by using a graduated cylinder.

On the other hands, the shut-down method measures directly the hold up of the dispersed phase. When the agitator turns off, the dispersed phase tends to coalesce and separate from the

continuous phase. After the complete separation of the two phases, it is possible to calculate the hold up, measuring the height of interface.

## 6.2 Mass transfer experimentation

After determining optimal conditions for different throughput and E/R ratio, it has been possible to begin extraction experiment. Aim of these experimental tests is getting important data to make comparison to the model and correlations, such as axial dispersion, concentration of acetone in different zones of the column, droplet size and hold-up.

Each test provides:

- Sample of Extract and raffinate outlet;
- Sample of feed concentration jump;
- Photos using Nikon D300;
- Sample of three sampling port along the column;
- Measure of hold up with shut down method.

Due to low flow rate, unit arrives to steady state after several times. At first, it's fundamental verifying that stability is reached in order to have consistent results. To verify it, it needs to monitor variation of solute concentration in function of the time. Each 30/60 minute a volume of liquid is sampled from outlet streams (extract and raffinate) and analysed using gas chromatography technique, which provides the exact mass concentration of acetone.

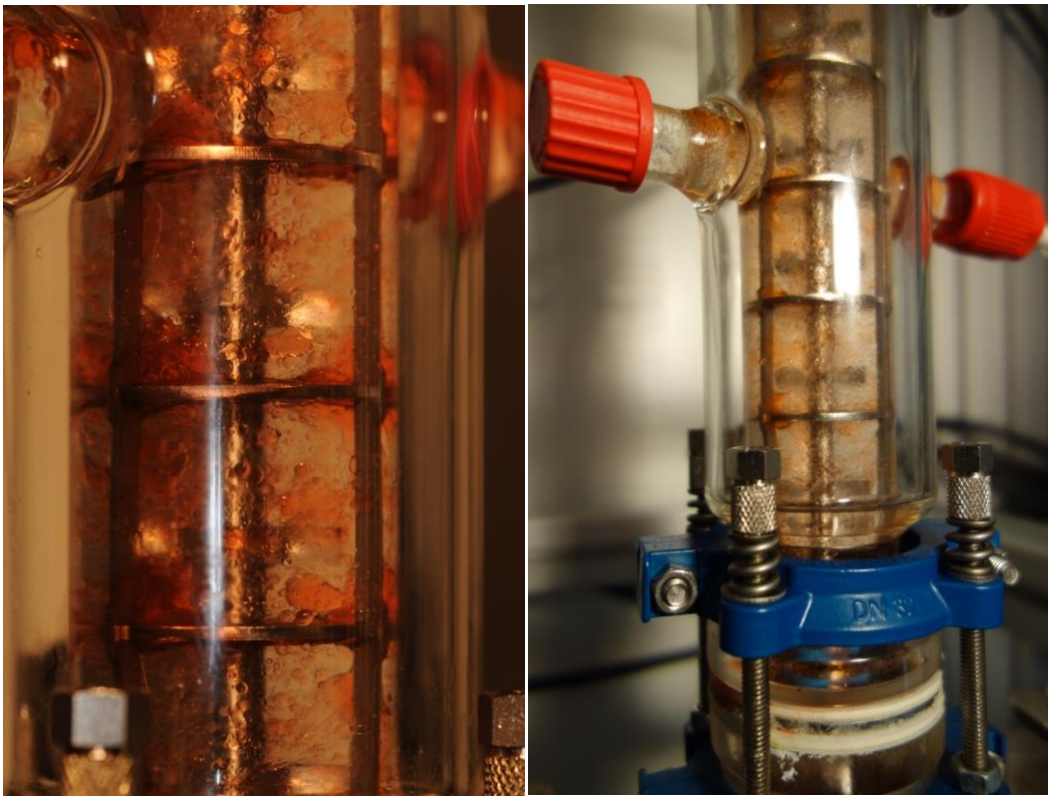

**Figure 6.2:** Kuhni DN32 column with the red Sudan dye in the dispersed phase

In order to evaluate the axial dispersion of the continuous phase, a little pipe connected to a syringe on the top of the column has been inserted close to the feed inlet, at the bottom of the column, and in this point a 20 ml sample has been taken.

A Nikon D300 professional has been utilize to photograph droplets. A particular led lamp and a halogen spot have been used, allowing to get clear photos. In order to distinguee the droplets from the continuous phase, the Sudan red chemical dye has been added into the butyl acetate charge. This dye, soluble in organic liquids, gives a stable red colour at the solvent phase. Figure 6.2 shows two photos of the unit with butyl acetate and Sudan red dye (dispersed phase) and water acetone (continuous phase). More than 100 photos have been taken for each experimental test.

Kuhni ECR32 column has eight injection/sampling ports which allow to take a part of liquid inside a section. By using a 100 ml separating funnel, sampling in section 1, 4 and 7 have been done. The two phases of the mixture taken aren't in equilibrium, so before the GC analysis it is necessary that biphasic system reaches it. So, after sampling it, at least 6 hours have been waited before analysing the sample. A mass balance has been done in order to evaluate the real concentration of acetone along the column.

# 7 Experimental results

## 7.1 Hydrodynamic

The line chart in Figure 7.1 shows the dispersed hold up trend using the fast sampling method. In the abscises, there's the impeller speed expressed in rpm and in the ordinate, hold up, and each curve indicates a specific throughput.

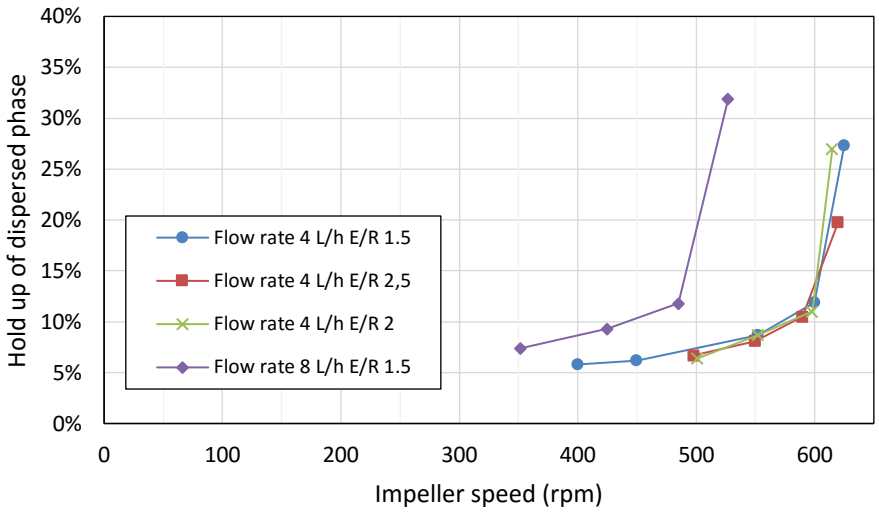


**Figure 7.1:** Fast sampling method hold up for several experimental tests

Shut down method is shown in Figure 7.2. The hold up, as already said, rises under a constant impeller increase, and it shows the exponential trend when the propeller speed reaches the critical agitation speed ($N_{crit}$). We define $N_{crit}$ as the number of revolution of impeller for reaching 30% hold up.

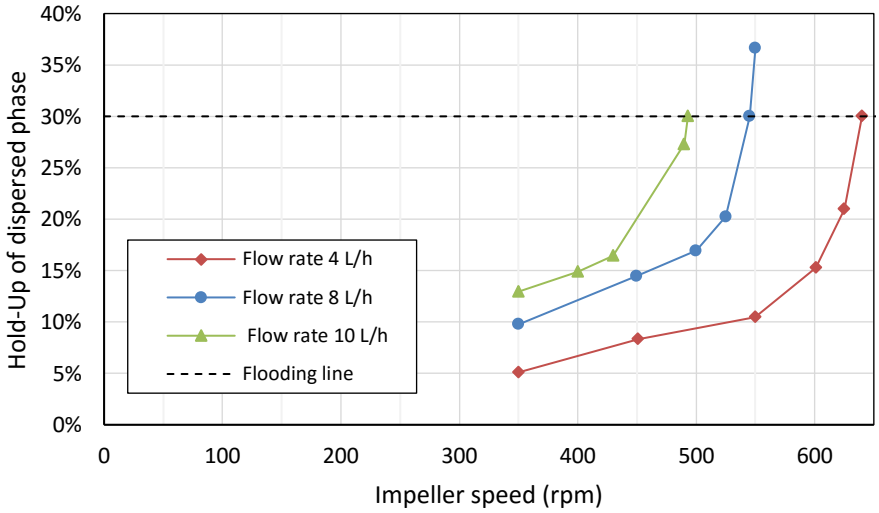


**Figure 7.2:** Shut down method hold up chart and flooding line (30%) for several experimental tests

Figure 7.3 shows a comparison from two experimental tests conducted by shut down method and fast sampling method. Overall the curves show the same tendency, but there is some significate variation. A difference around 5% of measured hold up occurs between two methods.

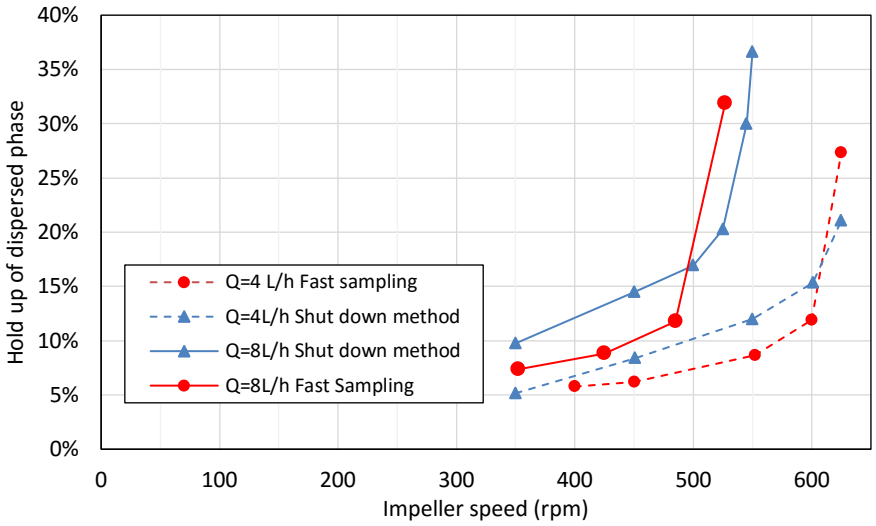


**Figure 7.3:** Shut down and fast sampling method comparison

The comparison between two methods shows a variation for the low/high values of the hold up. Firstly, the fast sampling-method performs a sampling in certain sampling port, giving information just for a certain compartment of the column. Secondly, for each method, operational and measure error may have influenced the final result. Second method may be resulted more reliable because it determines the average in the column.

After drawing hold up curves, it is possible extrapolating impeller speed critic ($N_{crit}$) for different flow rate. In Figure 7.4 shows the flooding curve for a E/R=1,5 and the working curve, related to an optimal rotational speed ($N_{opt}$) which is the 80% of $N_{crit}$.

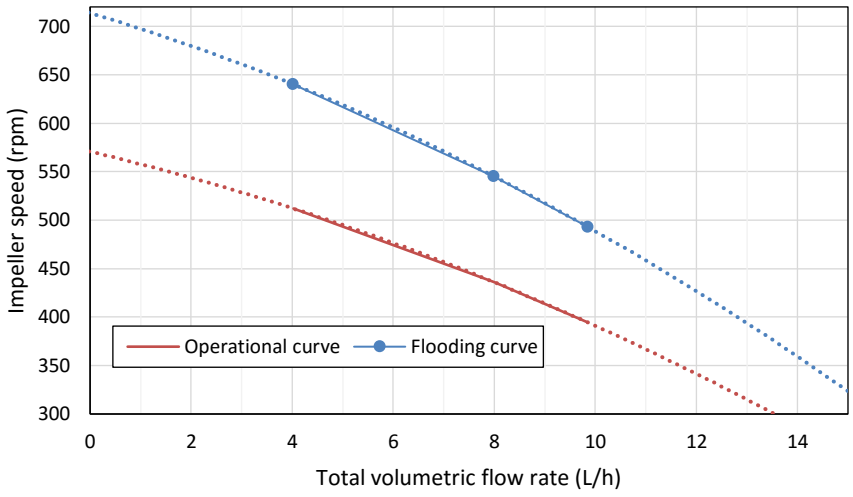


**Figure 7.4:** Flooding curve for Kuhni Column E/R=1.5 e=20% Water/Butyl-Acetate/Acetone system (shut down method)

In conclusion, it is possible to say:

- the hold up increases when the impeller speed rises;
- there is an impeller speed in which the hold up increases exponentially causing flooding;
- for high throughput, flooding happens with low speed of rotation;
- variations of hold up between fast sampling and shut down method has been found.
- working curve is the line that divide the map into two zones, allowed zone (below the line) and forbidden zone (above the line).

## 7.2 Mass transfer analysis

In Table 7.1 are shown the operating conditions of the experimental tests, direction of transfer and time to reach the stability.

**Table 7.1:** Operating condition for the experimental tests

| Test number | Mass transfer direction | E/R Extract Raffinate ratio (Theoretical) | Total flow rate (L/h) | Impeller speed (rpm) | Steady state (h) |
|---|---|---|---|---|---|
| D185-177 | c→d | 1,34 (1,5) | 10,7 | 396 | 2 |
| D185-178 | c→d | 1,47 (1,5) | 8,3 | 440 | 2,5 |
| D185-179 | c→d | 1,39 (1,5) | 4,2 | 517 | 4 |
| D185-180 | c→d | 2,41 (2,5) | 4,3 | 531 | 3,5 |

In the Table 7.2 is shown principal results of the tests.

**Table 7.2:** Main results of the tests at steady state

| Test number | Feed % w/w (acetone) | Extract % w/w (acetone) | Raffinate % w/w (acetone) | Hold up (shut down method) | NTS (Kremser's equation) |
|---|---|---|---|---|---|
| D185-177 | 10.40 | 7.64 | 0.11 | 14.9 | 9.5 |
| D185-178 | 10.40 | 7.29 | 0.07 | 14.8 | 10.3 |
| D185-179 | 12.47 | 8.77 | 0.17 | 9.3 | 8.1 |
| D185-180 | 9.59 | 4.23% | 0.01 | 13.1 | 6.6 |

For understanding the extraction performance of the column, it is possible to express it by using the number of theoretical stage (NTS), based on Kremser's equation (Laddha *et al.* 1978):

$$NTS = \frac{ln\left[\left(\frac{x_{ace}^{F} - x_{ace}^{S}/m}{x_{ace}^{R} - x_{ace}^{S}/m}\right)\left(1 - \frac{1}{E}\right) + \frac{1}{E}\right]}{ln\, E} \quad (7.1)$$

Where E is the mass extraction factor:

$$E = m_{mass}\frac{\dot{m}_s}{\dot{m}_F} \quad (7.2)$$

According to for the determination of the Sauter mean diameter of a drops population, Laso (1986) and Kentish (1997) suggested that a number minimum of 300 drops is necessary to provide a reasonable degree of accuracy in the determination of Sauter mean diameter. For each test, several snapshots have been used to evaluate this parameter.

The Sauter mean diameter is calculated according to the following equation:

$$d_{32} = \frac{\sum_{i=1}^{N} n_i d_i^3}{\sum_{i=1}^{N} n_i d_i^2} \quad (7.3)$$

**Table 7.3:** Sauter mean diameter and NTS obtained by experimentation

| Test number | d32 calculated from photography (mm) | Number of droplets |
|---|---|---|
| D185-177 | 0.97 | 307 |
| D185-178 | 0.81 | 333 |
| D185-179 | 0.51 | 297 |
| D185-180 | 0.50 | 225 |

The sampling with the syringe at the top of the column near the feed inlet, allowed to evaluate the jump concentration to justify the presence of the continuous axial dispersion. In fact, as it can be seen in Table 7.4 there's a concentration jump around the feed inlet, that confirms the presence of the axial dispersion in the continuous phase.

**Table 7.4:** Concentration jump at the inlet of the continuous phase

| Test number | Aqueous acetone feed inlet (%w/w) | Aqueous acetone near feed inlet(%w/w) | Aqueous acetone jump (%w/w) |
|---|---|---|---|
| D185-177 | 10.38 | 9.05 | 1.33 |
| D185-178 | 10.40 | 8.49 | 1.91 |
| D185-179 | 12.42 | 8.82 | 3.6 |
| D185-180 | 9.59 | 5.28 | 4.31 |

# 8 Post processing and model comparison

First of all, a sensitivity study about the principal parameters has been done. Five parameters of dispersion model have been taken under consideration:

- $K_{Ov}$;
- $D_{axc}$;
- $D_{axd}$;
- $d_{32}$;
- Holdup.

Each parameter has been multiplied by a factor from 0.1 to 1.5, taking the others constant. Simulations for an extraction case continuous to dispersed for a low throughput has been done. NTS and the incremental ratio have been calculated. The incremental ratio, shown in equation 8.1, allows to identify how much a variable affects the solution.

$$\left.\frac{\Delta \mathrm{NTS}}{\Delta x}\right|_{i+1} = \frac{NTS_{i+1} - NTS_i}{x_{i+1} - x_i} \tag{8.1}$$

Figure 8.1 shows the average incremental ratio for NTS for several parameters (Hold-up, $D_{ax}$, $d_{32}$, $K_{ov}$). The most susceptible parameters for the performance calculated by the model is the droplets size followed by mass transfer coefficient ($K_{ov}$) and Dispersed axial dispersion. The model shows a low sensitivity to hold up and axial dispersion coefficients for the continuous phase.

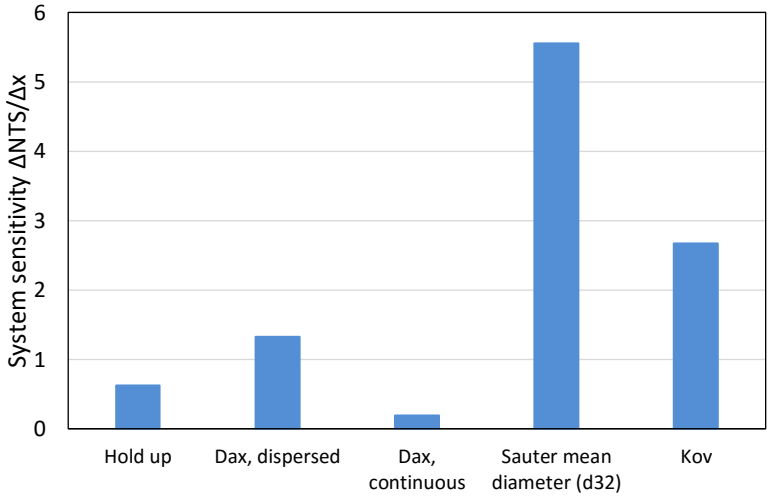


**Figure 8.1:** Sensitivity study of the five parameters of the dispersion model

The hold up data has compared to correlation, by using a direct method and a physical method. The same for d32. Furthermore, the two correlations have been modified after a sensibility studies to fit the experimental to the correlation results.

In order to find the best set, some parameter has to be fixed. In fact, there're too many degree of freedom, so it's necessary fix one correlation. Mass transfer correlation based on study of

Kumar and Hartland (1999) has been taken, because experimentation based on single drop mass transfer has a good degree of accuracy.

Furthermore, the study of sensibility has demonstrated that performance is not susceptible to the axial dispersion of the continuous phase. For this reason, the coefficient has been evaluated by Steinmetz's equation (2007) developed for a DN32.

## 8.1 Hold up and Sauter mean diameter direct method

### *8.1.1 Hold up*

Firstly, a comparison between holdup experimental and calculated by Kumar's correlation has been done. The given Figure 8.2 shows a parity plot of the experimental hold up to the hold-up correlation of Kumar and Hartland (1995). Two kinds of points have been plotted, Extract Raffinate ratio 1.5 and 2.5. A deviation around +40% between correlation and experimental points occurred.

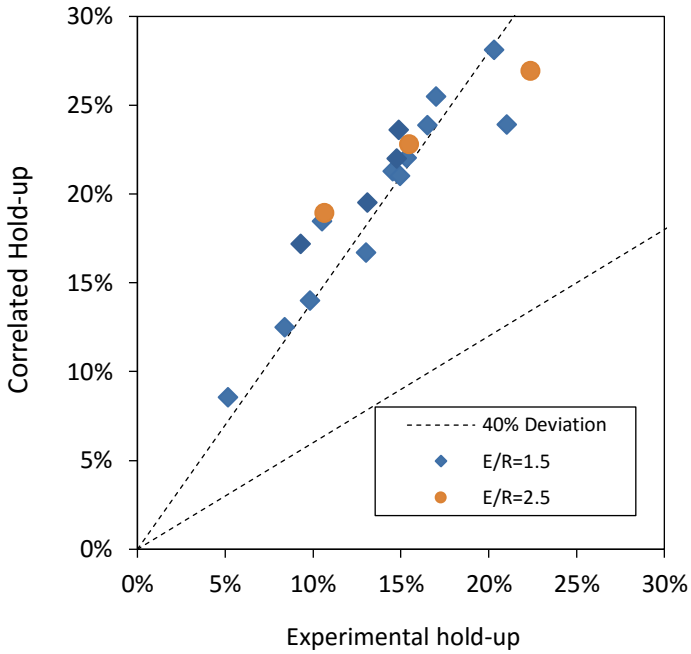


**Figure 8.2:** Parity plot of hold-up obtained by correlation of Kumar and Hartland (1995) and experimental values, using shut down method for two cases E/R 1.5 and 2.5

Kumar and Harland hold up equation is developed for a wide range of geometrical and operating condition, but this DN32 miniplant geometry are outside the range chosen by authors.

In order to fit the results, a modification of this correlation has been proposed. As already said, this correlation is a power law formed by different no dimensional groups, where each group has an exponent determined by the experimental way. A sensitivity study has allowed to identify that the dimensionless group has a greater influence on the hold up. Exponent n1 and n2 have been modified in order to obtain the minimum AARE possible. By using the average absolute value of the relative error (AARE), it's possible making a cmparison between the experimental data and the correlation results. AARE is defined as:

$$\text{AARE} = \frac{1}{\text{NDP}} \sum_{i=1}^{\text{NDP}} \frac{|\text{predicted value} - \text{experimental value}|}{\text{experimental value}} \tag{8.2}$$

NDP is the number of data points. In the Figure 8.3 a parity plot shows the comparison between experimental hold up values and modified Kumar and Hartland's correlation with an average error of 6.5%.

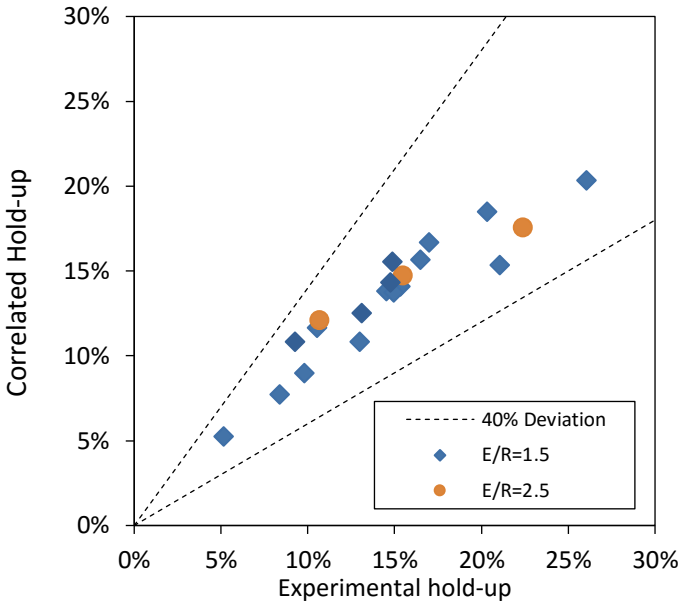


**Figure 8.3:** Parity plot of experimental hold up (shut down method) versus modified Kumar and Hartland's (1995) correlation with a 40% of deviation (dotted line)

After the modification, the correlation range of application is reduced. In the Table 8.1, constant value and range of applicability are given.

**Table 8.1:** Constant value and operating condition for modified Kumar Hartland's hold up correlation

| System | Mass transfer direction | Total flow rate (L/h) | Impeller speed (rpm) | $n_1$ constant | $n_2$ constant |
|---|---|---|---|---|---|
| Butyl acetate – water - acetone | c→d | 4-10 | 350-640 | 0.8292 | 0.7120 |

### *8.1.2 Sauter mean diameter direct method*

Droplets size has been evaluated by using two correlations reported in section 5.2.1. In the parity plot in Figure 8.4 is shown diameters calculated by different correlations. As it can be seen, all of them shows an average deviation lower than 25%. Experimental hold-up has been used for Fisher's correlation (it's hold-up dependent), and two constants (Hufnagl et al. 1991 and Lo et al. 1983). A modification of some constants of Kumar and Hartland's equation has been tested. In order to minimize AARE, after a sensitive study, two constants have been

chosen and varied. This modified equation is shown on the parity plot (Figure 8.5) compared to Kumar and Hartland's original correlation.

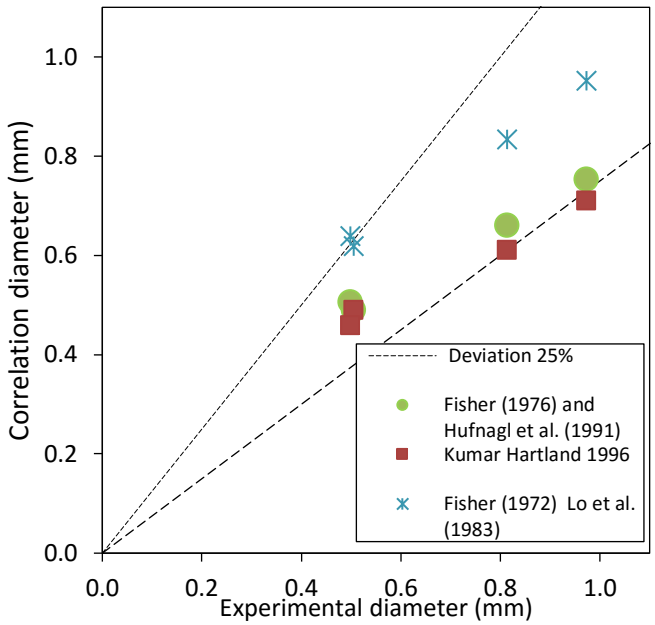


**Figure 8.4:** Parity plot of experimental diameter (photographic method) versus three different correlations and the deviation of 25% (dotted line)

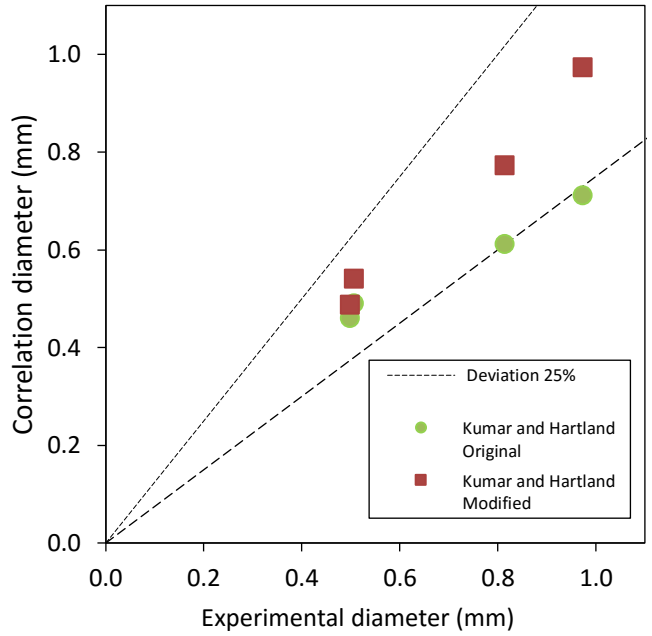


**Figure 8.5:** Parity plot of experimental diameter (photographic method) versus Kumar and Hartland's original correlation and Kumar and Hartland's modified correlation

The result of fitting the correlation to obtain the best match has a good accuracy with experimental values, but the range of application is narrow (Table 8.2). It's important remember that Kumar and Hartland's equation has been developed for a wide range of conditions and a modification can limit the range of validity.

**Table 8.2:** Constant values and operating condition for modified Kumar Hartland's correlation

| System | Mass transfer direction | Total flow rate (L/h) | Impeller speed (rpm) | $n_1$ constant | $C_\Pi$ constant |
|---|---|---|---|---|---|
| Butyl acetate – water - acetone | c→d | 4-10 | 390-540 | 1.6758 | 0.4267 |

## 8.2 Hold up and Sauter mean diameter physical method

### *8.2.1 Hold up and Sauter mean diameter implicit method*

As already said in section 5.3, in order to evaluate d32 or hold-up a physical method has been taken under consideration. This model offers a good approach to calculate hold up from d32 or d32 from hold up. In the first case, explicating hold-up from the equation (5.2) it's possible to obtain (Garthe 2006):

$$\varphi = \frac{v_{rs} - v_c + v_d}{2 \cdot v_{rs}} - \sqrt{\left(\frac{v_{rs} - v_c + v_d}{2 \cdot v_{rs}}\right) - \frac{v_d}{v_{rs}}} \tag{8.3}$$

And, remembering the "physical" equation (5.20) for calculating slip velocity:

$$v_{rs} = u_k(1 - \varphi)^m \tag{8.4}$$

It's possible to develop an iterative scheme that allows to calculate the hold-up from d32.Starting from d32 value, the impeller speed, the superficial velocity for each phase, these variables allow to determine the terminal velocity, the slowing factor. The first try of the hold-up has been chosen and it will allow to calculate the swarm factor and the slip velocity using the equation 8.4. Now, by using the equation 8.3 a new value of the hold-up is calculated and re-iterated until that the difference between the two hold up values is nil (Figure 8.6).Two possible scenarios have been tested. First is composed by Vignes' model for terminal velocity, Godfrey and Slater's for the swarm effect and Steinmetz for slowing factor. Otherwise, the second uses the model of Fang (Fang *et al.* 1995) for slowing factor (Table 8.3).

**Table 8.3:** Different scenarios for Hold up evaluation

| Scenario | Terminal velocity | Slowing factor | Swarm model |
|---|---|---|---|
| Scenario 1 | Vignes (1965) | Steinmetz (2007) | Godfrey and Slater (1991) |
| Scenario 2 | Vignes (1965) | Fang (1995) | Godfrey and Slater (1991) |

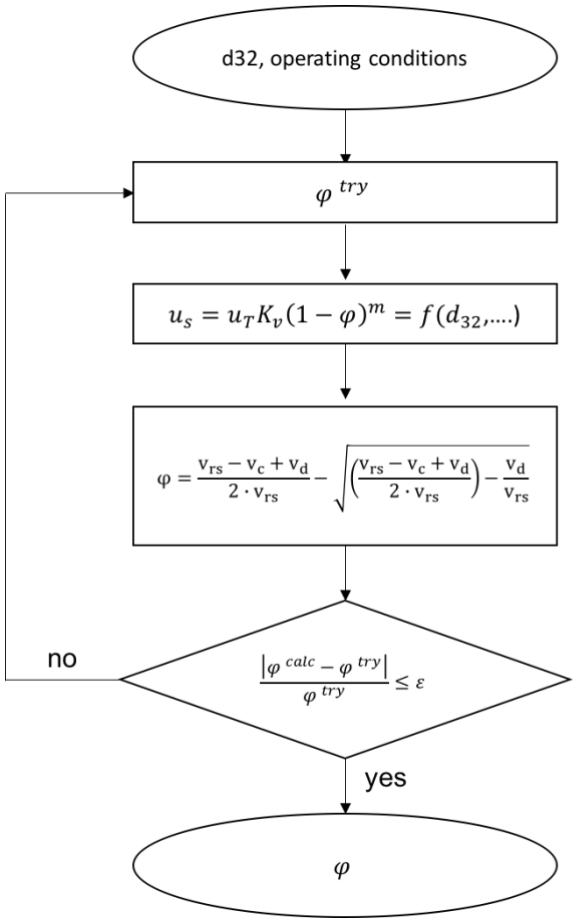


**Figure 8.6:** Iterative scheme for hold-up evaluation with a "physical" approach

In the Figure 8.7 a parity plot for scenario 1 is reported. Overall, the results by using this scenario show a huge deviation to the experimental points. Several points positioned on the x-axes haven't converged.

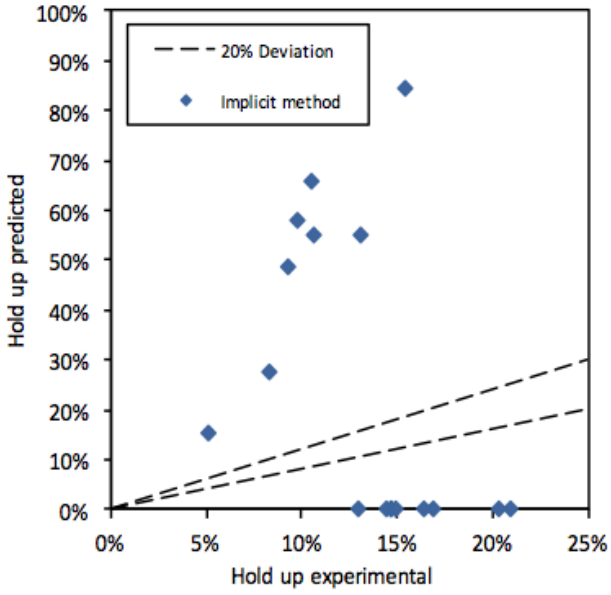


**Figure 8.7:** Parity plot of Scenario 1 (Vignes, Steinmetz, Godfrey and Slater) by using implicit method

By analysing scenario 2 (Figure 8.8) a high variation occurs between experimental and predicted hold up. Overall, second scenario offers a better result than the first scenario, which the presence of not converged points makes it an unstable method to use.

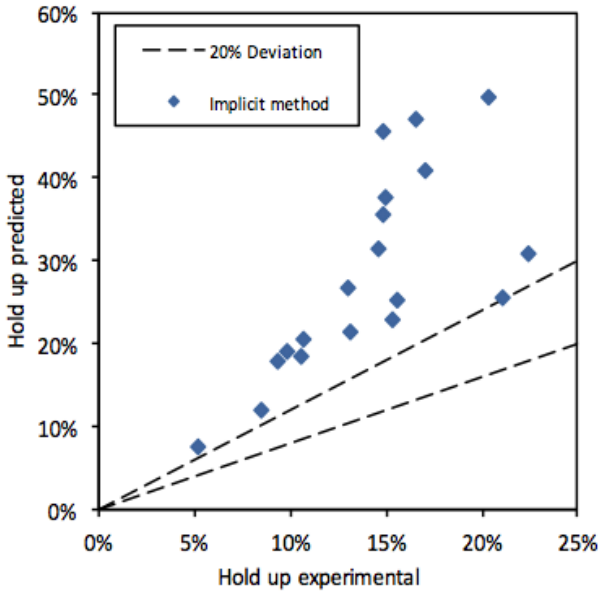


**Figure 8.8:** Parity plot of Scenario 2 (Vignes, Fang, Godfrey and Slater) by using implicit method

In order to fit the results, a modification of Fang's equation (equation 5.28 and 5.29) has been done. Parity plot of the Fang's modified equation is reported in Figure 8.9.

$$\gamma = 1.077 \cdot 10^{-5} Re_R \,/\, e \tag{8.5}$$

Overall hold-up predicted by using this method allows to obtain the results with an overall deviation lower than 20%

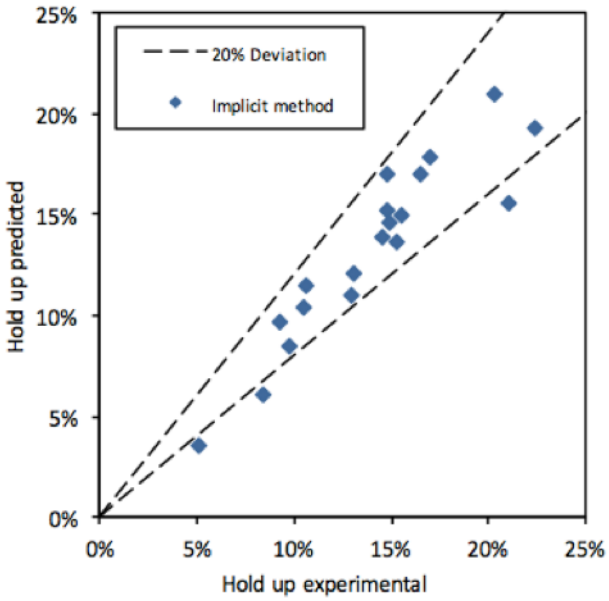


**Figure 8.9:** Parity plot of Scenario 2 (Vignes, Fang modified, Godfrey and Slater) by using implicit method

## 8.3 Dispersed axial coefficient correlation

In order to determine the best correlation for dispersed axial dispersion coefficient, an identification procedure has been applied. A group of simulations by using dispersion model has been conducted taking account of experimental values for d32 and hold up, and Kumar (1999) for mass transfer and Steinmetz (2007) for continuous axial dispersion.

**Table 8.4:** Parameters chosen for Dax,d evaluation

| Hold-up | Droplets size | Axial dispersion (continuous) | Mass transfer coefficient |
|---|---|---|---|
| Experimental | Experimental | Steinmetz (2007) (1) | Kumar and Hartland (1999) |

For each simulation, different correlations of Dax,d have been tested and compared to experimental NTS and then averaged. According to Hlawitschka (2013), best result is representing by Bauer's correlation.

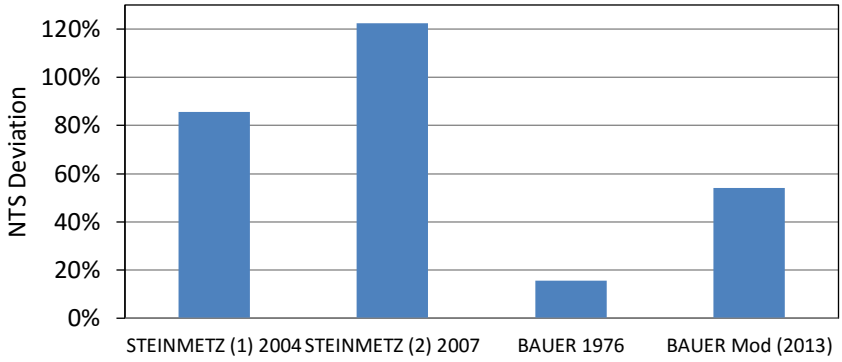


**Figure 8.10:** NTS Experimental deviation for several Dax,d correlation

## 8.4 Correlation comparison

In order to choose best set a comparison between the different set scenarios has been done. A scenario represents a set of correlations, modified or not modified which will be tested on the 1D axial simulator. After, solutions in term of d32, hold-up and NTS have been compared to experimental values. The criteria of choice selected was:

- A set composed by correlation less modified as possible, because modifications reduce the range of applicability of an equation;
- Minimum error committed.

First criterion is more important than the other, because aim of this work is to find the best correlations from literature, tested with several experimental points. In this case the number of experimental tests doesn't allow a number satisfactory of data to create a good extensible correlation. But in the case that no good solutions occur with this analysis, a modification of correlation has been taking under consideration.

In section 8.1 mass transfer and continuous axial dispersion coefficient correlations have been chosen for the reasons already mentioned. In section 8.2 two ways for evaluating d32 and

hold up have been explained. In the table Table 8.5 two scenarios have been taking under consideration.

**Table 8.5:** Two different scenarios chosen

| | **Hold-up** | **Droplets size** | **Axial dispersion (continuous)** | **Axial dispersion (dispersed)** | **Mass transfer coefficient** |
|---|---|---|---|---|---|
| Scenario 1 | Kumar and Hartland (1995) | Kumar and Hartland (1996) | Steinmetz (2007) (1) | Bauer (1976) | Kumar and Hartland (1999) |
| Scenario 2 | Fang (1995) Godfrey and Slater (1991) Vignes | Kumar and Hartland (1996) | Steinmetz (2007) (1) | Bauer (1976) | Kumar and Hartland (1999) |

Each scenario is a combination of two fixed correlations plus three variables correlations. These last three have been implemented original and modified, so total number of simulation for scenario are nine (Table 8.6).

In the bar chart (Figure 8.11, Figure 8.12) are shown the results of simulation, where the bar represents the deviation between the predicted and experimental values (NTS, d32, hold up). Overall, it's possible to see that the best result of course is that modified completely. But this not respect the criteria of choice that we have already discussed. By comparing 000 of the two scenarios, no significant deviations occur. The error on the performance is limited. In fact, the most of simulations, NTS has an error less than 10%.

**Table 8.6:** Nine simulations for each scenario. Code is the name

| **Code** | **Hold up** | **d32** | **Dax,d** |
|---|---|---|---|
| OOO | Original | Original | Original |
| MOO | Modified | Original | Original |
| MMO | Modified | Modified | Original |
| MMM | Modified | Modified | Modified |
| OMM | Original | Modified | Modified |
| OOM | Original | Original | Modified |
| MOM | Modified | Original | Modified |
| OMO | Original | Modified | Original |

The principal issue of scenario 1, it's that the implicit method doesn't reach convergence. In the simulations 000, M00, MM0, calculated hold-up from several iterations exceeds 100%, that's not possible. 00M offers a good solution with just one modification of Fang's correlation (equation 8.5).

Simulation with original correlation of the scenario 2 (000) also if there's a significant deviation of the hold up, the result in terms of performance is satisfactory. By following the criteria already discussed, simulation 000 has been chosen as final set of correlation.

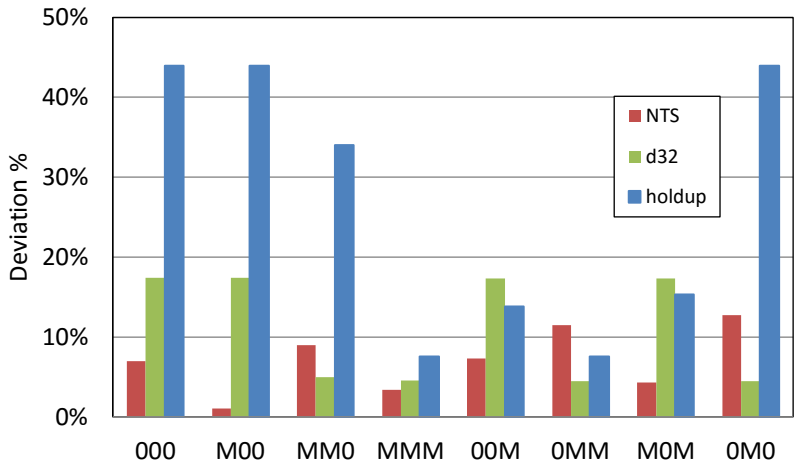


**Figure 8.11:** Scenario 1, Implicit method for hold up, Bauer and Kumar and Hartland (1996) for d32

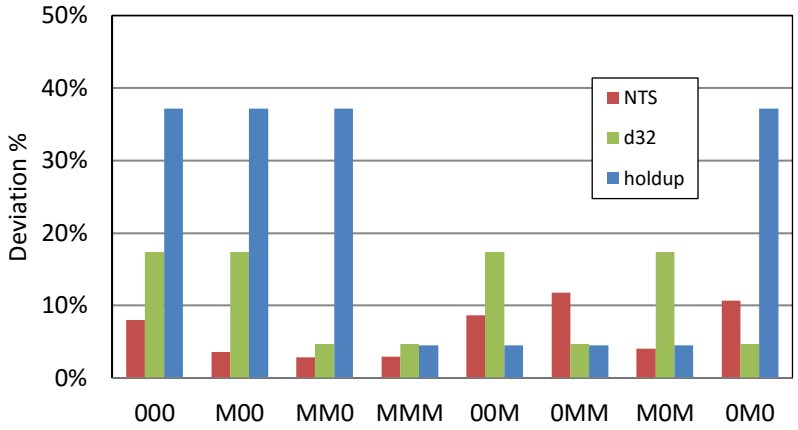


**Figure 8.12:** Scenario 2, Kumar and Hartland for hold up, Bauer and Kumar and Hartland (1996) for d32

## 8.5 Final result

In the Table 8.7 the final set of correlation chosen is shown. Axial dispersion model needs five parameters and six correlations to work.

**Table 8.7:** Final set of correlation chosen

| Hold-up | Droplets size | Axial dispersion (continuous) | Axial dispersion (dispersed) | Mass transfer coefficient |
|---|---|---|---|---|
| Kumar and Hartland (1995) | Kumar and Hartland (1996) | Steinmetz (2007) (1) | Bauer (1976) | Kumar and Hartland (1999) |

Figure 8.13 reports in abscises concentration of acetone in weight of the continuous aqueous phase and in ordinates acetone in organic dispersed phase. Each point of azure curve or operating line is the concentration of solute in each point through the column. A deviation is

also possible to see by observing the raffinate values. In this case effect of measuring system, operational mode has affected the result. Furthermore, the low concentration of acetone can be affected by an instrumental (GC) error. However, the good agreement model/system evidences the presence of axial dispersion in the Kuhni column.

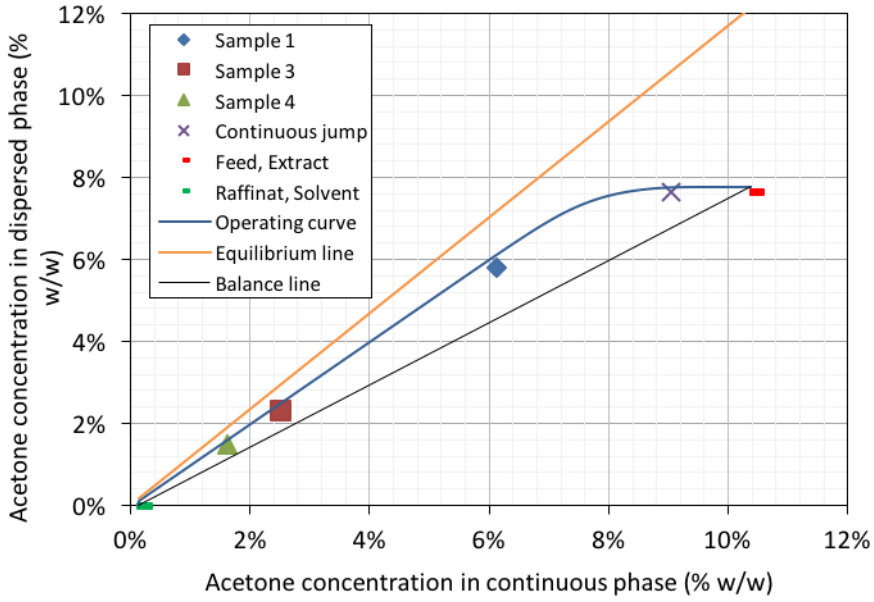


**Figure 8.13:** D185-177 model and experimental values concentration plot comparison. E/R=1.5, Q=10.7 L/h and N=396 rpm.

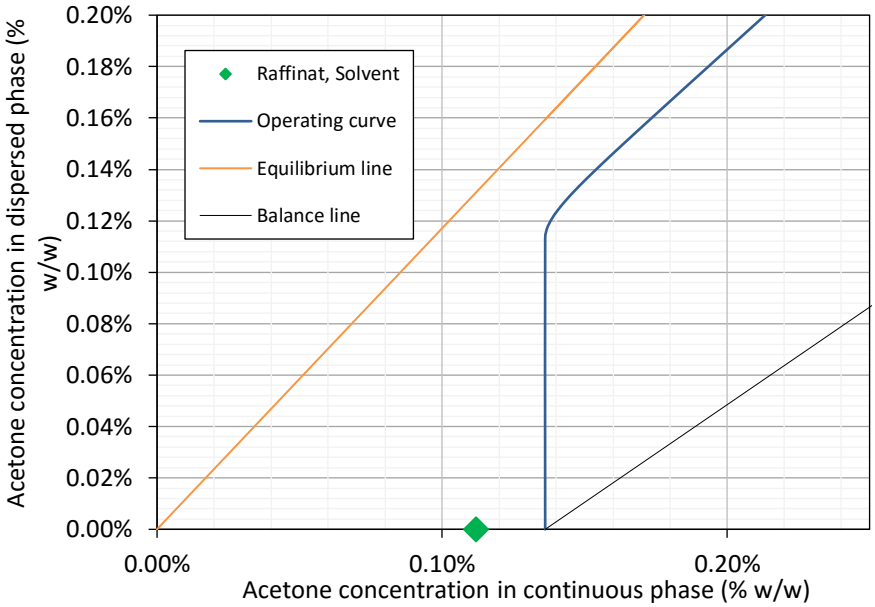


**Figure 8.14:** D185-177 raffinate concentration model/experiment zoomed near the raffinate outlet

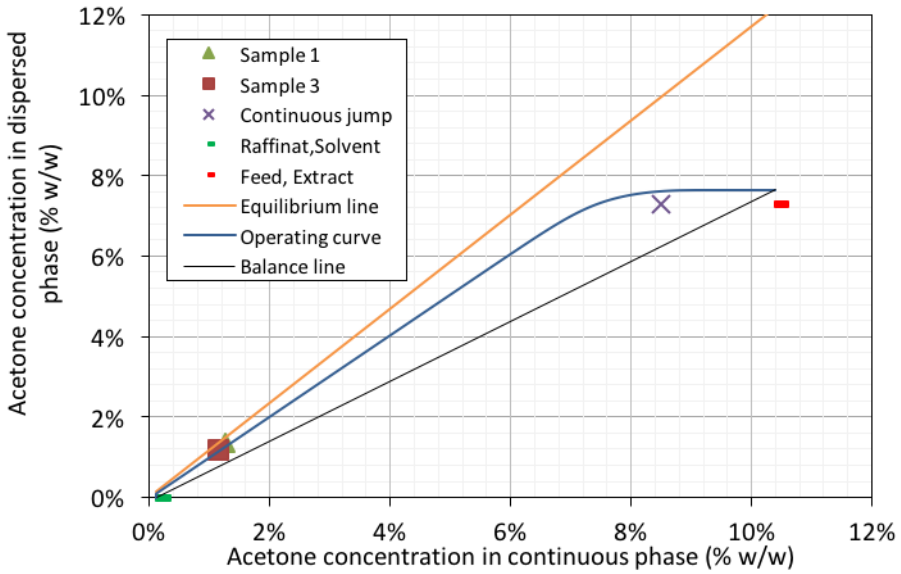


**Figure 8.15:** D185-178 model and experimental values concentration plot comparison. E/R=1.5, Q=8.3 L/h and N=440 rpm.

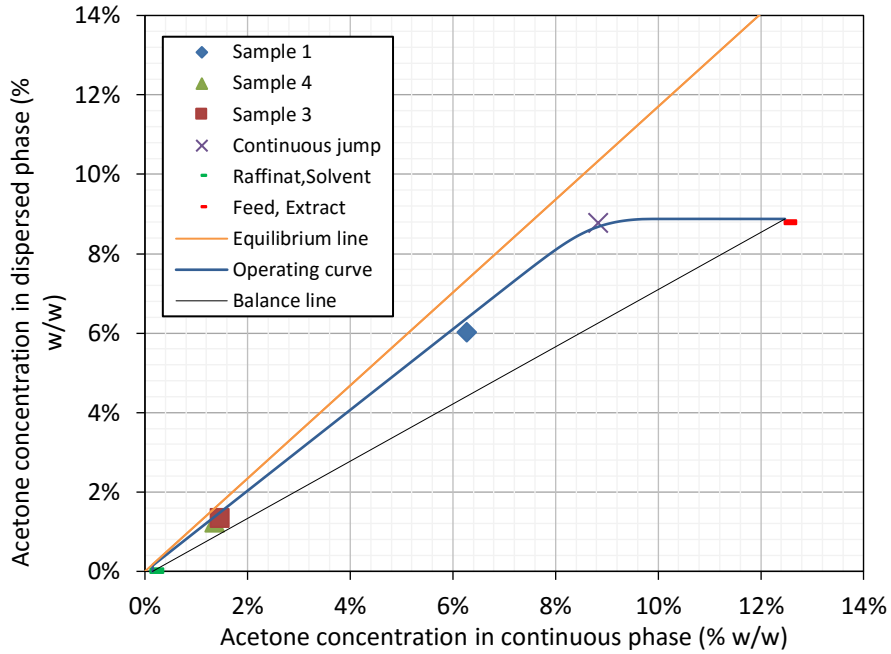


**Figure 8.16**: D85-179 model and experimental values concentration plot comparison E/R=1.5, Q=4.2 L/h and N=517 rpm

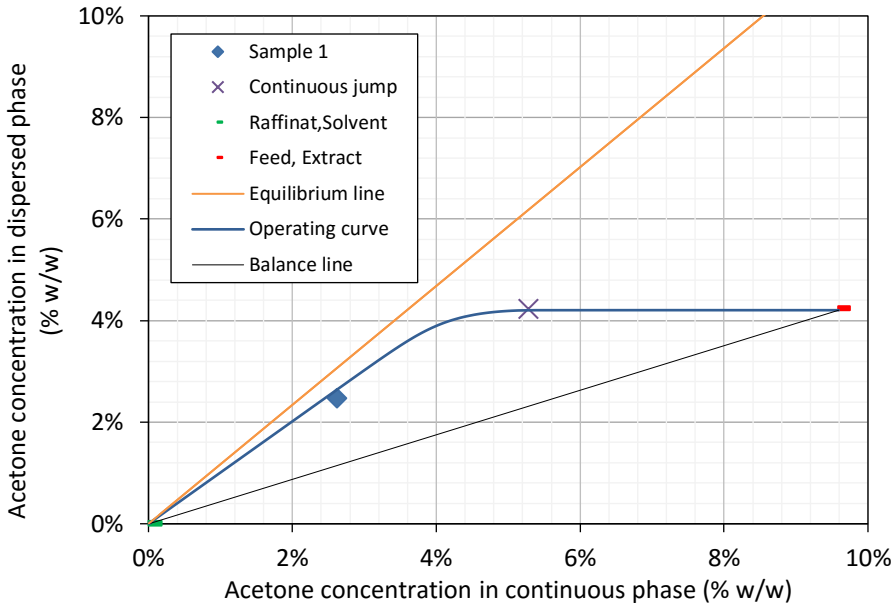


**Figure 8.17:** D180 model and experimental values concentration plot comparison. E/R=2.5, Q=4.3 L/h and N=513 rpm

**Table 8.8**: Hold up droplet size and NTS experimental/ predicted

| N° Test | Hold up % | | Droplet size (mm) | | NTS | |
|---|---|---|---|---|---|---|
| | Experimental | Calculated | Experimental | Calculated | Experimental | Calculated |
| D185-177 | 14.9 | 22.6 | 0.97 | 0.69 | 9.5 | 8.9 |
| D185-178 | 14.8 | 22.4 | 0.81 | 0.59 | 10.3 | 9.0 |
| D185-179 | 9.3 | 17.2 | 0.51 | 0.48 | 8.1 | 8.5 |
| D185-180 | 13.1 | 20.0 | 0.50 | 0.46 | 6.6 | 7.1 |

# 9 Axial dispersion 1D model applied to real system

The application of the axial dispersion model to the real system is the next step of this work. Model and correlation identification of a standard system has allowed the possibility to describe with an easy way a complicated series of chemical and physical phenomena with a good degree of accuracy. An improvement of the previous model has been done (equation 9.1).

$$\begin{cases} (1-\varphi)\dfrac{dC_{c,i}}{dt} = D_{axc,i}\dfrac{d^2C_{c,i}}{dz^2} - \dfrac{d(v_c \cdot C_{c,i})}{dz} - k_{Oc}a\left(C_{c,i} - C^*_{c,i}\right) - R_{i,c} \\ \varphi\dfrac{dC_{d,i}}{dt} = D_{axd,i}\dfrac{d^2C_{d,i}}{dz^2} + \dfrac{d(v_d \cdot C_{d,i})}{dz} + k_{Oc}a\left(C_{c,i} - C^*_{c,i}\right) - R_{i,d} \end{cases} \tag{9.1}$$

The 1D axial dispersion reaction model considers the effects of volumetric flow rate change along the column, the chemical reactions and the effect of variable coefficient of distribution. A model has been developed (IFP 2016) that correlates distribution ratio in function of A and B, E ratio.

$$\mathrm{m}^{\frac{aq}{org}} = m_i^0\left(m_i^{min} + (1 - m_i^{min})\exp(-\frac{T}{\tau})\right) \tag{9.2}$$

where:

$$\mathrm{T} = \frac{m_A + m_B}{m_E} \tag{9.3}$$

And $m_i^0$, $m_i^{min}$, $\tau$ are parameters in function to the component "i".

In order to solve the system of equation differential for multicomponent system (more than 3 components) a mathematical simulator in Fortran has used. A modification of the 1-D model already developed (IFP 2016) has allowed to taking account these effects.

## 9.1 Comparison between two models

In order to verify Fortran simulator, a comparison with analytical solutions for same operating condition has been done.

Two ways are proposed to verify the simulator:

- Comparison of a chemical extraction by using the analytical model (dispersion model in Appendix A.2);
- Comparison of a chemical reaction in a PFR.

### *9.1.1 Analytical extraction vs numerical extraction*

For a fixed operating condition, an extraction problem has been resolved by using the two methods. Figure 9.1 shows the two solutions, analytical (blue) and numerical (red) in concentration plot. As it can be seen there is no significate deviation between two trends.

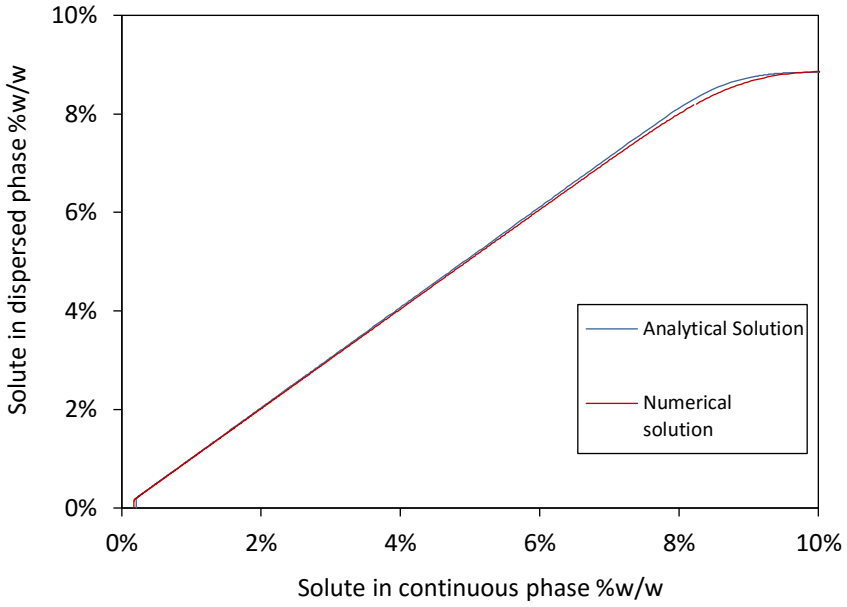


**Figure 9.1:** Numerical and analytical solution comparison for a 1D dispersion extraction problem

### *9.1.2 Analytical vs numerical plug flow reactor*

A plug flow reactor performs a generic chemical reaction described by 2A+B→C (with an inert D). The solutions in Figure 9.2 shows a slight deviation between two methods, that can be related to numerical error, but no significant differences occur.

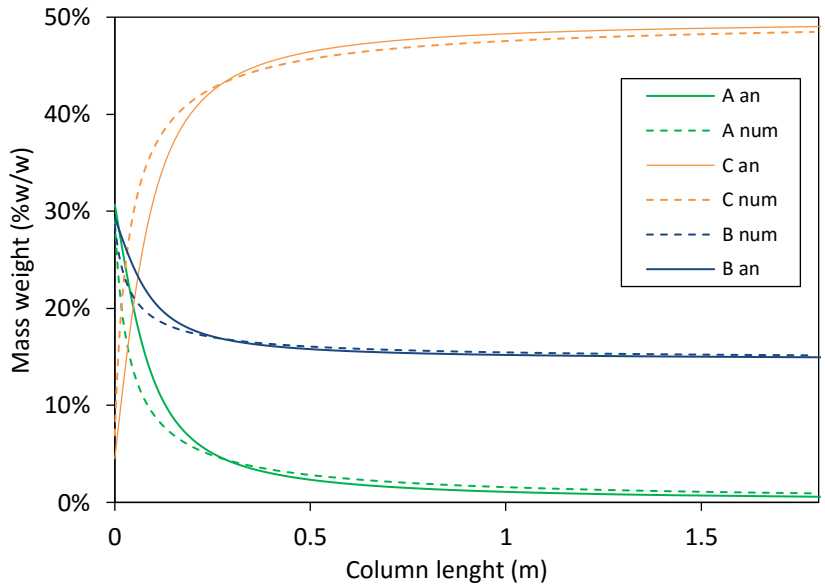


**Figure 9.2:** Numerical (Num, dotted line) and analytical (an, continuos line) solution comparison for a PFR 2A+B→C reaction problem. Plot of concentration of species in function of the length of the reactor

## 9.2 Real system extraction

### *9.2.1 Washing zone - Extraction*

Two series of experimental tests of washing (without chemical reaction) with synthetic charge feed (26) and real feed (27) has been compared to the mathematical model. These first simulations have been conducted by using the experimental hold up and the others parameters have been derived from best set of correlation found in the previous chapter.

In the bar chart (Figure 9.3), the comparison between experimental and predicted by simulator efficiency of separation for several species in the charge has shown. Green bar represents the simulation while the red bars experimental results. For the D185-26 test, for several species, the simulator predicts with a low deviation, but there's the presence of a high deviation for J.

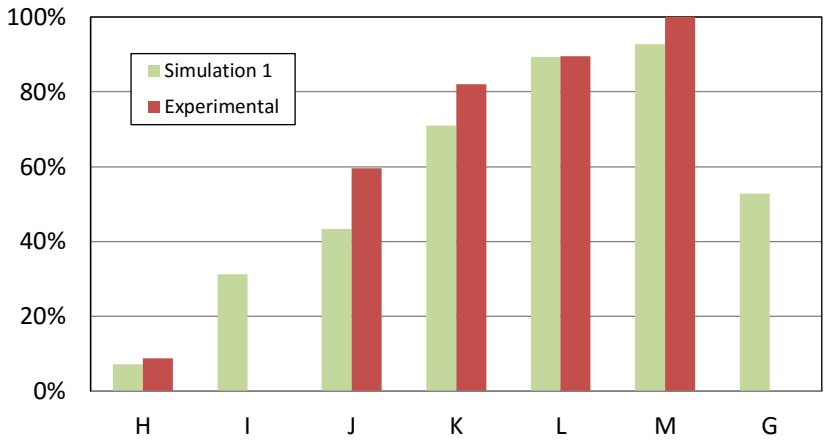


**Figure 9.3:** D185-26 Experimental test efficiency comparison

In Figure 9.4 the bar chart for D0185-27 has shown. Some component predicted by model shows a high deviation respect to experimental value. N, L and J show an abnormal behaviour respect the D0185-26.

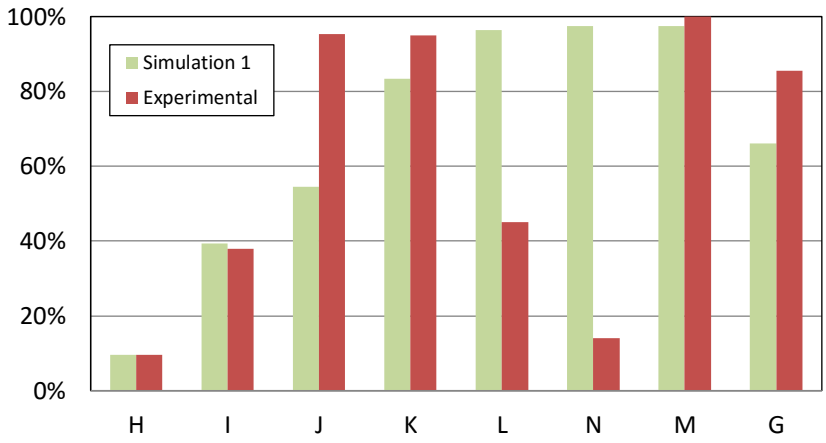


**Figure 9.4:** D185-27 Experimental test efficiency comparison

Overall, the dispersion model with distribution ratio variables remains correct for certain species but incorrect for others. It has been verified that the system, at the operating condition concerned, is sensitive to distribution ratio and interfacial tension and hence, mass transfer

condition and droplet size. On the other hand, it has to take account the presence in the real system of more hundreds of components that can affect the final result.

### *9.2.2 Back washing zone – Extraction with reaction*

The aim of backwashing zone, as already said, is to convert G into A and B. Augier et al. (IFP 2017) have found operating condition to allow a good conversion of G. High residence time with low throughput allows at the reaction to proceed. Hence, in this case it's possible to say that there's no a high influence of the result of the mass transfer, in fact high residence time allows the system to reach the equilibrium. By using the simulator and imposing the set of correlation simulations have been done. Chemical reaction has been described by equation 9.4:

$$G + E \leftrightarrow 2\,A + B \tag{9.4}$$

where the kinetic form proposed is expressed in equation 9.5:

$$\mathrm{R} = k_{dir}[G][E] - k_{inv}[A]^2[B] \tag{9.5}$$

The effect of the homogenous catalyser ($[H^+]$) has been taken account into the kinetic constant, derived from experimental test conducted.

In Figure 9.5 is shown the parity plot of G's efficiency of separation between experimental and predicted values of 20 different experiments (for 1% and 3%). Overall, the model predicts the efficiency of separation of G with good accuracy. Three tests (3% of Acid) have shown a high deviation respect the others.

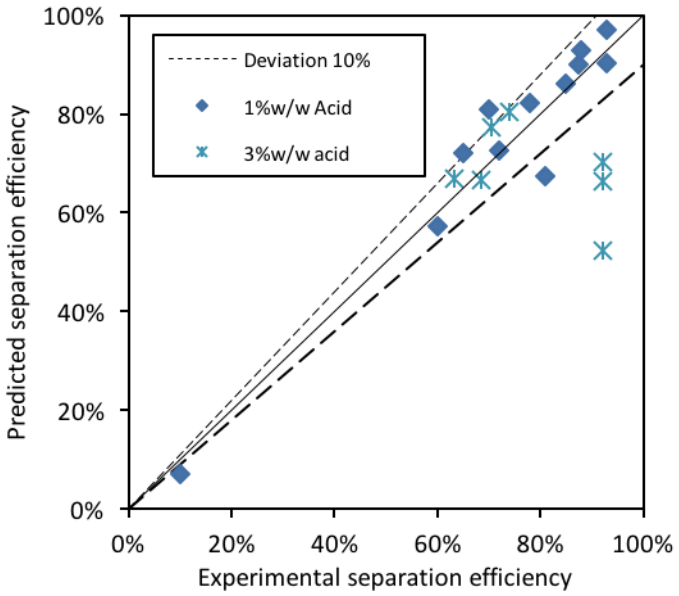


**Figure 9.5:** Parity plot of G's separation efficiency between the experimental values (x-axis) and the model prediction (y-axis)

Same results are shown in the bar chart Figure 9.6, for each experimental test. As it can be seen, in the same way, model prediction of D0185-37, D0185-38, D0185-39 provide different result respect the experimental tests. The other simulations show a low deviation (around 5%).

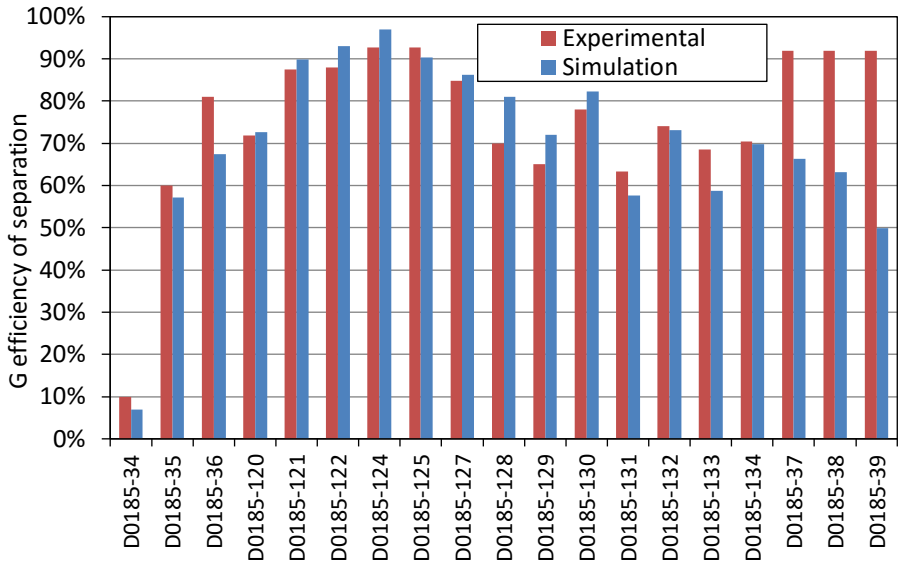


**Figure 9.6:** G's efficiency of separation for different operating condition

# 10 Conclusion

The modelling of a liquid-liquid extraction equipment for an IFP bio-sourced process project has taken under consideration.
It has been confirmed mathematically that for a DN32 ternary liquid system composed by two immiscible liquids and a solute, the column description by using a plug flow approach leads the deviation of the experimental value. In the Kuhni DN32 column, effect of back and forward mixing, channelling, and others aren't negligible. By taking account of these effects, using a model that describe the axial dispersion effect, it has been possible to predict the performance of the column with a good degree of accuracy, according to the experimental data. For the mathematical differential model concerned, it exists an analytical solution.
In order to solve the system of the equations of the axial dispersion model, five parameters (d32, hold-up, mass transfer coefficient, axial dispersion coefficient continuous and dispersed) have to be determined by correlations, which relate geometrical, physical and operating conditions. Several correlations are available in literature.

The aim of these parts was finding the best set of correlations to apply to axial dispersion model. Experimental tests, by using Kuhni DN32 and a standard ternary system, have been conducted. First of all, for several operating conditions, a series hydrodynamic tests allowed to know flooding curve and optimal working curve. Secondly, a series of mass transfer tests allowed to evaluate d32 (photographic method), concentration jump (correlated to axial dispersion), hold up, and raffinate and extract concentration. These collected data has allowed step by step to recognize the best correlations. On the cases studied, mathematical model shows that three parameters (mass transfer coefficient, d32 and Dax,d) affect significantly the performance of the column. By using different criteria of comparison, the best set of correlation has been found. The best set is composed by correlation of Kumar and Hartland (1995) for hold up, Kumar and Hartland (1996) for droplet size, Kumar and Hartland (1999) for mass transfer coefficients, Bauer (1976) for dispersed axial dispersion coefficient and Steinmetz (2007) for continuous axial dispersion coefficient. Performances in term of NTS and %w/w is well predicted by this model. On the other hand, the droplet size and hold up show a deviation from experimental data.
Implicit method to evaluate hold-up, based on a physical model doesn't report a good accuracy. The issues can be related to the mathematical iterative scheme or, for certain phenomena present into the column, which, the physical model to slip velocity doesn't able to describe. Nevertheless, this method offers the possibility to calculate without empirical correlation this important parameter, and it performs an alternative way for evaluating hold-up.

The predictive set of correlations applied to axial dispersion model has been tested on a washing and back washing case of the Biobutterfly project. Thanks to the experimental data collected (IFP 2017, IFP 2016 and IFP 2015) a comparison has been possible. In washing tests, the model reports a good response for certain chemical species as in the test D0185-26, but the others show a fluctuant deviation (D0185-27). That's can be related to the presence of many compounds in the feed, which could affect the thermodynamic conditions of the system, or distribution ratios. But not only, the limitation of the model/correlation.
The performance of separation, as it has been possible to see in D0185-26 are slightly less in the model than in experimental data. This could be a related not only to distribution ration, but also to an error of the empirical correlation especially of $d_{32}$ and axial dispersion equations which overestimate the real values (reducing the performance). In D0185-27 the fluctuating deviations (and not a systematic error occurs as in the previous simulation) between

experimental and model allows to understand that in this case the error may be caused by a distribution ratio and propriety (interfacial tension) deviation firstly, but also the effect of variation of the model as already said.

For the back-washing application, only the G's performance of extraction has been studied. The model reports a good result to experimental data. A huge deviation is shown for three different points. Here, high residence time of the phases allows to have a less influence to parameters which play a fundamental role in mass transfer (axial dispersion, d32, mass transfer coefficient). The variables important to know in the case of back washing are distribution ratio and kinetic constant which represent the rate determining step.

Overall, this model can perform satisfactory results without using a complicated method of calculation. An improvement useful to study hydrodynamics and for a better degree of accuracy is using dispersed model with balance population model (BPM) (Mohanty 2000 and Buchbender 2012). This model takes account the droplets size distribution in function to time, position and physical and operating conditions. In the BPM model the knowledge of source term as coalescence and sink term as breakage is required. The calculation of droplets velocity used to determine parameter into the population model is based on terminal velocity, swarm factor and slowing factor described in chapter 5.
Another improvement of balance population dispersed model, that allows a better degree of accuracy is the application of a CFD (3D system) and balance population mode (CFD-BPM) (Hlawitschka 2013). CFD-BPM allows a good description of the hydrodynamics (hold-up and also d32) and mass transfer phenomena along the column. Several recent studies have reported the power of this method which requires, on the other hand, a severe deep mathematical implementation, complicated parameters and correlations, long time for computing (10-20 days for each simulations) and sometimes expensive software.

# Bibliography


Augier F., 2001, Structure locale du champ hydrodynamique dans le écoulements disperses liquide-liquide concentres. Ph.D. dissertation, Institut National Polytechnique de Toulouse, Toulouse, France.

Bauer R., 1976, Die Längsvermischung beider Phasen in einer gerührten Fest/Flüssig-Extraktionskolonne. Ph.D. dissertation, ETH, Zürich, Switzerland.

Breysse J., Bühlmann U. and Godfrey J. C., 1983, Axial Mixing Characteristics of industrial and Pilot Scale Kuhni Column. *AIChE Symp*. **80** (238), 94-101.

Buchbender F., 2013, Single Drop Based Modelling of Drop Residence Times in Kuhni. Ph.D. dissertation, RWTH Aachen University, Aachen, Germany.

Buchbender F., Onink F., Meindersma W., de Haan A. and Pfnnig A., 2012, Simulation of aromatics extraction with anionic liquid in a pilot-plant Kuhni extractor based on single-drop experiments. *Chem. Eng. Science.* **82**, 167-176.

Fang J., Godfrey J. C., Mao Z.-Q., Slater M. J. and Gourdon C., 1995, Single Liquid Drop Breakage Probabilities and Characteristic Velocities in Kühni Columns. *Chem. Eng. Technol*. **18**, 41-48.

Fischer E. A., 1973, Hydrodynamik und Stoffaustausch in einer Flüssig-Flüssig-Rührextraktionskolonne. Zürich Juris Druck Verlag, Zürich, Switzerland.

Garthe D., 2006, Fluiddynamics and Mass Transfer of Single Particles and Swarms of Particles in Extraction Columns. Ph.D. dissertation, Lehrstuhl für Fluidverfahrenstechnik Technische Universität, München, Germany.

Godfrey J. C. and Slater M. J., 1991, Slip Velocity Relationships for Liquid-Liquid Extraction Columns. *Trans. I.Chem.E*. **69** (3) Part A, 130-141.

Gourdon C., Casamatta G. and Muratet G., 1994, Population balance based modelling of solvent extraction columns. In: Godfrey and Slater M.J., *Liquid-liquid extraction equipment,* John Wiley & Sons, New York, USA, 137-226.

Grace J. R., Wairegi T. H. and Nguyen N. T., 1976, Shapes and Velocities of Single Drops and Bubbles Moving Freely Through Immiscible Liquids. *Trans. Inst. Chem. Eng.* **54**, 167-173.

Grand View Research, 2016, Petrochemicals Market Analysis By Product By And Segment Forecasts, 2014-2025, San Francisco, USA.

Hemmati A., Torab-Mostaedi M. and Asadollahzadeh M., 2015, Mass transfer coefficients in a Kuhni extraction column. *AIChE J.* **93,** 747-754.

Hamielec A. E. and Johnson A. I., 1962, Viscous flow around fluid spheres at intermediate Reynolds numbers. *Can. J. Chem. Eng.* **40**, 41-45.

Henschke M., 2004, Auslegung Pulsierter Siebbodenextraktionskolonnen. Shaker Verlag, Aachen, Germany.

Hlawitschka M., 2013, Computational Fluid Dynamics Aided Design of Stirred Liquid-Liquid Extraction Columns. Ph.D. dissertation, Technischen Universität Kaiserslautern zur Verleihung, Kaiserslautern, Germany.

Hufnagl H., McIntyre M. and Blaß E., 1991, Dynamic behaviour and simulation of a liquid-liquid extraction column. *Chem. Eng. Technol*. **14**, 301-306.

Kolb P., Bart H.-J. and Fischer L., 2002, Liquid-Liquid miniplant extractor - a novel tool for process design. *International solvent extraction conference ISEC* (2002), Cape Town, South Africa, 17-21 March 2002,1382-1387.

Kumar A. and Hartland S., 1999, Correlations for Prediction of Mass Transfer Coefficients in Single Drop Systems and Liquid-Liquid Extraction Columns. *Trans. I. Chem. Eng*. **77** (Part A), 372-84.

Kumar A. and Hartland S., 1995, A unified correlation for the prediction of dispersed- phase hold-up in liquid–liquid extraction columns. *Ind. Eng. Chem. Res*. **34**, 3925–3940.

Kumar A. and Hartland S., 1996, Unified correlations for the prediction of drop size in liquid–liquid extraction columns. *Ind. Eng. Chem. Res*. **35**, 2682–2695.

Leybros J., 2004, Extraction liquide-liquide - Modélisation des colonne. *Techniques de l'Ingénieur* **J2765**, 1-20.

Laddha G. S. and Degaleesan T. E., 1978, *Transport Phenomena in Liquid Extraction,* McGraw-Hill, New York, USA.

Lo T. C., Baird M. H. and Hanson I. C., 1983, *Handbook of Solvent Extraction,* Wiley-Interscience, New York, USA.

Misek T., Berger R. and Schoter J., 1985, *Standard test systems for liquid extraction 2nd ed.,* EFCE Pub, Rugby, United Kingdom.

Modes G., 2000, Populationsdynamik einer Extraktionskolonne auf Basis von Einzeltropfenun- tersuchungen. Ph.D. dissertation, Technischen Universität Kaiserslautern zur Verleihung, Kaiserslautern, Germany.

Mohanty S., 2000, Modeling of Liquid-Liquid Extraction Column: A Review. *Rev. in Chem. Eng.* **16**(3), 199-248.

Pratt H.R.C. and Hanson C., 1982, Selection, Pilot Testing and Scale-up of Commercial Extractors. In: Lo T. C., Baird M. H. I. and Hanson C. *Handbook of Solvent Extraction, John Wiley & Sons*, New York, USA.

Rydberg J., 2004, *Solvent Extraction Principles and Practice, Revised and Expanded,* CRC Press, Boca Raton, USA.

Seikova I., Gourdon C. and Casamatta G., 1992, Single drop transport in a Kuhni extraction column. *Chem. Eng. Sci*. **47**, 4141–4154.

Steinmetz T., 2007, Tropfenpopulationsbilanzgestu¨tztes Auslegungsverfahren zur Skalierung einer geru¨hrten Miniplant-Extraktionskolonne. Ph.D. dissertation, Technischen Universität Kaiserslautern zur Verleihung, Kaiserslautern, Germany.

Steinmetz T. and H.-J. Bart, 2004, Droplet Hydrodynamics in a Kühni-Miniplant Extraction Column. *CHISA 2004, 16th International Congress of Chemical and Process Engineering,* Prague, Czech Republic, 22 -26 August 2004, 1111 – 1121.

Ziegler N. N. and Li E. N., 1967, Effect of mass transfer axial mixing. *Ind. Eng. Chem.* ***59*** (3), 30–36.

# Ringraziamenti

Desidero ringraziare i miei colleghi dell'IFP-EN, i miei supervisori, prof. Frédéric Augier, l'ing. Damien Leinkugel e l'ing. Helena Gonzàlez Peñas. I miei colleghi del Politecnico, Andrea, Gabriele, Giacomo, Luigi, Mariachiara, Simone e Vincenzo. Ringrazio inoltre Carlotta e la mia famiglia.

# Appendix 1: PID Kuhni DN32

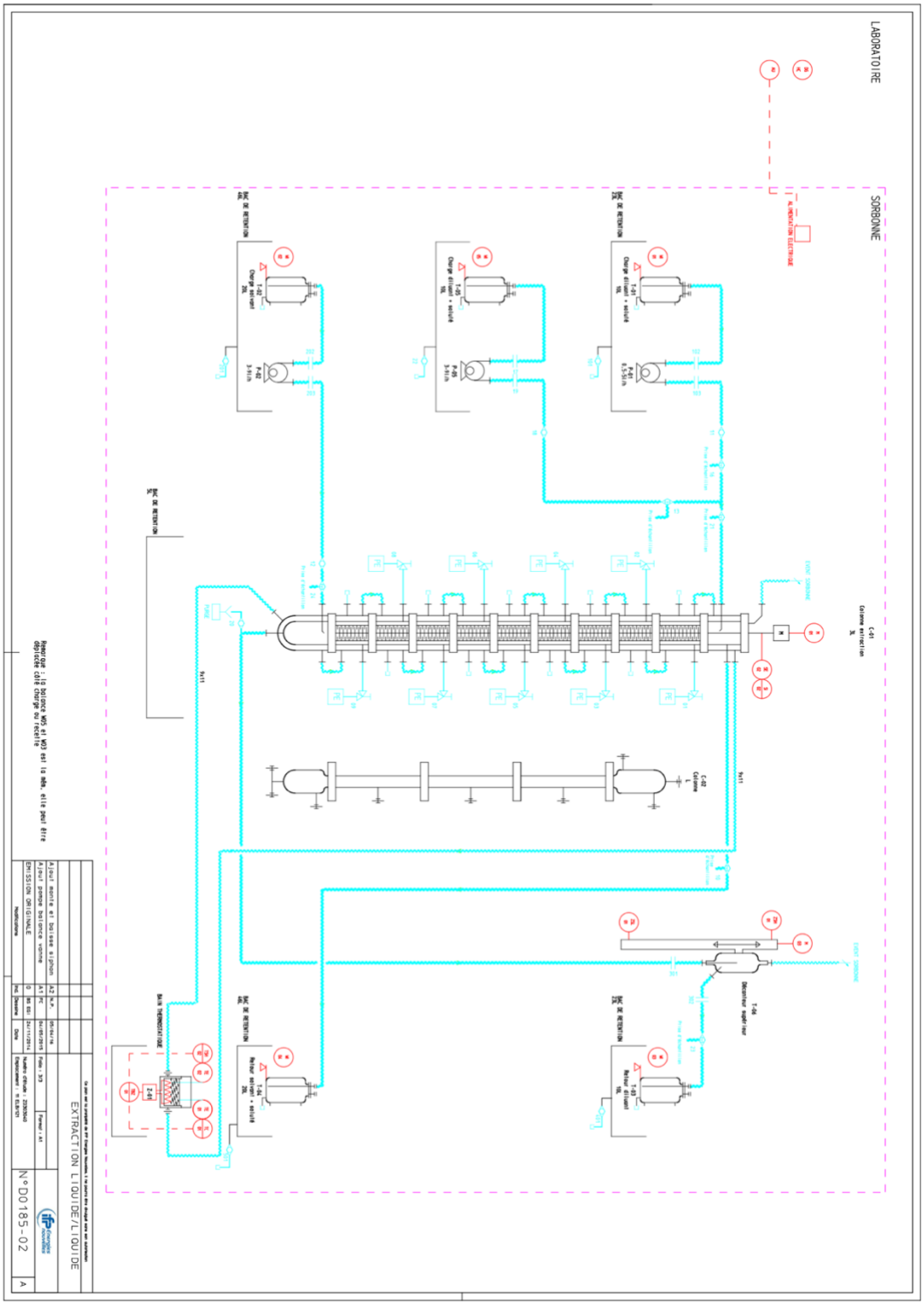

## Appendix 2: 1D Dispersion model analytical solution

Equation reported in section 4 can be expressed in dimensionless form as follows:

$$X = \frac{c_x - c^*_{x,1}}{c_{x,0} - c^*_{x,1}} = \frac{c_x - (c_{y,1} - q)/m}{c_{x,0} - (c_{y,1} - q)/m} \tag{A.1}$$

$$Y = \frac{c_y - c_{y,1}}{mc_{x,0} - (c_{y,1} - q)} \tag{A.2}$$

with m and q parameters of distribution ratio. (0 x inlet and 1 y inlet:

$$\frac{d^2X}{dZ^2} - Pe_x B \frac{dX}{dZ} - N_{ox} Pe_x B(X - Y) = 0 \tag{A.3}$$

$$\frac{d^2Y}{dZ^2} + Pe_y B \frac{dY}{dZ} + EN_{ox} Pe_x B(X - Y) = 0 \tag{A.4}$$

where:

$$Pe_x = \frac{v_c H_c}{D_{ax,c}} \tag{A.5}$$

$$Pe_y = \frac{v_d H_c}{D_{ax,d}} \tag{A.6}$$

$$B = \frac{H}{H_C} \tag{A.7}$$

$$N_{ox} = \frac{k_{Ov,x} aH}{v_x} \tag{A.8}$$

$$a = \frac{6\varphi}{d_{32}} \tag{A.9}$$

$$\frac{d^4Y}{dZ^4} - \alpha \frac{d^3Y}{dZ^3} - \beta \frac{d^2Y}{dZ^2} - \gamma \frac{dY}{dZ} = 0 \tag{A.10}$$

$$\boldsymbol{E} = m \frac{\dot{V}_s}{\dot{V}_F} = m \frac{u_x}{u_y} \tag{A.11}$$

$$\alpha = \mathrm{B}(\mathrm{Pe_x} - \mathrm{Pe_y}) \tag{A.12}$$

$$\beta = \mathrm{N_{ox}B}(\mathrm{Pe_x} + \mathbf{E}\mathrm{Pe_y}) \tag{A.13}$$

$$\gamma = \mathrm{N_{ox}Pe_xPe_yB^2}(1 - \mathbf{E}) \tag{A.14}$$

$$\mathrm{Y} = \sum_{i=1}^{4} A_i a_i \exp(\lambda_i Z) \tag{A.15}$$

$$\mathrm{X} = \sum_{i=1}^{4} A_i \exp(\lambda_i Z) \tag{A.16}$$

where $\lambda_1 = 0$

and the remaining $\lambda_i$ are the roots of the characteristic equation:

$$\lambda^3 - \alpha\lambda^2 - \beta\lambda - \lambda = 0 \tag{A.17}$$

The $a_i$ are given by:

$$a_i = 1 + \frac{\lambda_i}{\mathrm{N_{ox}}} - \frac{{\lambda_i}^2}{\mathrm{N_{ox}}\lambda_i B} = \frac{\mathbf{E}(1 - \lambda_i/(\mathrm{Pe_x}B))}{1+\lambda_i/(\mathrm{Pe_y}B)} \tag{A.18}$$

The roots of $\lambda_i$ can be evaluated by:

$$\lambda_i = \frac{\alpha}{3} + 2p^{1/2}\cos(\frac{u}{3} + k) \tag{A.19}$$

with k=0°, 120°, 240° for $\lambda_2$ $\lambda_3\lambda_4$ respectively and:

$$p = \left(\frac{\alpha}{3}\right)^2 \tag{A.20}$$

$$q = \left(\frac{\alpha}{3}\right)^2 + \frac{\alpha\beta}{6} + \frac{\gamma}{2} \tag{A.21}$$

$$u = cos^{-1}\left(\frac{q}{p^{3/2}}\right) \tag{A.22}$$

This solution is valid only for:

$$q^2 - p^3 < 0 \tag{A.23}$$

For $Pe_x$ $Pe_y$ L $H_{Ox}$ Finite, and **E**.

$$A_i = \frac{D_{Ai}}{D_{A1} - D_A} \tag{A.24}$$

$$D_A = \begin{Vmatrix} 1 - \frac{\lambda_2}{P_x B} & 1 - \frac{\lambda_3}{P_x B} & 1 - \frac{\lambda_4}{P_x B} \\ a_2\lambda_2 & a_3\lambda_3 & a_4\lambda_4 \\ a_2 e^{\lambda_2} & a_3 e^{\lambda_3} & a_4 e^{\lambda_4} \end{Vmatrix} \tag{A.25}$$

$$D_{A1} = \begin{Vmatrix} a_2\lambda_2 & a_3\lambda_3 & a_4\lambda_4 \\ a_2 e^{\lambda_2} & a_3 e^{\lambda_3} & a_4 e^{\lambda_4} \\ a_2 e^{\lambda_2} f(\lambda_2) & a_3 e^{\lambda_3} f(\lambda_3) & a_4 e^{\lambda_4} f(\lambda_4) \end{Vmatrix} \tag{A.26}$$

with

$$f(\lambda_i) = \left(1 + \frac{\lambda_i}{\mathrm{Pe_y} B}\right) \tag{A.27}$$

$$D_{A2} = \lambda_4\lambda_3\left(a_4 e^{\lambda_3} - a_3 e^{\lambda_4}\right) \tag{A.28}$$

$$D_{A3} = \lambda_2\lambda_4\left(a_2 e^{\lambda_4} - a_4 e^{\lambda_2}\right) \tag{A.29}$$

$$D_{A4} = \lambda_2\lambda_3\left(a_3 e^{\lambda_2} - a_2 e^{\lambda_3}\right) \tag{A.30}$$

Limit case and simplified solutions are available in Handbook of Solvent Extraction.

## Appendix 3: Henshke's model for terminal velocity

Henschke (2004) proposed a model more complicated composed by velocities of spherical, deformed and oscillating droplets. This model can be used for a wide range of droplet diameter, describing well effect of circulations within a drop, unfortunately this model includes several fitting parameters. Henschke's model has been proposed here for information only:

$$u_t = \frac{u_{def,os} u_{sph}}{\left(u_{def,os}^{p3} + u_{sph}^{p3}\right)^{1/p3}} \tag{A.31}$$

with:

$$u_{def,os} = \left(u_{def}^{p5} + u_{os}^{p5}\right)^{1/p3} \tag{A.32}$$

$$u_{def,os} = \left(u_{def}^{p5} + u_{os}^{p5}\right)^{1/p3} \tag{A.33}$$

$$u_{def} = \left(\frac{d_p g \Delta\rho}{2\rho_c}\right)^{1/2} \tag{A.34}$$

$$u_{os} = \left(\frac{2p_2\sigma}{d_p\rho_c}\right)^{1/2} \tag{A.35}$$

The terminal velocity of spherical droplets $u_{sph}$ reads:

$$u_{sph} = \frac{\mu_c Re_{sph}}{d_p \rho_c} \tag{A.36}$$

with:

$$Re_{sph} = (1 - f)Re_{rigid} + fRe_{circ} \tag{A.37}$$

$$f = 2(K_{HR} - 1),\ K_{HR} = \frac{3(\mu_c + \frac{\mu_d}{\beta})}{2\mu_c + 3\mu_d/\beta},\ \beta = 1 - \frac{1}{\left(1 + (d_p/p_1)^{p4}\right)} \tag{A.38}$$

In order to calculate the Reynolds numbers $Re_{rigid}$ $Re_{circ}$:

$$Re_{circ} = \frac{Ar}{12(0.065Ar + 1)^{1/6}} \tag{A.39}$$

$$\mathrm{Re_{rig}} = \left(\frac{4\mathrm{Ar}}{3\mathrm{Cd}}\right)^{1/2} \tag{A.40}$$

$$\mathrm{C_D} = \frac{432}{\mathrm{Ar}} + \frac{20}{\mathrm{Ar}^{1/3}} + \frac{0.51\mathrm{Ar}^{1/3}}{\mathrm{Ar}^{1/3} + 140} \tag{A.41}$$

The original has five parameters p1…p5 but two of them were constant in the respective investigations by Bertakis et al (2010). In the study of Baumler et al. (2010) all five parameters are regarded as free parameters in order to get the best approximation to experimental data.

**Table A.1:** List of parameters used for Henschke's model

| System | $p_1$ (mm) | $p_2$ (-) | $p_3$ (-) | $p_4$ (-) | $p_5$ (-) |
|---|---|---|---|---|---|
| Toluene/Water | 8.87 | 1.60 | 12.32 | 9.25 | 2.03 |
| n-butyl Acetate/water | 37.57 | 1.40 | 9.36 | 23.78 | 1.54 |
| n-butanol/water | 1.63 | 3.76 | 2.98 | 10.00 | 8.00 |

# Appendix 4: Experiments

In this section show the results of the experimental tests of Kuhni ECR32 Miniplant.

Two different technique for measuring hold-up, photography method for valuation of the Sauter mean diameter and complete analysis are been proposed.

Fast-sampling method:

In this section of appendix more experimental detail are been reported. (open free area 20%,

| Experiment test | Transfer direction | Impeller speed (rpm) | Total volumetric flow rate(L/h) | E/R real | Solvent flow rate (L/h) | Feed flow rate (L/h) | Hold-up | | | |
|---|---|---|---|---|---|---|---|---|---|---|
| | | | | | | | T1% | T4% | T7% | Av% |
| D0185-142 | c→d | 400 | - | - | - | - | 7,2 | 5,7 | 4,5 | 5,8 |
| D0185-143 | c→d | 450 | 4,3 | 1,43 | 2,5 | 1,75 | 7,6 | 5,8 | 5,3 | 6,2 |
| D0185-144 | c→d | 552 | 4,2 | 1,44 | 2,5 | 1,74 | 11,5 | 8,1 | 6,4 | 8,7 |
| D0185-145 | c→d | 600 | 3,9 | 1,44 | 2,3 | 1,61 | 15,0 | 10,6 | 9,9 | 11,9 |
| D0185-146 | c→d | 625 | 4,2 | 1,44 | 2,5 | 1,73 | 16,2 | 32,0 | 33,8 | 27,3 |
| D0185-147 | c→d | 501 | 4,2 | 1,92 | 2,76 | 1,44 | 7,8 | 5,7 | 5,57 | 6,4 |
| D0185-148 | c→d | 501 | 4 | 1.4 | 2.6 | 1.44 | 11,9 | 7,5 | 6,8 | 8,7 |

| | | | | | | | | | | |
|---|---|---|---|---|---|---|---|---|---|---|
| D0185-149 | c→d | 598 | 4,2 | 1,9 | 2,8 | 1,45 | 14,1 | 10,2 | 8,7 | 11,0 |
| D0185-150 | c→d | 615 | - | - | - | - | 17,3 | 48 | 16 | 27 |
| D0185-151 | c→d | 498 | 4,2 | 2,3 | 3,0 | 1,29 | 7,7 | 6,1 | 5,6 | 6,7 |
| D0185-152 | c→d | 550 | 4,2 | 2,3 | 3,0 | 1,29 | 9,7 | 7,2 | 7,2 | 8,1 |
| D0185-153 | c→d | 590 | 4,3 | 2,31 | 2,99 | 1,29 | 13,0 | 9,8 | 8,8 | 10,5 |
| D0185-154 | c→d | 620 | 4,3 | 2,39 | 3,03 | 1,27 | 14,8 | 34,4 | 10,2 | 19,8 |
| D0185-155 | c→d | 352 | 8,5 | 1,39 | 4,95 | 3,57 | 9,1 | 7,4 | 5,6 | 7,4 |
| D0185-156 | c→d | 425 | 8,5 | 1,40 | 4,96 | 3,54 | 11,9 | 9,0 | 7,0 | 9,3 |
| D0185-157 | c→d | 485 | 7,9 | 1,26 | 4,42 | 3,51 | 15,3 | 10,0 | 10,0 | 11,8 |

Shut-down method:

| **Experiment test** | **Transfer direction** | **Impeller speed (rpm)** | **Total volumetric flow rate(L/h)** | **E/R real** | **Solvent flow rate (L/h)** | **Feed flow rate (L/h)** | **Hold up** |
|---|---|---|---|---|---|---|---|
| D0185-158 | c→d | 451 | 3.95 | 1.41 | 2.31 | 1.64 | 8.40% |
| D0185-159 | c→d | 601 | 4.01 | 1.37 | 2.32 | 1.69 | 15.34% |
| D0185-160 | c→d | 625 | 4.03 | 1.36 | 2.32 | 1.71 | 21.06% |
| D0185-161 | c→d | 550 | 4.06 | 1.32 | 2.31 | 1.75 | 10.54% |
| D0185-162 | c→d | 350 | 4.03 | 1.37 | 2.33 | 1.70 | 5.16% |
| D0185-163 | c→d | 350 | 8.00 | 1.42 | 4.69 | 3.30 | 9.83% |
| D0185-164 | c→d | 450 | 7.72 | 1.47 | 4.59 | 3.13 | 14.55% |
| D0185-165 | c→d | 500 | 7.57 | 1.43 | 4.46 | 3.11 | 17.00% |
| D0185-166 | c→d | 525 | 7.60 | 1.43 | 4.47 | 3.13 | 20.33% |
| D0185-167 | c→d | 350 | 9.89 | 1.29 | 5.57 | 4.32 | 13.01% |
| D0185-168 | c→d | 400 | 9.85 | 1.35 | 5.66 | 4.19 | 14.97% |
| D0185-169 | c→d | 430 | 9.84 | 1.32 | 5.60 | 4.24 | 16.51% |
| D0185-170 | c→d | 490 | 9.86 | 1.35 | 5.66 | 4.19 | 26.06% |
| D0185-171 | c→d | 525 | 4.15 | 2.37 | 2.92 | 1.23 | 10.69% |
| D0185-173 | c→d | 625 | 4.15 | 2.40 | 2.93 | 1.22 | 22.40% |